

### **Archive ouverte UNIGE**

https://archive-ouverte.unige.ch

Thèse 2020

**Open Access** 

This version of the publication is provided by the author(s) and made available in accordance with the copyright holder(s).

Aspects of Eigenstate Dynamics: A Holographic Approach

\_\_\_\_\_\_

Vielma Blanco, Manuel Vidal

#### How to cite

VIELMA BLANCO, Manuel Vidal. Aspects of Eigenstate Dynamics: A Holographic Approach. Doctoral Thesis, 2020. doi: 10.13097/archive-ouverte/unige:143593

This publication URL: <a href="https://archive-ouverte.unige.ch/unige:143593">https://archive-ouverte.unige.ch/unige:143593</a>

Publication DOI: <u>10.13097/archive-ouverte/unige:143593</u>

© This document is protected by copyright. Please refer to copyright holder(s) for terms of use.

# Aspects of Eigenstate Dynamics: A Holographic Approach

### THÈSE

présentée à la Faculté des Sciences de l'Université de Genève pour obtenir le grade de Docteur ès sciences, mention Physique

par

Manuel Vidal VIELMA BLANCO

de

Mérida (Venezuela)

Thèse  $N^{o}$  5502

GENÈVE Atelier d'impression de l'Université de Genève Septembre 2020 A cierto lugar del norte de América del Sur. Y a los que, desde aquellos palacios de infancia ahora desplomados o desde la diáspora en su distancia, lo añoran.

# Contents

M	lemb	ers of	the Jury	vii
$\mathbf{A}$	ckno	wledge	ements	ix
$\mathbf{R}$	ésum	ıé		xi
1	Intr	roducti	ion	1
	1.1	Chaos	and thermalization	4
		1.1.1	Chaos and Random Matrix Theory	6
		1.1.2	Some results from random matrix theory	8
	1.2	Quant	cum thermalization and ETH	15
		1.2.1	ETH	16
	1.3	Towar	ds quantum chaos	20
		1.3.1	The OTOC as a signature of quantum chaos	20
		1.3.2	Fast scramblers and a bound on chaos	23
	1.4	The S	achdev-Ye-Kitaev model	25
		1.4.1	Schwinger-Dyson equation and the IR limit	32
		1.4.2	Schwarzian theory	36
		1.4.3	Four-point functions and the OTOC	38

2 ETH in the SYK model: a numerical study						
	2.1	Summary of results				
	2.2 The complex SYK model			42		
	2.3 One point functions and eigenstate thermalization			45		
		2.3.1	On-diagonal terms are thermal	45		
		2.3.2	Off-diagonal terms	48		
	2.4	Correl	ation functions and chaotic behavior	51		
		2.4.1	The spectral form factor	51		
		2.4.2	The two-point function	52		
		2.4.3	The four-point function	58		
	2.5	Discus	ssion	59		
		2.5.1	Comments on putative bulk dual	60		
	2.A	Full sp	pectrum & ETH for other operators	63		
		2.A.1	Density of states	63		
		2.A.2	ETH for the hopping operator	64		
	2.B	Rando	om matrix theory	64		
		2.B.1	Off-diagonal matrix elements	66		
		2.B.2	Spectral form factor	66		
3	ETI	H in th	ne conformal SYK model	69		
	3.1 Introduction		luction	69		
	3.2	Releva	ant Properties of the SYK system	72		
		3.2.1	Vertex expansion	73		
		3.2.2	The IR theory & Schwarzian contribution	76		
	3.3	Heavy	States in Conformal Three-point Correlators	77		
		3.3.1	Operators and states	77		
		3.3.2	Fermion six-point functions and OPE coefficients	79		
		3.3.3	Thermalization in a generalized free theory?	84		
	3.4	Summ	ary and Discussion	86		
	3.A	Collec	tive field action	88		
	3.B		nance of Planar diagrams	89		
	3.C	Expres	ssions for $\mathcal{I}_{mkn}^{(1)}$ and $\mathcal{I}_{mkn}^{(2)}$	90		

3	3.D	Regularised Kronecker delta function				
3	3.E	Lack o	f ETH in Free fields	93		
4 I	$\mathbf{Ext}$	ended	eigenstate Thermalization in the Schwarzian theory	95		
4	1.1	Introd	uction	95		
		4.1.1	Summary of results	97		
4	1.2	Pure s	tates in Liouville and the Schwarzian	102		
		4.2.1	Boundary Liouville theory and Schwarzian coherent states	102		
		4.2.2	Descending to the Schwarzian	107		
		4.2.3	Boundary conditions as States of the theory	110		
4	1.3	Semicl	assical results	113		
		4.3.1	One-point function and effective temperature	114		
		4.3.2	Semiclassical OTOC and chaos conjecture	117		
		4.3.3	An alternative derivation	121		
4	1.4	Exact	results	124		
		4.4.1	Computations between ZZ branes	124		
		4.4.2	Computations between ZZ and FZZT branes	133		
		4.4.3	Computations between two FZZT branes	135		
4	1.5	Discus	sion	137		
Bib	liog	graphy		140		

# Members of the Jury

### Prof. Julian Sonner

Département de Physique Théorique Université de Genève, Switzerland

### Prof. Anton Alekseev

Section de Mathématiques Université de Genève, Switzerland

### Prof. Kyriakos Papadodimas

High Energy, Cosmology and Astroparticle Physics International Center for Theoretical Physics, Italy

# Acknowledgements

First and foremost, I would like to thank Julian Sonner for his guidance and support throughout my PhD. I am most honored to have carried out my doctoral studies under his tutelage and to have learned from him a great deal about Physics in particular and about the scientific endeavor in general.

It was my great pleasure to undertake part of my research in collaboration with Pranjal Nayak. I thank him immensely for all the things he has taught me and for being a good friend to me.

My gratitude goes also to the many other friends and colleagues which populate the fondest memories I keep from my happy stay in Geneva.

I would like to extend my thanks to Anton Alekseev and Kyriakos Papadodimas for agreeing to serve on this thesis' committee, and to Hong Liu for hosting me during my delightful scientific visit to his institution.

Last but not least, many thanks to my family for their love and continuos encouragement.

# Résumé

Via la dualité holographique (ou 'AdS / CFT'), les trous noirs sont décrits par des états thermiques d'une théorie quantique des champs. Le processus de formation et d'évaporation des trous noirs correspond au processus de thermalisation de certaines théories quantiques de champs unitaires, évoluant depuis des états initiaux hors-équilibre vers l'équilibre thermique. Cependant, de nombreuses questions importantes concernant cette image d'une simplicité attravante restent mystérieuses, comme exprimé notamment dans le paradoxe de l'information et ses ramifications plus récentes. Un aspect important d'une résolution satisfaisante de ces énigmes dans l'holographie est une compréhension précise de la relation entre la perte d'information, l'évolution unitaire et la thermalisation de la théorie défini sur la frontière, au sens holographique. Pour résumer, la question de savoir à quel point un état propre générique de haute énergie dans une théorie avec un dual holographique est thermique, est étroitement liée à la question de savoir jusqu'à quel point il est légitime de considérer la géométrie duale de cet état pur comme un trou noir. Il est donc important de comprendre le mécanisme détaillé de la thermalisation dans tout modèle de théorie des champs dual donné, ainsi que d'extraire des leçons pour la classe générale des théories avec duales sur le volume, dans la mesure où l'on trouve de tels modèles. Comme c'est souvent le cas, les points de départ les plus prometteurs sont les instances les plus simples qui contiennent encore suffisamment de structure pour permettre d'aborder les subtilités également présentes dans les théories de grande dimension et plus complexes auxquelles on est souvent intéressé. Pour cette raison, les modèles holographiques de plus basse dimension, tels que AdS<sub>3</sub>/CFT<sub>2</sub> (c'est-à-dire la gravité tridimensionnelle), ainsi que le cas encore plus bas de NAdS<sub>2</sub>/NCFT<sub>2</sub> ('Near AdS<sub>2</sub>', 'Near CFT<sub>2</sub>') sont à nouveau au premier plan.

Le sujet de la présente thèse est un système quantique à plusieurs corps composé de fermions en interaction proposé pour la première fois par Alexei Kitaev en 2015 : l'ainsi connu 'modèle Sachev-Ye-Kitaev' (SYK). Il s'agit d'un système quantique à désordre trempé avec des couplages aléatoires entre tous les fermions, qui montre une invariance conforme

approximative émergente dans l'infrarouge ainsi qu'une entropie étendue à basse température. De plus, il a également été démontré que le modèle présente un chaos quantique maximal, diagnostiqué par un certain exposant de Lyapunov ( $\lambda_L$ ) extrait des fonctions de corrélation thermique à quatre points connues comme OTOCs (out-of-time-order correlators). Dans le modèle SYK donc, la question de la thermalisation est celle du comportement d'un simple Hamiltonien à plusieurs corps sous évolution unitaire, c'est-à-dire l'étude de la thermalisation dans des systèmes quantiques fermés à plusieurs corps. Il y a eu beaucoup de progrès dans l'étude de telles situations et nous passons en revue certaines de ces découvertes. La simplicité du modèle SYK fait de lui un parfait candidat pour une étude détaillée du mécanisme de thermalisation dans le cadre de la dualité holographique avec accès au régime quantique profonde.

En raison du moyennage d'ensemble implicite dans le modèle, il existe des subtilités potentielles dans la connexion des résultats du modèle SYK à la physique des trous noirs. Pour adresser ce point, il a été montré que certaines théories tensorielles définies sans moyennage sur un ensemble, donnent lieu à la même limite de grand N que les modèles SYK. Ici nous étudions également la question de la thermalisation dans une réalisation aléatoire donnée du modèle SYK, pour laquelle la mise en garde précédente ne s'applique pas. Dans la mesure où l'on se limite à des quantités auto-moyennées, il en va de même pour le modèle moyenné sur le désordre.

Dans cette thèse, nous démontrons en détail que le modèle SYK satisfait les propriétés de l'hypothèse de thermalisation de l'état propre (eigenstate thermalisation hypothesis – ETH) et établissons donc ce scénario comme le mécanisme approprié de thermalisation dans cet exemple prototypique de dualité holographique. L'ETH, qui s'appuie sur les résultats du chaos classique et de la théorie des matrices aléatoires, est une hypothèse sur les propriétés du spectre des Hamiltoniens à plusieurs corps pour les systèmes présentant un comportement thermique. Son importance est qu'elle explique le comportement thermique de certains opérateurs dans les systèmes quantiques fermés via les propriétés des états stationnaires de l'Hamiltonien. La thermalisation pour les opérateurs locaux (ou non extensifs) se produit dans cette image dans le sens où les moyennes à long terme des observables se rapprochent de l'attente dans l'ensemble microcanonique.

Notre étude implique des tests numériques approfondis ainsi que, dans les régimes où le modèle peut être ainsi approché, divers tests analytiques. Ils ont permis d'élucider plus généralement la structure thermique inhérente aux états purs, conduisant notamment à une conjecture sur l'applicabilité de l'ETH à des observables impliquant plusieurs opérateurs, à l'observation de phases ergodiques et non ergodiques analogues au comportement connu dans une transition chaotique-intégrable, et, dans les secteurs concernés du modèle, aux progrès autour de la physique des micro-états associés holographiquement.

## Summary

Via holographic duality (or 'AdS/CFT') black holes are described by thermal states of a dual quantum field theory. The process of black hole formation and evaporation corresponds to the process of thermalization of certain (unitary) quantum field theories, evolving from nonequilibrium initial states towards thermal equilibrium. However, many important questions pertaining to this attractively simple picture remain mysterious, as expressed notably in the information loss paradox [1], and its more recent ramifications [2]. An important aspect of a satisfactory resolution of these puzzles within holography is a precise understanding of the relation between information loss, unitary evolution and thermalization of the boundary theory. Put succinctly the question of how thermal [3, 4] a generic high-energy eigenstate looks in a theory with a holographic dual is closely tied to the question of how legitimately one may consider the dual geometry of this pure state to be a black hole. It is therefore important to understand the detailed mechanism of thermalization in any given dual field theory model, as well as to extract lessons for the general class of theories with bulk duals, wherever these are available. As is often the case, the most promising starting points are the simplest instances which still contain enough structure to allow one to address the subtleties also present in the higher-dimensional, more complicated theories of primary concern. For this reason, lower-dimensional holographic models, such as AdS<sub>3</sub>/CFT<sub>2</sub> (i.e. three-dimensional

gravity) [5–8], as well as the even lower-dimensional case of  $NAdS_2/NCFT_2$  ('Near  $AdS_2$ ', 'Near  $CFT_2$ ') [9–12] have once again risen to the fore.

The subject of the present thesis is a many-body quantum mechanical system of interacting fermions first proposed by Alexei Kitaev in 2015 [9], closely related to an older one with a controllable spin-glass ground state [13], the so-called Sachev-Ye-Kitaev (SYK) model. This is a quenched disorder quantum system with random all-to-all couplings, which shows emergent approximate conformal invariance in the infrared as well as an extensive entropy at low temperature [9–11,14]. Furthermore, it has also been demonstrated [9] that the model exhibits maximal quantum chaos (in the sense of [15]), diagnosed by a certain Lyapunov exponent ( $\lambda_L$ ) extracted from four-point out-of-time-order correlators (OTOCs) [9,11,14]. In the SYK model then, the question of thermalization is one about the behavior of a simple many-body Hamiltonian under unitary evolution, i.e. the study of thermalization in closed many-body quantum systems. Much has been learned about such situations, and we will review some of it and will provide some relevant references in this Chapter. The simplicity of the SYK model means that it is a perfect candidate for a detailed study of the mechanism of thermalization within the setting of holographic duality with access to the deeply quantum regime.

Owing to the ensemble average implicit in the model, there are potential subtleties in connecting results in the SYK model to black-hole physics. To start addressing this issue, [23–25] have shown that certain tensor theories defined without averaging over an ensemble, give rise to the same large-N limit as the SYK models. Here we also study the question of thermalization in a given random realization of the SYK model, for which the previous cautionary remark does not apply. To the extent that one limits oneself to self-averaging quantities the same then holds for the disorder averaged model.

Here we demonstrate in detail that the SYK model satisfies the properties of the eigenstate thermalization hypothesis (ETH) and therefore establish this scenario as the appropriate mechanism for thermalization in this prototypical example of holographic duality. The ETH, which builds on results from classical chaos and random matrix theory, is an assumption on the properties of the spectrum of many-body Hamiltonians for systems showing thermal

<sup>&</sup>lt;sup>1</sup>Simple enough that various experimental approaches have been put forward [18–21].

behavior. Its significance is that it explains thermal behavior of certain operators in closed quantum systems via properties of stationary states of the Hamiltonian. Thermalization for local (on non-extensive) operators occurs in this picture in the sense that long-time averages of observables approach the microcanonical ensemble expectation.

Our studies involve thorough numerical tests as well as, in the regimes where the model can be thus approached, various analytic checks. They have allowed us to elucidate the thermal structure inherent in pure states more generally, leading in particular to a conjecture regarding the applicability of the ETH to observables involving multiple operators, to the observation of ergodic and non ergodic phases akin to the known behavior across a chaotic-integrable transition, and to advancements regarding the physics, in the relevant sectors of the model, of the microstates associated in lower dimensional holography.

### Structure of this thesis

The structure of this thesis is naturally dictated by that of the works on which it is based, namely

- J. Sonner and M.V., "Eigenstate Thermalization in the Sachdev-Ye-Kitaev Model," JHEP 11 (2017) 149, arXiv:1707.08013 [hep-th]
- P. Nayak, J. Sonner, and M.V., "Eigenstate Thermalisation in the Conformal Sachdev-Ye-Kitaev: an Analytic Approach," JHEP 10 (2019) 019, arXiv:1903.00478 [hep-th]
- P. Nayak, J. Sonner, and M.V., "Extended Eigenstate Thermalization and the Role of FZZT Branes in the Schwarzian Theory," JHEP 03 (2020) 168, arXiv:1907.10061 [hep-th]

Chapter 2, wherein we establish numerically that the SYK model satisfies the ETH, contains the material originally presented in the first of these references. In it we study one point functions of simple operators evaluated in energy eigenstates and observe the behavior predicted by this hypothesis. We also perform further checks on higher-point correlators, including a version of the so-called OTOC evaluated in energy eigenstates. Our findings here have naturally led us to conjecture that an extended version of the ETH applies to more

complicated quantities (such as the OTOC.) In the subsequent Chapters, based respectively on the second and third references, we undertake various analytical studies in the conformal-and Schwarzian-dominated regimes of the SYK, thus proving that ETH is indeed satisfied in this model as well as supporting our conjecture of extended ETH.

In the remaining of this Chapter we review some of the main technical and conceptual results relevant for the discussions we expand upon in subsequent Chapters. The material we are about to present has been long established, and the approach we have taken draws heavily upon the reviews [22], [27] and [28], in content as well as in structure, although certainly not in scope. The reader interested in further exploring aspects of the vast and currently very active field of quantum chaos and thermalization is encouraged to consult the fist reference. The other two reviews focus on the Sachdev-Ye-Kitaev model, which has served as basis for all of our computations.

### 1.1 Chaos and thermalization

From a microscopic, quantum mechanical point of view, the general question about the equilibration and thermalization of a system encounters an immediate puzzle: how is it possible to reconcile the time reversibility of most microscopic laws of nature with the apparent irreversibility of the laws of thermodynamics?

One way in which classical physics explains the process of thermalization (or its lack) is as follows: in a system with many constituents—a gas released in a container, say—almost all particle trajectories quickly begin looking alike, even if their initial points are very different. This is so because nonlinear equations drive them to explore ergodically the constant-energy manifold, covering it uniformly with respect to the microcanonical measure. However, if the system possesses further conserved quantities functionally independent from the Hamiltonian and each other, then time evolution is confined to a highly restricted hypersurface of the energy manifold. These constraints could be such that microcanonical predictions fail and the system does not thermalize.

In the above line of thought, the ergodic hypothesis –which states in that in the longtime limit the time spent in each region of phase-space is proportional to its volume– is invoked and time averages are taken to be equivalent to ensemble averages, which are the ones ultimately computed. This essentially implies that the equal probability assumption embedded in the construction of the microcanonical ensemble is the key ingredient to capture long-time averages of observables.

Now, long-time averages of observables do not necessarily coincide with the values of the observables at long times, and ideally one would like to prove thermalization in the latter, strong sense; that is, one would like to prove that instantaneous values of observables approach the equilibrium value predicted by the microcanonical ensemble and remain close to it subsequently, up to Poincaré recurrences. These recurrences appear at very late times (exponential in the number of degrees of freedom) and can in any case be said to be irrelevant. However, in order for a system to explore all of its phase space, which is a key ingredient in the ergodic hypothesis, one should also wait a time exponential in the number of degrees of freedom. Therefore, the earlier and more physically relevant times are in fact not addressed by this hypothesis.

A second line of thought notes that almost all configurations are equivalent from a macroscopic point of view, i.e. macroscopic observables essentially exhibit the same values in most phase-space configurations compatible with a set of macroscopic constraints. Given that typical configurations vastly outnumber atypical configurations and that, under chaotic dynamics each configuration is reached with equal probability, atypical configurations quickly evolve into typical ones. From this point of view, thermalization boils down to reaching a typical configuration, which happens much faster than the full exploration of phase space required by ergodicity. Note, however, that this approach applies only when the measured quantity is macroscopic, as it is indeed meaningless to distinguish microscopic configurations by arbitrarily separating them into typical or atypical ones. Also, while most macroscopic configurations are by definition typical, it is in general cumbersome to prepare them experimentally without having to follow very slow protocols or letting the system evolve by itself [22].

As appealing as these explanations may be in the context of classical thermalization, one encounters a number of difficulties when trying to apply them in the realm of quantum thermalization. First of all, in isolated quantum systems the equation dictating the dynamics—the Schrödinger equation—is linear, as opposed to the non-linear ones which in classical

mechanics lead to the chaotic behavior responsible for "typicality". Also, it is not clear under what conditions conserved quantities provide independent constraints on relaxation dynamics since any operator commuting with a generic Hamiltonian is functionally dependent on it, implying that the conservation of energy is the only independent constraint [29]. On the other hand, even when operators are functionally dependent, their expectation values—considered as functionals of states—generally are not: for example, two states may have the same mean energies but different mean square-energies.

Remarkably, an approach combining ideas from classical chaos and random matrix theory (RMT) in a clear mathematical form was proposed independently in the 1990's by Srednicki and Deutsch which provides a possible explanation as to how thermalization comes about in quantum mechanics. This approach is known as the Eigenstate Thermalization Hypothesis (ETH) and can be formulated as an ansatz with strong predictive power. It focuses on physical observables and states that eigenstates of generic quantum Hamiltonians are typical in the sense that the statistical properties of physical observables approach the ones predicted by the microcanonical ensemble. We will have more to say more about this but before let us review some of the basic notions of classical chaos and RMT that inspired the ETH.

## 1.1.1 Chaos and Random Matrix Theory

Classically, a system is said to be chaotic if it exhibits a strong (exponential) sensitivity of phase-space trajectories to small perturbations, i.e. if

$$|\tilde{\mathbf{X}}(t) - \mathbf{X}(t)| \sim e^{\lambda_L t} \delta \mathbf{X}_0$$
 (1.1)

where  $\mathbf{X}(t) \equiv (\mathbf{q}(t), \mathbf{p}(t))$  is the phase space trajectory for initial conditions  $\mathbf{X}(0) = \mathbf{X}_0$ , and  $\tilde{\mathbf{X}}(t)$  is the trajectory for initial conditions  $\tilde{\mathbf{X}}(0) = \mathbf{X}_0 + \delta \mathbf{X}_0$ , where  $\delta \mathbf{X}_0$  is some small perturbation. The exponent  $\lambda_L$  is known as the *Lyapunov exponent* of the system, and is used to characterize its chaotic behaviour. A necessary, and often sufficient, condition for chaotic motion to occur is that the number of functionally independent conserved quantities (integrals of motion) is smaller than the number of degrees of freedom. When a system has as many integrals of motion as it has degrees of freedom, it is said to be *integrable*.

More concretely, consider a system of N degrees of freedom, with phase space coordinates  $\mathbf{q} \equiv (q_1, ..., q_N)$  and  $\mathbf{p} \equiv (p_1, ..., p_N)$  and Hamiltonian  $H(\mathbf{q}, \mathbf{p})$ . The system is integrable if it has as many functionally independent conserved quantities in involution as degrees of freedom, that is, if there exists  $\mathbf{I} = (I_1(\mathbf{q}, \mathbf{p}), ..., I_N(\mathbf{q}, \mathbf{p}))$  satisfying

$${I_j, H} = 0, \quad {I_j, I_k} = 0, \quad \text{for all } j, k = 1, ..., N.,$$
 (1.2)

where  $\{f,g\}$  denotes the Poisson bracket

$$\{f,g\} \equiv \sum_{k=1}^{N} \left( \frac{\partial f}{\partial q_k} \frac{\partial g}{\partial p_k} - \frac{\partial f}{\partial p_k} \frac{\partial g}{\partial q_k} \right) \tag{1.3}$$

for any two phase space functions  $f(\mathbf{q}, \mathbf{p})$  and  $g(\mathbf{q}, \mathbf{p})$ .

From Liouville's integrability theorem, it follows that there is a canonical transformation  $(p,q) \to (I,\Theta)$  (where  $I,\Theta$  are called action-angle variables) such that H(p,q) = H(I), [30]. As a result, the solutions of the equations of motion for the action-angle variables are trivial:  $I_j(t) = I_j^0 = \text{constant}$ , and  $\Theta_j(t) = \Omega_j t + \Theta_j(0)$ . Time evolution is by no means ergodic, hence integrable systems won't feature thermalization.

For example, the motion of a single particle without internal degrees of freedom in a one dimensional system described by a static Hamiltonian is integrable. This is so because in this case the energy provides a unique relation between its coordinate and its momentum. Fig. 1.1 illustrates the analogue phenomenon in a two-dimensional cavity and contrasts it with its chaotic cousin. Figure 1.1(a) shows the trajectory of a particle in an integrable circular cavity, which is a superposition of two periodic motions along the radial and angular directions. This is a result of the system having two conserved quantities, energy and angular momentum. Clearly, the long-time average of the particle density does not correspond to a uniform probability which covers phase space (it is not ergodic). Figure 1.1(b), on the other hand, shows a trajectory of a particle in a chaotic Bunimovich stadium [31], which looks completely random. If one compares two trajectories that are initially very close to each other in phase space one finds that, after a few bounces against the walls, they become uncorrelated both in terms of positions and directions of motion. This is a consequence of chaotic dynamics.

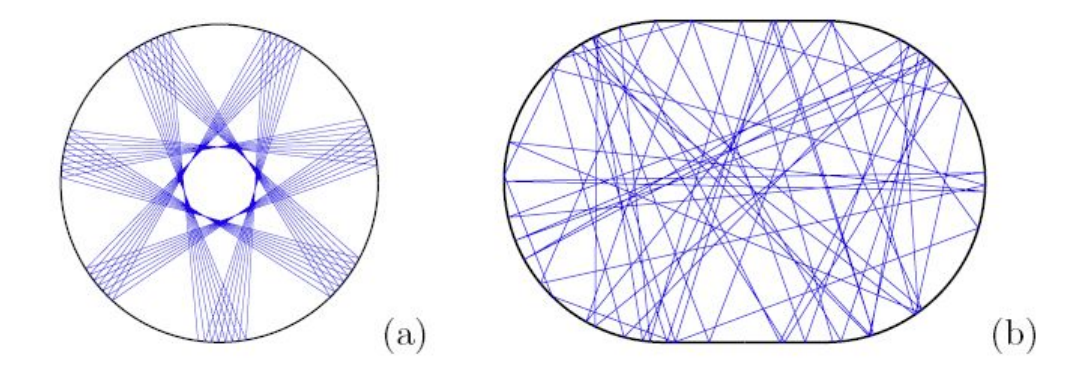


Figure 1.1: Examples of trajectories of a particle bouncing in a cavity: (a) non-chaotic circular (energy and angular momentum converved) and (b) chaotic Bunimovich stadium. Images taken from [22].

Examples of dynamical systems exhibiting chaos abound, in particular in the context of many-particle configurations, which are considered chaotic if they do not have an extensive number conserved quantities. For instance, an ensemble of noninteracting particles in high-dimensional systems is not chaotic in this sense, even if each particle exhibits chaotic motion in the part of phase space associated with its own degrees of freedom. This due to the fact that the energy of each particle is separately conserved. However, the general expectation is that interactions between the particles will lead to chaotic motion.

Generally speaking, it is difficult to rigorously prove the ergodicity of a system but it seems intuitive that it should be related to chaos. One could say that in a chaotic system trajectories quickly "forget" about their initial conditions and become undistinguishable from others with completely different initial data, a feature that is indeed present in systems that spread uniformly in phase space. For this reason, it may prove useful to study the chaotic properties of a system in order to see what consequences this has on the thermalization (or not) of it. Let us follow this line of thought.

## 1.1.2 Some results from random matrix theory

We said that classical chaos plays an important role when pondering about ergodicity and thermalization of a classical level but it is not yet clear how to extend these observations to what we may call quantum chaos. A first approach to this question could amount to consider quantization à la Wilson-Sommerfeld (or its formalization in the form of the Wentel-Kramers-Brillouin quantization). Here, along allowed trajectories, the classical reduced action satisfies the quantization condition

$$\oint pdq \approx 2\pi \hbar n \tag{1.4}$$

This approach would allow to treat the quantization of integrable systems but the form of this integral condition already signals its limitations to chaotic trajectories: the latter do not have closed trajectories in phase space.

For this reason, in modern discussions quantum chaos builds instead on a set of crucial results due to Wigner and Dyson that go under the name of random matrix theory (RMT) and that were originally developed for understanding the spectra of complex atomic nuclei. Wigner's original idea was to focus on the statistical properties of complex quantum mechanical systems instead of trying to predict their exact energy levels and corresponding eigenstates. His main insight was that, within small energy windows where the density of states is constant, in a generic basis the Hamiltonian looks essentially like a random matrix. Thus, it can be insightful to describe these systems by drawing their Hamiltonians from some statistical ensembles whose general properties could leave imprints on those of a single realization.

As an introductory example, let us treat the case of a system with a 2-dimensional Hilbert space whose Hamiltonian is given by

$$H = \begin{pmatrix} \varepsilon_1 & \frac{V}{\sqrt{2}} \\ \frac{V^*}{\sqrt{2}} & \varepsilon_2 \end{pmatrix} \tag{1.5}$$

where  $\varepsilon_1, \varepsilon_2$  and V are random numbers drawn from a Gaussian distribution with zero mean and variance  $\sigma$ . If the system is invariant under time reversal, then the Hamiltonian can be written as a real matrix  $(V = V^*)$ . The eigenvalues,  $E_{1,2}$ , can be easily found by diagonalizing the Hamiltonian. They are given by

$$E_{1,2} = \frac{\varepsilon_1 + \varepsilon_2}{2} \pm \frac{1}{2} \sqrt{(\varepsilon_1 - \varepsilon_2)^2 + 2|V|^2}$$
(1.6)

Using this we can study the level spacing statistics of the system. Setting  $\hbar = 1$ , the probability for the energy difference between the two eigenstates to be  $\omega$  is

$$P(\omega) = \frac{1}{(2\pi)^{3/2}\sigma^3} \int d\varepsilon_1 \int d\varepsilon_2 \int dV \, \delta\left(\sqrt{(\varepsilon_1 - \varepsilon_2)^2 + 2V^2} - \omega\right) \exp\left(-\frac{\varepsilon_1^2 + \varepsilon_2^2 + V^2}{2\sigma^2}\right).$$

which can be integrated [22] to obtain

$$P(E_1 - E_2 = \omega) \equiv P(\omega) = \begin{cases} \frac{\omega}{2\sigma^2} \exp\left(-\frac{\omega^2}{4\sigma^2}\right) & \text{if } V = V^* \\ \frac{\omega^2}{2\sqrt{\pi}(\sigma^2)^{3/2}} \exp\left(-\frac{\omega^2}{4\sigma^2}\right) & \text{if } V \neq V^* \end{cases}$$
(1.7)

When the system has time reversal symmetry  $(V \in \mathbb{R})$  the ensemble in question is the so called Gaussian Orthogonal Ensemble (GOE). When it does not, the ensemble is referred to as Gaussian Unitary Ensemble (GUE). In compact notation, (1.7) can be rewritten as

$$P(\omega) = \mathcal{A}_{\beta}\omega^{\beta} \exp\left(-\mathcal{B}_{\beta}\omega^{2}\right) \tag{1.8}$$

where  $\beta = 1, 2$  for GOE and GUE, respectively, and  $\mathcal{A}_{\beta}, \mathcal{B}_{\beta}$  are some constants that account for the normalization and the energy scale of the ensemble. Equation (1.8) is commonly referred to as Wigner's Surmise. A remarkable feature of these level statistics is that they show level repulsion, i.e.

$$P(\omega) \xrightarrow{\omega \to 0} 0 \tag{1.9}$$

For Hilbert spaces with more dimensions, generically in RMT one considers an ensemble of Hamiltonians with probability distribution given by the Gaussian

$$P(H) \propto \exp\left(-\frac{\beta}{2a^2} \operatorname{Tr} H^2\right) = \exp\left(-\frac{\beta}{2a^2} \sum_{ij} H_{ij} H_{ji}\right)$$
 (1.10)

where again  $\beta = 1, 2$  are related to GOE and GUE, a sets the energy scale of the ensemble, and  $\{H_{ij}\}$  are the matrix elements of the Hamiltonian in some basis. P(H) is independent on the choice of basis, as one should expect. Note that the Hamiltonian in (1.5) falls in the

category of (1.10).

Wigner's ideas proved very helpful in explaining the statistical properties of the spectra of complex nuclei. However, for a long time it was not clear for which "complex systems" RMT could be more generally applicable. In 1984, Bohigas, Giannoni, and Schmit, studying a single particle placed in an infinite potential well with the shape of a Sinai billiard, found that in the semiclassical limit (i.e. at high energies), the level statistics is described by the Wigner-Dyson distribution [32], provided that one looks at sufficiently narrow energy windows. Based on this, they conjectured that the level statistics of quantum systems that have a classically chaotic counterpart are described by RMT (this is known as the BGS conjecture). By convention, this behaviour of the spectrum is taken as a definition of quantum chaos even for systems without a classical counterpart.

In contrast to this, in integrable systems there are typically many conserved quantities and there can be arbitrarily close eigenstates that belong to different sectors of the spectrum that do not interact efficiently. The level spacing distribution for this kind of systems is therefore expected to be Poissonian. A simple example that illustrates this is an array of independent harmonic oscillators with incommensurate frequencies, such as the normal modes in a harmonic chain. Because these oscillators can be diagonalized independently, the many-body energy levels of such a system can be computed as

$$E = \sum_{j} n_{j} \omega_{j}, \tag{1.11}$$

where  $n_j$  are the occupation numbers and  $\omega_j$  are the mode frequencies. If we look into high energies, E, when the occupation numbers are large, nearby energy levels can come from very different sets of  $\{n_j\}$ . This means that the energy levels E are effectively uncorrelated with each other and can be treated as random numbers. Their distribution then should be described by Poisson statistics, that is, the probability of having n energy levels in a particular interval  $[E, E + \delta E]$  will be

$$P_n = \frac{\lambda^n}{n!} e^{-\lambda},\tag{1.12}$$

where  $\lambda$  is the average number of levels in that interval. Poisson and Wigner-Dyson statistics are very different in that in the former there is no level repulsion. For systems with Poisson

statistics, the distribution of energy level separations  $\omega$  is of the form

$$P_0(\omega) = e^{-\omega},\tag{1.13}$$

which is very different from the Wigner surmise (1.8). The statement that, for quantum systems whose corresponding classical counterpart is integrable, the energy eigenvalues generically behave like a sequence of independent random variables, that is, exhibit Poisson statistics, is now known as the Berry-Tabor conjecture [33]. While this conjecture describes what is seen in many quantum systems whose classical counterpart is integrable, and integrable quantum systems without a classical counterpart, there are examples for which it fails (such as the single particle in the harmonic potential described above and other harmonic systems [34]). Deviations from Poisson statistics are usually the result of having symmetries in the Hamiltonian that lead to extra degeneracies resulting in commensurability of the spectra.

So far we have described the implications of RMT on eigenvalues and their distributions but some important implications regarding eigenvectors of random matrices can also be extracted. In RMT, eigenstates will be given by random vectors with a certain correlation, since they need to be orthogonal to each other; however, for a Hilbert space with a large dimension, two random unit vectors will most likely be orthogonal, and hence they can be taken as independent random vectors. Also, the fact that the probability distribution in (1.10) is invariant under orthogonal (unitary) transformations for GOE (GUE) forces to impose the same restriction on the eigenvectors. For an eigenstate  $\psi$  normalized to unity with components  $(\psi_1, ..., \psi_N)$  in some (not fine-tuned) basis of the D-dimensional Hilbert space, its probability satisfies

$$P(\psi) \propto \begin{cases} \delta \left( \sum_{j=1}^{D} \psi_j^2 - 1 \right) & \text{GOE} \\ \delta \left( \sum_{j=1}^{D} |\psi_j|^2 - 1 \right) & \text{GUE} \end{cases}$$
 (1.14)

This can be used to study matrix elements of observables in the energy basis, which will have a very characteristic form in RMT. Given an hermitian observable  $\mathcal{O}$  with eigenvalues  $\mathcal{O}_i$  and eigenstates  $\{|\mathcal{O}_i\rangle\}_{i=1}^D$ , it can be decomposed as

$$\mathcal{O} = \sum_{i=1}^{D} \mathcal{O}_i |\mathcal{O}_i\rangle \langle \mathcal{O}_i| = \sum_{i,m,n=1}^{D} \mathcal{O}_i(\psi_i^m)^* \psi_i^n |m\rangle \langle n|$$
 (1.15)

with  $\psi_i^m \equiv \langle \mathcal{O}_i | m \rangle$ , i.e. the *i*-component of  $|m\rangle$  in the proper basis of  $\mathcal{O}$ . Crucially, the following relation holds

$$\overline{(\psi_i^m)^*(\psi_j^n)} = \frac{1}{D} \delta_{mn} \delta_{ij} + O\left(\frac{1}{D^2}\right)$$
(1.16)

where the overline denotes averaging over random eigenkets  $|m\rangle$  and  $|n\rangle$ . This can be used to compute the average and variance of the matrix elements of the observable  $\mathcal{O}$  in the energy basis,  $\langle m|\mathcal{O}|n\rangle \equiv \mathcal{O}_{mn}$ , to leading order in  $\frac{1}{D}$ . The average is given by

$$\overline{\mathcal{O}_{mn}} \cong \begin{cases}
\frac{1}{D} \sum_{i=1}^{D} \mathcal{O}_{i} \equiv \overline{\mathcal{O}} & \text{if } m = n \\
0 & \text{if } m \neq n
\end{cases}$$
(1.17)

whereas the standard deviation satisfies [22]

$$\frac{1}{\left|\mathcal{O}_{mn}\right|^{2}} - \left|\overline{\mathcal{O}_{mn}}\right|^{2} \simeq \begin{cases}
\frac{3-\beta}{D^{2}} \sum_{i=1}^{D} \mathcal{O}_{i}^{2} \equiv \frac{3-\beta}{D} \overline{\mathcal{O}}^{2} & \text{if } m = n \\
\frac{1}{D} \overline{\mathcal{O}}^{2} & \text{if } m \neq n
\end{cases} \tag{1.18}$$

where, again,  $\beta = 1, 2$  corresponds to GOE and GUE, respectively. Combining these expressions we see that, to leading order in 1/D, the matrix elements of any operator can be written as

$$\mathcal{O}_{mn} \simeq \overline{\mathcal{O}}\delta_{mn} + \sqrt{\frac{\overline{\mathcal{O}^2}}{D}}R_{mn}$$
 (1.19)

Here  $R_{mn}$  is a random Gaussian variable which is real for the GOE and complex for the GUE.

Equation (1.19) allows us to establish the relevance of RMT in the study of thermalization of a quantum mechanical system. For instance, consider a simple setup in which an isolated system is initially prepared in a pure state  $|\psi_I\rangle$  and evolves under a time-independent Hamiltonian  $\hat{H}$  with eigenvectors  $|m\rangle$  and eigenvalues  $E_m$ . The time-evolving wave function

is given by

$$|\psi(t)\rangle = \sum_{m} C_m e^{-iE_m t} |m\rangle,$$
 (1.20)

where  $C_m = \langle m | \psi_I \rangle$ . The time evolution of some observable  $\mathcal{O}$  expressed in the same basis is then given by

$$\mathcal{O}(t) \equiv \langle \psi(t) | \mathcal{O} | \psi(t) \rangle = \sum_{m,n} C_m^* C_n e^{i(E_m - E_n)t} \mathcal{O}_{mn}$$

$$= \sum_{m} |C_m|^2 \mathcal{O}_{mm} + \sum_{m,n \neq m} C_m^* C_n e^{i(E_m - E_n)t} \mathcal{O}_{mn}$$
(1.21)

where  $\mathcal{O}_{mn} = \langle m|\mathcal{O}|n\rangle$ . We say that the observable  $\mathcal{O}$  thermalizes if: (i) after some relaxation time, its average expectation value agrees with the microcanonical expectation value and (ii) temporal fluctuations about the microcanonical prediction are small at most later times.

Now, in the long-time average and in the absence of degeneracies, the last sum in the equation above averages to zero and we are left with the sum of the diagonal elements of  $\mathcal{O}$  weighted by  $|C_m|^2$ . The question is then how is it possible for  $\sum_m |C_m|^2 \mathcal{O}_{mm}$  to agree with the microcanonical average. We will see in the next subsection how to address this, but for now let us remark that if the Hamiltonian H ware a true random matrix, then using the RMT prediction for observables (1.19) one finds that the observables do thermalize. This is because the first sum in Eq. (1.21) becomes independent of the initial state

$$\sum_{m} |C_{m}|^{2} \mathcal{O}_{mm} \approx \bar{\mathcal{O}} \sum_{m} |C_{m}|^{2} = \bar{\mathcal{O}}, \tag{1.22}$$

that is, it agrees with the microcanonical result. Note that within RMT, the microcanonical ensemble has no energy dependence and is thus formally equivalent to the infinite temperature ensemble. It also becomes clear that exponentially long times may not be needed for relaxation. The off-diagonal matrix elements of  $\mathcal{O}$  are exponentially small so, by destroying phase coherence between a finite fraction of the eigenstates with a significant contribution to the expectation value, it is possible to approach the infinite-time prediction with high accuracy in a time much shorter than the inverse (many-body) level spacing, which is required to destroy coherence between all eigenstates. We will come back to this later.

In order to describe observables in experiments, however, one needs to go beyond the

RMT prediction. This is because in real systems thermal expectation values of observables depend on the energy density (temperature) of the system, and relaxation times are observable dependent. Hence, there is information in the diagonal and off-diagonal matrix elements of observables in real systems that cannot be found in RMT. In groundbreaking works throughout the 1990s, Srednicki provided the generalization of the RMT prediction that is needed to describe observables in physical systems [4, 35, 36]. Srednicki's ansatz is known as the eigenstate thermalization hypothesis (ETH). It was first shown to apply to realistic quantum systems, where thermalization was observed for a strikingly small number of particles (5 bosons in 21 lattice sites), by Rigol et al. [29].

# 1.2 Quantum thermalization and ETH

In order for a closed quantum system to thermally equilibrate under its own dynamics, the system must be able to act as its own reservoir, i.e. the dynamics must be such that for a subsystem that contains only a small fraction of the degrees of freedom of the entire system, the coupling to the rest of the system mimics a coupling to a reservoir. Indeed, for the full system, the dynamics is unitary and the total density matrix does not have a steady state limit  $\lim_{t\to\infty} \rho(t) \neq \rho_{eq}$  as it just picks up phase factors when written in the energy eigenbasis

$$\rho(t) = \sum_{nm} C_{nm} |n\rangle \langle m| e^{-i(E_n - E_m)t}$$
(1.23)

The memory of the local properties of the system's initial state is thus not erased by unitary time evolution but is rather 'hidden' if the system thermalizes: the spreading of quantum entanglement moves the information about the initial state so that at long times it is inaccessible if we are allowed to perform local measurements only on just a few degrees of freedom for which the remaining of the system acts as a reservoir<sup>2</sup>. The question about the thermalization of a quantum system then becomes one about its ability to act as reservoirs for their subsystems. For a long time it was assumed that generic interacting systems are always thermal in the sense that a statistical mechanical description holds given long enough times

<sup>&</sup>lt;sup>2</sup>This suggests that the essential function of a reservoir is to provide other quantum degrees of freedom that the subsystem gets entangled to such an extend that no information about the initial state of the subsystem remains locally observable [37]

but it was eventually found out that some systems exhibit a so-called many-body localized phase in which this fails to happen (see [37] for a review.)

### 1.2.1 ETH

What implications are there for a quantum mechanical system that does thermalize? It turns out that one way of reconciling quantum statistical mechanics and the dynamics of quantum thermalization involves imposing some constraints on the nature of eigenstates and observables. A natural extension of ideas from quantum chaos and random matrix theory, ETH allows to describe thermalization in isolated chaotic systems without even invoking the notion of an external bath. We will now see how.

The question about the thermalization of an isolated quantum system is naturally related to its dynamics as dictated by its time evolution. Consider again the evolution of an observable  $\mathcal{O}$  in a many-body quantum mechanical system as written in terms of the eigenstate energies

$$\langle \mathcal{O}(t) \rangle \equiv \langle \psi(t) | \mathcal{O} | \psi(t) \rangle = \sum_{\alpha, \beta} C_{\alpha}^* C_{\beta} e^{i(E_{\alpha} - E_{\beta})t} \mathcal{O}_{\alpha\beta}, \qquad (1.24)$$

As we discussed before, the long-time average of  $\langle \mathcal{O}(t) \rangle$  is simply

$$\overline{\langle \mathcal{O} \rangle} = \lim_{T \to \infty} \frac{1}{T} \int_0^T \sum_{\alpha,\beta} C_{\alpha}^* C_{\beta} \mathcal{O}_{\alpha\beta} e^{it(E_{\alpha} - E_{\beta})} = \sum_{\alpha} |C_{\alpha}|^2 \mathcal{O}_{\alpha\alpha}. \tag{1.25}$$

This can be seen as being the prediction of a diagonal ensemble, with  $|C_{\alpha}|^2$  the corresponding weight of the eigenstate  $|\alpha\rangle$ . If the mean of the observable thermalizes, we should have [29]

$$\sum_{\alpha} |C_{\alpha}|^{2} \mathcal{O}_{\alpha\alpha} = \langle \mathcal{O} \rangle_{\text{microcan.}} (E_{0})$$

$$= \frac{1}{\mathcal{N}_{E_{0}, \Delta E}} \sum_{\substack{\alpha \\ |E_{0} - E_{\alpha}| < \Delta E}} \mathcal{O}_{\alpha\alpha}, \qquad (1.26)$$

where  $E_0$  is the mean energy of the initial state,  $\Delta E$  is the half-width of an appropriately chosen energy window centered at  $E_0$ , and the normalization  $\mathcal{N}_{E_0,\Delta E}$  is the number of energy eigenstates with energies in the window  $[E_0 - \Delta E, E_0 + \Delta E]$ . Thermodynamical universality

arises in this equality in the sense that, while the left hand side depends on the details of the initial conditions through the set of coefficients  $C_{\alpha}$ , the right hand side depends only on the total energy, which is the same for many different initial conditions. Three possible scenarios that would account for this universality are [29]

- (i) Even for eigenstates close in energy, there are large eigenstate-to-eigenstate fluctuations of both the eigenstate expectation values  $\mathcal{O}_{\alpha\alpha}$  and  $|C_{\alpha}|^2$ . However, for physically interesting initial conditions, the fluctuations in the two quantities are uncorrelated. A given initial state then performs an unbiased sampling of the distribution of the eigenstate expectation values  $\mathcal{O}_{\alpha\alpha}$ , resulting in equation (1.26).
- (ii) For physically interesting initial conditions and between eigenstates that are close in energy, the eigenstate occupation numbers  $|C_{\alpha}|^2$  practically do not fluctuate at all. Again, equation (1.26) follows.
- (iii) The eigenstate expectation values  $\mathcal{O}_{\alpha\alpha}$  practically do not fluctuate at all between eigenstates that are close in energy. In that case equation (1.26) holds for *all* initial states narrow in energy.

In [3] and [4], Deutsch and Srednicki independently proposed the last scenario to be the one responsible for thermalization in quantum mechanical systems, what we now know as the Eigenstate Thermalization Hypothesis. The hypothesis can be summarized by the following ansatz.

$$\langle m|\mathcal{O}|n\rangle = \mathcal{O}(\bar{E})\delta_{mn} + e^{-S(\bar{E})/2}f_{\mathcal{O}}(\bar{E},\omega)R_{mn},$$
 (1.27)

Here  $\mathcal{O}(\bar{E})$  is a smooth function of the average energy  $\bar{E} = \frac{E_m + E_n}{2}$  that coincides with the microcanonical expectation value at energy  $\bar{E}$ , and  $f_{\mathcal{O}}(\bar{E},\omega)$  is a smooth function of the difference,  $\omega = E_m - E_n$ , in addition to  $\bar{E}$ . The remainder function  $R_{mn}$  is a Gaussian random variable (real or complex) with zero mean and unit variance. A few comments are in order:

• The most striking feature of this ansatz is that off-diagonal matrix elements are suppressed by a large number, more precisely the thermodynamic entropy  $S(\bar{E})$ , while diagonal elements are of order one.

• In order to have thermalization of all initial states that could potentially be experimentally prepared, it seems that it is enough if ETH holds for almost all eigenstates [37]. Numerical results strongly support the proposal that there are systems where at least almost all eigenstates obey the ETH [22]. But the simpler and perhaps more physically plausible scenario is that if the ETH is true for a given system at a given temperature, then it is true there for all its eigenstates. In any case, if there were certain rare eigenstates that violate the ETH, we would need to understand what is so special about these rare eigenstates.

• When the ETH is true, the way to construct out-of-equilibrium states would be by establishing a special structure off the diagonal when  $\rho$  is written in the energy eigenbasis. This would imply a special coherence patterns between eigenstates of different energies. Quantum thermalization of an out-of-equilibrium initial state requires that the contributions of this off-diagonal coherence to local observables must vanish at long times.

Srednicki's ansatz (1.27) is similar to the RMT result in (1.19), with the crucial difference that the diagonal matrix elements are not constant but depend on the energy of the eigenstates, and that for the off-diagonal matrix elements, there is an envelope function  $f_{\mathcal{O}}(\bar{E},\omega)$  on top of the small Gaussian fluctuations. This ansatz is consistent with results obtained in the semi-classical limit of quantum systems whose classical counterpart is chaotic [3, 4, 38, 39].

The ETH ansatz reduces to the RMT prediction if one focuses on a very narrow energy window where the function  $f_{\mathcal{O}}(\bar{E},\omega)$  is constant. In single-particle diffusive systems, this scale is given by the so-called Thouless energy, which is essentially equal to Planck's constant divided by the diffusion time [22]

$$E_T = \frac{\hbar D}{L^2},\tag{1.28}$$

with D the diffusion constant and L the linear size of the system. Our previous comments imply that there is no structure in the eigenstates of ergodic Hamiltonians in an energy window narrower than the Thouless energy. As this window vanishes in the thermodynamic limit, RMT has in principle a very limited range of applicability. Note, however, that the level spacing vanishes much faster with the system size, which means that there is still an

exponentially large number of energy levels in the region where RMT applies. The ETH ansatz does not have these limitations and is believed to apply to arbitrary energies. The dependence of  $f_{\mathcal{O}}(E,\omega)$  on  $\omega$  determines the decay of nonequal-time correlation functions as well as the relaxation time following a small perturbation about equilibrium [22], and, as we will see, it also serves as a good indicator of when we have RMT behavior as  $f_{\mathcal{O}}(E,\omega)$  is structureless (constant) for  $\omega < E_T$ .

While there is no rigorous understanding of which observables satisfy ETH and which do not, it is generally expected that Eq. (1.27) holds for all physical observables, namely, observables for which statistical mechanics applies. Specifically, ETH has been numerically verified for few-body observables in a variety of lattice models, no matter whether they are local or not. By few-body observables we mean n-body observables with  $n \ll N$ , where N is the number of particles, spins, etc, in the system. This is the class of observables that can be experimentally studied in macroscopic systems.

As a last important remark, it is worth noticing that the function  $f_{\mathcal{O}}(\bar{E},\omega)$  is operatordependent and indeed specifies the dynamical properties of the observable. This becomes clear if we consider, for instance, the connected 2-point function evaluated on the energy eigenstate  $|n\rangle$ 

$$\langle n|\mathcal{O}(t)\mathcal{O}(0)|n\rangle^{(c)} := \langle n|\mathcal{O}(t)\mathcal{O}(0)|n\rangle - \langle n|\mathcal{O}(0)|n\rangle^{2} =$$

$$= \sum_{\substack{m \in \mathcal{H} \\ m \neq n}} e^{it(E_{n} - E_{m})} e^{-S\left(\frac{E_{m} + E_{n}}{2}\right)} \left| f_{\mathcal{O}}\left(\frac{E_{m} + E_{n}}{2}, E_{m} - E_{n}\right) \right|^{2} |R_{mn}|^{2}$$

$$(1.29)$$

We can now take the continuum limit, considering that the factors  $|R_{mn}|^2$  average out to 1 and replacing  $\sum_{\substack{m \in \mathcal{H} \\ m \neq n}} \mapsto \int d\omega \Omega(E_n + \omega)$ , where the density of states is given by  $\Omega(E_n + \omega) \sim e^{S(E_n + \omega)}$ . This yields

$$\langle n | \mathcal{O}(t) \mathcal{O}(0) | n \rangle^{(c)} \propto \int d\omega e^{-i\omega t} \left| f_{\mathcal{O}} \left( E_n + \frac{\omega}{2}, \omega \right) \right|^2 e^{S(E_n + \omega) - S\left(E_n + \frac{\omega}{2}\right)}$$
 (1.30)

We then conclude that the function  $f_{\mathcal{O}}$  is related to the Fourier transform of the connected two-point function. In a similar fashion, susceptibilities and linear response functions can be computed in terms of the characteristic functions appearing in the ETH ansatz (1.27) [22].

## 1.3 Towards quantum chaos

Having introduced some insights as to how quantum thermalization comes about, it is natural to ask whether something can be said about quantum chaos, if there is such a thing at all. The latter in indeed not obvious: the Schrödinger equation is a linear equation, leaving no room for chaos in the classical sense of having nonlinear dynamics. Another problem with the proper definition of the term 'quantum chaos' has its origin in the concept of phase-space trajectories, which is only meaningful in the semiclassical region. Furthermore, uncertainty relation prevents a precise determination of the initial conditions.

Generally speaking, the term quantum chaos is understood to comprise all problems concerning the quantum mechanics of classically chaotic systems, and different quantities exist to identify the crossover from the integrable to the non-integrable regime in quantum systems (level spacing distribution and level number variance, for example.) One approach to studying quantum chaos has recently gained attention which is based on the study of a particular kind four-point out-of-time order correlators (OTOCs). We now follow [27] to introduce the main features of this approach whose significance in the context of holographic systems was made clear thanks to the groundbreaking work [15].

## 1.3.1 The OTOC as a signature of quantum chaos

As we said before, classically chaotic systems are characterized by the exponential divergence

$$\left| \left\{ q^i(t), p^j(0) \right\} \right| = \left| \sum_{k=1}^N \frac{\partial q^i(t)}{\partial q^k(0)} \frac{\partial p^j(0)}{\partial p^k(0)} - \frac{\partial q^i(t)}{\partial p^k(0)} \frac{\partial p^j(0)}{\partial q^k(0)} \right| = \left| \frac{\partial q^i(t)}{\partial q^j(0)} \right| \sim e^{\lambda t}, \tag{1.31}$$

Naturally, we could attempt to generalize this by replacing the Poisson brackets with a commutator of the corresponding quantum mechanical operators, since the former is nothing but the semiclassical limit of the latter:

$$\{q^{i}(t), p^{j}(0)\} \rightarrow -\frac{i}{\hbar} [\hat{q}^{i}(t), \hat{p}^{j}(0)], \text{ as } \hbar \rightarrow 0.$$
 (1.32)

Note that the position and momentum operators act at different times, so the expression (1.32) is not trivial. This correspondence can be used to extend the concept of classical

chaos and Lyapunov exponent to quantum systems [9,40,41]. What we want to derive is a quantity that correctly captures the sensitivity of the quantum system to a change in initial conditions and reproduces the exponential growth in the limit  $\hbar \to 0$  if the system is chaotic. The simplest expression of this kind is the amplitude

$$A_{in-out} = \langle out | \left[ q^i(t), p^j(0) \right] | in \rangle, \tag{1.33}$$

where  $|in\rangle$  and  $|out\rangle$  are initial and final wave-functions of the system in consideration. However, this expression has the drawback that, due to the dependence on the specific states, the quantity (1.33) varies significantly for the same system. In order to eliminate the dependence on  $|in\rangle$  and  $|out\rangle$  we can sum over final states and average over a suitable initial ensemble, say over the thermal one

$$C(t) = \sum_{n} \sum_{out} \frac{1}{Z} e^{-\beta E_n} \langle n | \left[ q^i(t), p^j(0) \right]^{\dagger} | out \rangle \langle out | \left[ q^i(t), p^j(0) \right] | n \rangle = -\langle \left[ q^i(t), p^j(0) \right]^2 \rangle_{\beta}, \quad (1.34)$$

where  $\beta$  is the inverse temperature,  $E_n$  is the energy of the *n*-th energy level,  $Z = \sum_n e^{-\beta E_n}$  is the partition function and  $\langle \cdots \rangle_{\beta}$  denotes the averaging over the thermal ensemble.

This quantity can be generalized to an arbitrary quantum system with a large number of degrees of freedom

$$C(t) = -\langle [V(t), W(0)]^2 \rangle_{\beta},$$
 (1.35)

where V and W are Hermitian operators with vanishing one-point function  $(\langle V \rangle_{\beta} = \langle W \rangle_{\beta} = 0)$  acting on  $\mathcal{O}(1)$  degrees of freedom. We say that the system is chaotic if C(t), as defined by (1.35), grows exponentially for all possible pairs<sup>3</sup> of operators V and W. The exponent characterizing this growth is referred to as the "quantum Lyapunov exponent". The time  $t_*$  at which C(t) saturates is called the "scrambling time".

Note that in practice the correlator (1.35) should be regularized because it contains the product of operators at coincident times. A common approach to avoid this is to smear uniformly the thermal distribution between the two commutators (which amounts to smearing

<sup>&</sup>lt;sup>3</sup>In integrable systems the function C(t) can grow for some, but not all pairs of operators. See e.g. [?].

the operators in the imaginary time)

$$C(t) = -\text{tr}\left(\rho^{\frac{1}{2}}[V(t), W(0)]\rho^{\frac{1}{2}}[V(t), W(0)]\right), \tag{1.36}$$

where  $\rho = \frac{1}{Z}e^{-\beta H}$  is the density matrix (see [42] for a detailed discussion about the possible ways to smear this correlator).

Let us now expand the commutators in (1.36) and rewrite C(t) as the sum of four fourpoint correlation functions

$$C(t) = 2\operatorname{tr}\left(V(t)\rho^{\frac{1}{2}}V(t)W\rho^{\frac{1}{2}}W\right) - \operatorname{tr}\left(\rho^{\frac{1}{2}}V(t)W\rho^{\frac{1}{2}}V(t)W\right) - \operatorname{tr}\left(\rho^{\frac{1}{2}}WV(t)\rho^{\frac{1}{2}}V(t)W\right) =$$

$$= 2 \times \operatorname{TOC}(t) - \operatorname{OTOC}\left(t - \frac{i\beta}{4}\right) - \operatorname{OTOC}\left(t + \frac{i\beta}{4}\right),$$
(1.37)

with  $W \equiv W(0)$  and where we have introduced the time-ordered correlator (TOC) and outof-time ordered correlator (OTOC) given by

$$TOC(t) \equiv tr\left(V(t)\rho^{\frac{1}{2}}V(t)W\rho^{\frac{1}{2}}W\right), \quad OTOC(t) \equiv tr\left(\rho^{\frac{1}{4}}V(t)\rho^{\frac{1}{4}}W\rho^{\frac{1}{4}}V(t)\rho^{\frac{1}{4}}W\right). \quad (1.38)$$

There are two important time scales for C(t). The first one is the dissipation time  $t_d$ , at which two-point correlation functions decay exponentially:  $\langle V(t)V\rangle_{\beta} \sim \langle W(t)W\rangle_{\beta} \sim \langle V(t)W\rangle_{\beta} \sim e^{-t/t_d}$ . At this time scale both the TOC and the OTOC are approximately equal to the product of two disconnected two-point functions, so the commutator C(t) is close to zero [15]

$$TOC(t) \approx OTOC(t) \approx \langle VV \rangle_{\beta} \langle WW \rangle_{\beta} + \mathcal{O}\left(e^{-t/t_d}\right) + \mathcal{O}\left(\frac{1}{N}\right),$$
 (1.39)

where  $\langle VV \rangle_{\beta}$  denotes  $\langle V(-i\beta/2) V \rangle_{\beta} = \operatorname{tr}\left(\rho^{\frac{1}{2}}V\rho^{\frac{1}{2}}V\right)$ .

The second time scale is the scrambling time  $t_*$ , which is parametrically larger than  $t_d$ . If the system is chaotic, well after the dissipation time and well before the scrambling time, C(t) grows exponentially and the OTOC decays rapidly

$$C(t) \sim \frac{1}{N} e^{\lambda_L t}, \quad \text{OTOC}(t) \sim \langle VV \rangle_{\beta} \langle WW \rangle_{\beta} - \frac{A}{N} e^{\lambda_L t},$$
 (1.40)

where A is some numerical coefficient. At later times, C(t) is saturated and the OTOC

becomes zero. Since the TOC is approximately constant at such times, the growth of C(t) and the exponential decay of the OTOC signal the same thing: quantum chaos. In particular, by studying the temporal behavior of the OTOC, it is possible to extract the quantum Lyapunov exponent  $\lambda_L$ , which is expected to coincide with its classical version in the semiclassical limit. Let us now explore the significance of this quantum chaotic behavior and its relation to the scrambling of information.

### 1.3.2 Fast scramblers and a bound on chaos

Consider a complex quantum system with a large number of degrees of freedom N that has been originally prepared in some pure state and let this state evolve under the action of the unitary operator  $U = e^{-iH}$ . If ETH is satisfied, it is to be expected that after a long enough time the system thermalizes although its quantum state remains pure. By this time the information about the initial state of the system has been smeared throughout the system one needs to measure  $\mathcal{O}(N)$  degrees of freedom to restore it. The system is then said to be scrambled.

In a scrambled system, the information about small perturbations of a few degrees of freedom will again smear across all degrees of freedom. The time needed to return to the initial scrambled state after a small perturbation is known as *scrambling time* [43].

The original motivation for studying OTOCs was the fast scrambling conjecture, which states that the scrambling time of any system cannot be less than  $t_*^{min} \sim \beta \log N$  [43]. Interestingly, it was proved that black holes saturate the bound, making them "the fastest scramblers in nature by a wide margin" [43], triggering a fruitful activity which led to some insights regarding the implications of the fast scrambling conjecture for information cloning and the black hole information paradox [?].

The correlators introduced in the previous section are sensitive to the scrambling time. To see this, note that the OTOC can be rewritten as a two-sided correlation function in a perturbed thermofield double state

$$OTOC(t) = \left(V\left(t - \frac{i\beta}{4}\right)W\left(0\right)V\left(t + \frac{i\beta}{4}\right)W\left(\frac{i\beta}{2}\right)\right)_{\beta} = \langle\psi|W_LW_R|\psi\rangle, \tag{1.41}$$

where V and W are local Hermitian operators,  $W_L = W^{\dagger} \otimes 1$  acts on the left subsystem,  $W_R = 1 \otimes W$  acts on the right subsystem and the perturbed state is as follows

$$|\psi\rangle = V_L \left(t + \frac{i\beta}{4}\right) |TFD\rangle = \frac{1}{\sqrt{Z}} \sum_{mn} e^{-\frac{\beta}{4}(E_m + E_n)} V(t)_{nm} |m\rangle_L \otimes |n\rangle_R, \tag{1.42}$$

where the thermofield-double state is defined as  $|TFD\rangle = \frac{1}{\sqrt{Z}} \sum_n e^{-\frac{1}{2}\beta E_n} |n\rangle_L \otimes |n\rangle_R$ .

At small times the operator V affects only  $\mathcal{O}(1)$  degrees of freedom and cannot change significantly the global pattern of correlations, so the perturbed state is close to  $|TFD\rangle$ . The left and right subsystems are then highly entangled and the correlator approaches  $OTOC(t) \approx \langle VV \rangle_{\beta} \langle WW \rangle_{\beta}$ . However, as time evolves the perturbation involves other degrees of freedom and destroys the fragile pattern of correlations, which translates in a decay to zero of the OTOC. In this setting, scrambling time is simply the time at which the OTOC saturates:  $OTOC(t_*) \approx 0$  or, equivalently,  $C(t_*) \approx 2\langle VV \rangle_{\beta} \langle WW \rangle_{\beta}$ .

Of major interest here is the rate at which the OTOC approaches zero. On general grounds, one expects that in the large N limit and for small evolution times the first correction to OTOC is of the order of  $\mathcal{O}\left(\frac{1}{N}\right)$  [15]

$$\frac{\text{OTOC}(t)}{\langle VV \rangle_{\beta} \langle WW \rangle_{\beta}} = 1 - \frac{A}{N} f(t) + \mathcal{O}\left(\frac{1}{N^2}\right), \tag{1.43}$$

where A is some positive  $\mathcal{O}(1)$  number and f(t) is some monotonically growing function. Extending this approximation to large times, one can qualitatively estimate the scrambling time as  $t_* \sim f^{-1}(N/A)$ , where  $f^{-1}$  is the inverse of f,  $f \circ f^{-1} = f^{-1} \circ f = 1$ . At the same time, the fast scrambling conjecture states that  $t_* \gtrsim \beta \log N$ . Therefore, the function f cannot grow faster than exponentially in time,  $f(t) \lesssim e^{\lambda_L t}$ . The exponent of this growth is also bounded,  $\lambda_L \leq \frac{B}{\beta}$ , where B is a universal positive  $\mathcal{O}(1)$  numerical constant. This analog of the fast scrambling conjecture for OTOCs was proven in [15], yielding the widely studied "bound on chaos":

$$\frac{d}{dt} \Big[ \langle VV \rangle_{\beta} \langle WW \rangle_{\beta} - \text{OTOC}(t) \Big] \le \frac{2\pi}{\beta} \Big[ \langle VV \rangle_{\beta} \langle WW \rangle_{\beta} - \text{OTOC}(t) \Big], \quad \text{i.e.} \quad \lambda_L \le \frac{2\pi}{\beta}. \quad (1.44)$$

## 1.4 The Sachdev-Ye-Kitaev model

It was shown in [15] that black holes saturate the aforementioned bound on chaos. Another example of a maximally chaotic system was later found by Kitaev which provided what has proved to be a very useful ground (as it solvable in the large N limit) to test and understand the main features of maximally chaotic systems and their connections to black hole dynamics: the Sachdev-Ye-Kitaev [9] model. In this section we summarize some of the main properties of this model that are relevant for our analysis, leaving further details for our discussions in the coming Chapters.

We work mainly with the Majorana version of the model, to be introduced shortly and reviewed in more detail, for example in [27,28,44]. However, as will become clear, our results apply equally to the complex 'Dirac' model [10] that we will introduce later on. Without further ado, here is the Hamiltonian of the Majorana fermion SYK model generalized to q-body interactions,

$$H = i^{q/2} \sum_{i_1 < i_2 < \dots < i_q \le N} J_{i_1 \dots i_q} \psi_{i_1} \psi_{i_2} \dots \psi_{i_q}.$$
 (1.45)

We will mostly focus our attention on the disorder-averaged theory, where the couplings  $J_{i_1...i_q}$  are averaged over a Gaussian random ensemble, with vanishing mean coupling and variance  $\overline{J_{i_1...i_q}^2} = J^2(q-1)!/N^{q-1}$ . For clarity, we will work for now with the q=4 version of the model, which was the focus of the foundational works  $[9,11]^4$ . The corresponding action is given by

$$I_{SYK} = \int d\tau \left[ \frac{1}{2} \sum_{i=1}^{N} \psi_i(\tau) \dot{\psi}_i(\tau) - \frac{1}{4!} \sum_{i,j,k,l=1}^{N} J_{ijkl} \, \psi_i(\tau) \psi_j(\tau) \psi_k(\tau) \psi_l(\tau) \right], \tag{1.46}$$

where we have included the kinetic term, in which  $\dot{\psi}_i = \partial \psi_i / \partial \tau$ . The fermions furnish a representation of the Clifford algebra

$$\{\psi_i, \psi_j\} = \delta_{ij}, \quad i, j = 1, ..., N,$$
 (1.47)

 $<sup>^4</sup>$ Some simplifications occur in the large q limit. We will consider this important case in the relevant sections in later Chapters.

where  $\{.,.\}$  is the usual anticommutator. In this case, we can build a Hermitian  $(\psi_i = \psi_i^{\dagger})$  representation of the algebra by introducing a new, complex basis

$$c_i = \frac{1}{\sqrt{2}}(\psi_{2i} - i\psi_{2i+1}), \quad c_i^{\dagger} = \frac{1}{\sqrt{2}}(\psi_{2i} + i\psi_{2i+1}), \quad i = 1, ..., K,$$
 (1.48)

which satisfies

$$\{c_i, c_j\} = \{c_i^{\dagger}, c_j^{\dagger}\} = 0, \quad \{c_i, c_j^{\dagger}\} = \delta_{ij}.$$
 (1.49)

Note that in this case we have N=2K even. We recognize the familiar canonical anticommutation relations for fermionic modes, which are thus equivalent to the Clifford algebra relation (1.47). The use of creation and annihilation operators clarifies how to build the representation: we pick a vacuum annihilated by all the modes  $c_i|0\rangle = 0$ , and construct the basis of the representation as

$$(c_1^{\dagger})^{n_1}...(c_K^{\dagger})^{n_K}|0\rangle, \quad n_k = 0, 1.$$
 (1.50)

There are  $2^K = 2^{\frac{N}{2}}$  such states, corresponding to whether or not a given mode is occupied by a fermion. One can also give an explicit recursion relation for the representation matrices [28]:

$$\psi_{i}^{(K)} = \psi_{i}^{(K-1)} \otimes \begin{pmatrix} -1 & 0 \\ 0 & 1 \end{pmatrix}, \quad i = 1, ..., N - 2, 
\psi_{N-1}^{(K)} = \frac{1}{\sqrt{2}} I_{2^{K-1}} \otimes \begin{pmatrix} 0 & 1 \\ 1 & 0 \end{pmatrix}, 
\psi_{N}^{(K)} = \frac{1}{\sqrt{2}} I_{2^{K-1}} \otimes \begin{pmatrix} 0 & -i \\ i & 0 \end{pmatrix},$$
(1.51)

where the superscript indicates the dimension N=2K, and  $I_d$  is the d-dimensional identity matrix. It is clear that  $\psi_i^{(K)}$  are  $2^K \times 2^K$  matrices if we start the recursion with  $2 \times 2$  matrices. These initial matrices are given by

$$\psi_1^{(1)} = \frac{1}{\sqrt{2}} \begin{pmatrix} 0 & -i \\ i & 0 \end{pmatrix}, \quad \psi_2^{(1)} = \frac{1}{\sqrt{2}} \begin{pmatrix} 0 & 1 \\ 1 & 0 \end{pmatrix}. \tag{1.52}$$

Let us turn our attention to the integration interva in (1.46). Here  $\tau$  denotes Euclidean time, for which we will usually consider two intervals: the Euclidean line (zero temperature quantum-mechanics):  $\tau_{\text{line}} \in (-\infty, \infty)$ , and the Euclidean circle (thermal state of temperature  $T = \frac{1}{\beta}$ ):  $\tau_{\text{circle}} \in \left[\frac{\beta}{2}, \frac{\beta}{2}\right)$ ,  $\tau + \beta \sim \tau$ . We can use the following real and monotonic function to build a map between the two

$$\tau_{line} = \tan \frac{\pi \tau_{circle}}{\beta}.$$
 (1.53)

As for the coupling constants, antisymmetry of the fermions and Hermiticity of the Hamiltonian impose the constraints

$$J_{ijkl} = -J_{jikl}, \quad J_{ijkl} = -J_{ijlk}, \quad J_{ijkl} = J_{klij}^{\star}. \tag{1.54}$$

The remaining independent coupling constants in  $J_{ijkl}$  are drawn from a Gaussian distribution with zero mean. The variance

$$\overline{\left|J_{ijkl}\right|^2} = \frac{3!J^2}{N^3}$$
 (1.55)

sets the average strength of the coupling, which has to scale with the number of sites N as shown to ensure a well-behaved large-N limit.

These properties allow to simplify expressions involving products of the couplings. There is a Wick-type decomposition for the average of even number of couplings. For instance

$$\overline{J_{i_1 i_2 i_3 i_4} J_{j_1 j_2 j_3 j_4} J_{k_1 k_2 k_3 k_4} J_{l_1 l_2 l_3 l_4}} = \overline{J_{i_1 i_2 i_3 i_4} J_{j_1 j_2 j_3 j_4}} \overline{J_{k_1 k_2 k_3 k_4} J_{l_1 l_2 l_3 l_4}} 
+ \overline{J_{i_1 i_2 i_3 i_4} J_{k_1 k_2 k_3 k_4}} \overline{J_{j_1 j_2 j_3 j_4} J_{l_1 l_2 l_3 l_4}} 
+ \overline{J_{i_1 i_2 i_3 i_4} J_{l_1 l_2 l_3 l_4} J_{j_1 j_2 j_3 j_4} J_{k_1 k_2 k_3 k_4}},$$
(1.56)

and the disorder average of two arbitrary couplings is in turn given by

$$\overline{J_{i_1 i_2 i_3 i_4} J_{j_1 j_2 j_3 j_4}} = \frac{3! J^2}{N^3} \sum_{\sigma} \operatorname{sgn} \sigma \delta_{i_1 \sigma(j_1)} \delta_{i_2 \sigma(j_2)} \delta_{i_3 \sigma(j_3)} \delta_{i_4 \sigma(j_4)},$$
(1.57)

which implies

$$\sum_{k,l,m=1}^{N} \overline{J_{iklm} J_{jklm}} = \frac{3!J^2}{N^3} \sum_{k,l,m=1}^{N} \delta_{ij} \delta_{kk} \delta_{ll} \delta_{mm} + \dots = \frac{3!J^2}{N^3} \left( N^3 \delta_{ij} + \mathcal{O}(N^2) \right) = 3!J^2 \delta_{ij} + \mathcal{O}\left(\frac{1}{N}\right). \tag{1.58}$$

Note also that, since in the free theory the Hamiltonian is zero, operators are constant in the Heisenberg picture. Using this fact we can compute the Green functions

$$G^{\text{free}}(\tau) = \frac{1}{N} \sum_{i=1}^{N} \langle 0 | \mathcal{T} \psi_i(\tau) \psi_j(0) | 0 \rangle = \frac{1}{N} \sum_{i=1}^{N} (\theta(\tau) \langle 0 | \psi_i \psi_j | 0 \rangle - \theta(-\tau) \langle 0 | \psi_j \psi_i | 0 \rangle)$$
$$= \frac{1}{2} \operatorname{sgn} \tau \delta_{ij}, \tag{1.59}$$

and

$$G_{\beta}^{\text{free}}(\tau) = \frac{1}{N} \sum_{i=1}^{N} \langle \mathcal{T} \psi_i(\tau) \psi_j(0) \rangle_{\beta} = \frac{1}{2} \operatorname{sgn} \left( \sin \frac{\pi \tau}{\beta} \right) \delta_{ij}. \tag{1.60}$$

where  $\mathcal{T}$  denotes time ordering,  $\theta(\tau)$  is the Heaviside function,  $|0\rangle$  denotes the vacuum state in the free theory, and  $\langle \cdots \rangle_{\beta}$  denotes the averaging over the thermal distribution

$$\langle \cdots \rangle_{\beta} \equiv \frac{\operatorname{tr}\left[e^{-\beta H} \cdots\right]}{\operatorname{tr}\left[e^{-\beta H}\right]}.$$
 (1.61)

Let us now turn on the interaction term to calculate disorder-averaged loop corrections to the free propagators. The evolution operator in Lorentzian time is given by

$$U(t_1, t_2) \equiv \mathcal{T}\exp\left[-i\int_{t_2}^{t_1} dt H(t)\right] = 1 - i\int_{t_2}^{t_1} dt H(t) - \int_{t_2}^{t_1} dt \int_{t_2}^{t} dt' H(t) H(t') + \cdots, \quad (1.62)$$

from where we have

$$G(t)\delta_{ab} = \left\langle \mathcal{T} \left[ \psi_{a}(t)\psi_{b}(0) - \frac{i}{4!} \sum_{i,j,k,l} \overline{J_{ijkl}} \int_{-\infty}^{+\infty} dt' \psi_{a}(t)\psi_{b}(0)\psi'_{i}\psi'_{j}\psi'_{k}\psi'_{l} - \frac{1}{2} \frac{1}{(4!)^{2}} \sum_{i,j,k,l,p,q,r,s} \overline{J_{ijkl}J_{pqrs}} \int_{-\infty}^{+\infty} dt' \int_{-\infty}^{+\infty} dt'' \psi_{a}(t)\psi_{b}(0)\psi'_{i}\psi'_{j}\psi'_{k}\psi'_{l}\psi''_{p}\psi''_{q}\psi''_{r}\psi''_{s} + \mathcal{O}(J^{3}) \right] \right\rangle,$$

$$(1.63)$$

with  $\psi_i' \equiv \psi_i(t')$  and  $\psi_i'' \equiv \psi_i(t'')$ .

Now one sees that the rules (1.56) and (1.57) single out the nontrivial contributions. The disconnected part of the averages factorizes, and odd orders in  $J_{ijkl}$  die out after the disorder

averaging. The connected part of (1.63) thus reduces to

$$G(t) - G^{\text{free}}(t) = \frac{2 \cdot 4 \cdot 4!}{2(4!)^2} \frac{1}{N} \sum_{i,k,m,n} \overline{J_{ikmn} J_{jkmn}} \delta_{ij} \int dt' dt'' G^{\text{free}}(t - t') G^{\text{free}}(t' - t'')^3 G^{\text{free}}(t'') + \mathcal{O}(J^4)$$

$$= J^2 \int dt' dt'' G^{\text{free}}(t - t') G(t' - t'')^3 G(t'') + \mathcal{O}\left(\frac{J^2}{N}\right) + \mathcal{O}(J^4).$$
(1.64)

where in the last line we have used (1.58) to identify the leading contribution.

Using Wick's theorem and the relation (1.57) one can write down higher order corrections that correspond to higher-order diagrams. We switch back to Euclidean time and follow [28]<sup>5</sup> to summarize the perturbative procedure:

• For each realization of the model, there is a four leg vertex

$$\frac{l}{i}$$
  $\frac{k}{j}$ 

proportional to  $J_{ijkl}$ .

• We calculate Feynman diagrams in each realization of the model. Then we average the diagram over disorder. Each diagram will contain a number of  $J_{ijkl}$  and since the distribution is Gaussian, we evaluate these expectation values using Wick's theorem and the two point expectation value

$$\overline{J_{i_1j_1k_1l_1}J_{i_2j_2k_2l_2}} = 3! \frac{J^2}{N^3} \delta_{i_1i_2} \delta_{j_1j_2} \delta_{k_1k_2} \delta_{l_1l_2}$$
(1.65)

• The first contribution to the two point function is the tadpole. However, since it is linear in  $J_{ijkl}$ , this contribution vanishes:

$$\left\langle \frac{Q_k}{i} \right\rangle_J \sim \overline{J_{ijkl}} = 0$$

• The next diagram is the melon (or settling sun)

<sup>&</sup>lt;sup>5</sup>We thank Sárosi for giving us his permission to partially reproduce here the diagrams and the text accompanying them.

$$\left\langle \begin{array}{c} \\ \hline \\ \\ J \end{array} \right\rangle_{J} = \frac{l_{1}}{l_{2}} \underbrace{\begin{pmatrix} i \\ j \\ k \end{pmatrix}}^{l_{2}} = 3! \frac{J^{2}}{N^{3}} G_{ii}^{\text{free}} G_{jj}^{\text{free}} G_{kk}^{\text{free}} \delta_{l_{1}l_{2}} = 3! J^{2} (G^{\text{free}})^{3} \delta_{l_{1}l_{2}}$$

where the dashed line denotes the disorder pairing with (1.65), and doubled indices are summed over. Note that the result does not scale with N.

• There are multiple order  $J^4$  diagrams, with multiple pairings. For illustration, let us check one diagram with two different types of pairings. When the pairing happens inside the melon, we get

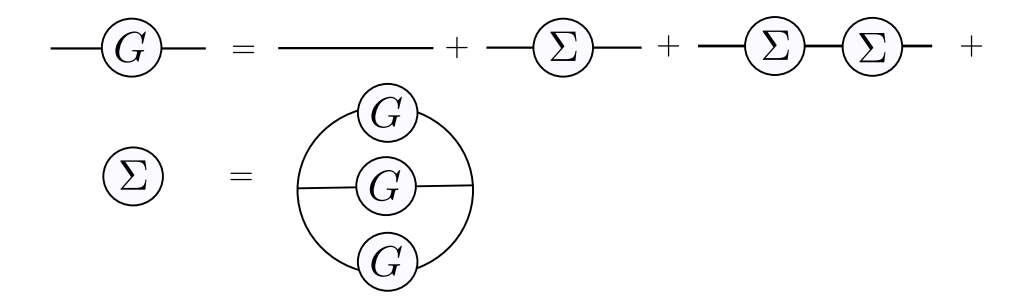
$$\frac{l_{1} - l_{1}}{k_{3}} = \frac{J^{4}}{N^{6}} (G_{ll}^{\text{free}})^{5} G_{l_{1}l_{3}}^{\text{free}} G_{l_{1}l_{3}}^{\text{free}} \delta_{k_{3}k_{4}} = \frac{1}{2} J^{4} (G^{\text{free}})^{6} \delta_{k_{3}k_{4}}$$

where we have used that  $G_{l_1l_3}^{\text{free}}G_{l_1l_3}^{\text{free}} = \frac{1}{2}NG^{\text{free}}$ , because of (??). This again does not scale with N. The other pairing is

We see that this is suppressed as  $N^{-2}$  compared to the previous nonzero diagrams.

This last lesson is a general one: the only diagrams that are not suppressed by some power of  $N^{-1}$  are the ones when the disorder average pairs vertices inside a single melon. Therefore, the two point function has an iterated structure

All this can be summarized in the following closed set of consistency equations [28]



where  $\Sigma$  is the self energy and is defined to contain all the iterated melon diagrams.

Using the following notation for the bilinear kernels

$$(AB)(\tau,\tau') = \int d\tau'' A(\tau,\tau'') B(\tau'',\tau'), \tag{1.66}$$

the first of this pictorial equations reads

$$G = G^{\text{free}} + G^{\text{free}} \Sigma G^{\text{free}} + G^{\text{free}} \Sigma G^{\text{free}} \Sigma G^{\text{free}} + \cdots$$

$$= G^{\text{free}} \left[ 1 + \Sigma G^{\text{free}} + \Sigma G^{\text{free}} \Sigma G^{\text{free}} + \cdots \right]$$

$$= G^{\text{free}} \left[ 1 - \Sigma G^{\text{free}} \right]^{-1}$$

$$= \left[ (G^{\text{free}})^{-1} - \Sigma \right]^{-1},$$

$$(1.67)$$

where the third line is obtained after resumming the geometric series. The inverse of the free propagator is just the kernel in the bilinear kinetic term in the action

$$(G^{\text{free}})^{-1}(\tau, \tau') = \delta(\tau - \tau')\partial_{\tau'}, \tag{1.68}$$

so we can use the shorthand notation

$$G = \left[\partial_{\tau} - \Sigma\right]^{-1}.\tag{1.69}$$

The second pictorial equation is just

$$\Sigma(\tau, \tau') = J^2 [G(\tau, \tau')]^3. \tag{1.70}$$

,

In summary, to leading order in 1/N, the two point function is given by solving a set of integral equations (the Schwinger-Dyson equations). For general q, only the second equation changes, and we have [11]

$$G = \left[\partial_{\tau} - \Sigma\right]^{-1},$$

$$\Sigma(\tau, \tau') = J^{2} \left[G(\tau, \tau')\right]^{q-1}.$$
(1.71)

While our sketch of the computation has been done in the limit  $\beta \to \infty$ , the results can be easily generalized to the finite-temperature case, because the averaging over the disorder does not depend on the temperature and always singles out melonic diagrams.

### 1.4.1 Schwinger-Dyson equation and the IR limit

Let us now study the IR limit of our Schwinger Dyson equations

$$G(\tau_{1}, \tau_{2}) = G^{\text{free}}(\tau_{1}, \tau_{2}) + \int d\tau_{3} d\tau_{4} G^{\text{free}}(\tau_{1}, \tau_{3}) \Sigma(\tau_{3}, \tau_{4}) G(\tau_{4}, \tau_{2}),$$

$$\Sigma(\tau_{1}, \tau_{2}) \equiv J^{2} G(\tau_{1}, \tau_{2})^{3}.$$
(1.72)

Due to translational invariance, the exact propagator depends on the time difference  $G(\tau_1, \tau_2) = G(\tau_1 - \tau_2)$ ,  $\Sigma(\tau_1, \tau_2) = \Sigma(\tau_1 - \tau_2)$  and we can Fourier-transform equation (1.72) to obtain

$$G^{-1}(\omega) = -i\omega - \Sigma(\omega), \tag{1.73}$$

where we used the explicit form of the tree-level propagator:

$$G^{\text{free}}(\omega) \equiv \int_{-\infty}^{\infty} d\tau e^{i\omega\tau} \frac{1}{2} \operatorname{sgn}\tau = \frac{i}{\omega + i0}, \quad \text{i.e.} \quad \frac{1}{G^{\text{free}}(\omega)} = -i\omega.$$
 (1.74)

Equation (1.72) can be treated analytically in the limits of low frequency,  $\omega \ll J$  (i.e.  $J\tau \gg 1$ ), and strong coupling,  $\beta J \gg 1$ . Consider for now the zero-temperature case  $\beta = \infty$ . On dimensional grounds, we expect that in the limit under consideration the exact propagator decays as  $G(\tau) \sim \tau^{-\frac{1}{2}}$ . Hence, the left-hand side of the equation (1.72) is negligible and the equation reduces to the following form

$$0 = G^{\text{free}}(\tau_1, \tau_2) + \int_{-\infty}^{\infty} d\tau_3 \int_{-\infty}^{\infty} d\tau_4 G^{\text{free}}(\tau_1, \tau_3) \Sigma(\tau_3, \tau_4) G(\tau_4, \tau_2), \tag{1.75}$$

from where it follows

$$\int d\tau \Sigma(\tau_1, \tau) G(\tau, \tau_2) = -\delta(\tau_1 - \tau_2). \tag{1.76}$$

To obtain the second identity we have differentiated (1.75) over  $\tau_1$ , then took the integral over  $\tau_3$  and used the differential equation which  $G^{\text{free}}(\tau_1 - \tau_2)$  does obey. Clearly, the same equation arises when one drops the inverse tree-level propagator in (1.73)

$$G^{-1}(\omega) \approx -\Sigma(\omega), \quad \text{or} \quad \Sigma(\omega)G(\omega) \approx -1,$$
 (1.77)

which is nothing else than the Fourier transformation of the equation (1.76). Note that in the limit in question the DS equation (1.75) is invariant under reparametrizations of time,  $\tau \to f(\tau)$ ,  $f'(\tau) > 0$ 

$$G(\tau_{1}, \tau_{2}) \to G[f(\tau_{1}), f(\tau_{2})] f'(\tau_{1})^{\Delta} f'(\tau_{2})^{\Delta},$$
  

$$\Sigma(\tau_{1}, \tau_{2}) \to \Sigma[f(\tau_{1}), f(\tau_{2})] f'(\tau_{1})^{3\Delta} f'(\tau_{2})^{3\Delta},$$
(1.78)

with  $\Delta = \frac{1}{q} = \frac{1}{4}$ . This can be checked explicitly

$$\int df(\tau) \Sigma \left[ f(\tau'), f(\tau) \right] G \left[ f(\tau), f(\tau'') \right] = \frac{\int d\tau \Sigma(\tau', \tau) G(\tau, \tau'')}{f'(\tau')^{\frac{1}{4}} f'(\tau'')^{\frac{3}{4}}} = \frac{-\delta(\tau' - \tau'')}{f'(\tau')} = -\delta \left[ f(\tau') - f(\tau'') \right], \tag{1.79}$$

We then conclude that, in the IR limit, fermions acquire an anomalous conformal dimension  $\Delta = \frac{1}{q} = \frac{1}{4}$ , which hints at the following ansatz to solve the SD equation

$$G_c(\tau_1, \tau_2) = B \frac{\operatorname{sgn} \tau_{12}}{|J\tau_{12}|^{2\Delta}},$$
 (1.80)

where  $\tau_{12} \equiv \tau_1 - \tau_2$  and B is some numerical constant to be determined. The subscript "c" stands for "conformal". Using the following identity

$$\int_{-\infty}^{\infty} d\tau e^{i\omega\tau} \frac{\operatorname{sgn}\tau}{|\tau|^{2D}} = 2i\Gamma(1 - 2D)\cos(\pi D)|\omega|^{2D - 1}\operatorname{sgn}\omega, \tag{1.81}$$

we can confirm that our ansatz does solve the equation (1.75), and find the numerical factor B

$$G_c(\tau) = \frac{1}{(4\pi)^{\frac{1}{4}}} \frac{\operatorname{sgn}\tau}{|J\tau|^{2\Delta}}.$$
 (1.82)

Note that this solution decays as  $J(\tau_1 - \tau_2) \to \infty$ , which confirms the self-consistency of the approximation in which the equation (1.75) was obtained.

Finally, reparametrization invariance (1.78) allows one to find the finite-temperature exact propagator by means of the map (1.53), which does satisfy the condition  $f'(\tau) > 0$ 

$$G_c^{\beta}(\tau) = \frac{\pi^{\frac{1}{4}}}{\sqrt{2\beta J}} \frac{\operatorname{sgn}\left(\sin\frac{\pi\tau}{\beta}\right)}{|\sin\frac{\pi\tau}{\beta}|^{2\Delta}}, \quad \tau \in \left[-\frac{\beta}{2}, \frac{\beta}{2}\right). \tag{1.83}$$

Note that in the limit  $\tau \ll \beta$  expressions (1.82) and (1.83) coincide.

We remind that  $G_c(\tau)$  and  $G_c^{\beta}(\tau)$  are approximately equal to the exact propagators  $G(\tau)$  and  $G^{\beta}(\tau)$  only for relatively large times  $\tau \gg 1/J$ . At the same time, in the UV limit  $(\tau \ll 1/J)$  exact propagators are approximately equal to the bare ones,  $G_0(\tau)^6$  and  $G_0^{\beta}(\tau)$  correspondingly. In the intermediate region  $G(\tau)$  and  $G^{\beta}(\tau)$  interpolate between these functions.

After the analytic continuation of (1.83) to the Lorentzian time  $t = -i\tau$  one obtains the following two-point function:

$$G_c^{\beta}(t) = \frac{(\pi)^{\frac{1}{4}}}{\sqrt{2\beta J}} \frac{1}{|\sinh\frac{\pi t}{\beta}|^{2\Delta}} \propto e^{-\frac{2\pi\Delta}{\beta}t}, \quad \text{as} \quad t \gg \frac{1}{J}.$$
 (1.84)

This function becomes exponentially small after the time  $t_d = \frac{\beta}{2\pi\Delta} \sim \beta$ , which is usually called as dissipation time.

### The effective action

An analysis of the conformally invariant and non-invariant contributions can be done at the level of the effective action. The partition function associated to the SYK Hamiltonian is

<sup>&</sup>lt;sup>6</sup>We use the notations  $G_0$  and  $G^{\text{free}}$  interchangeably

written as a path integral

$$Z(J_{ijkl}) = \int D\psi_i \exp\left(-\int d\tau \left[\frac{1}{2}\sum_i \psi_i \partial_\tau \psi_i + \sum_{1 \le i < j < k < l \le N} J_{ijkl} \psi_i \psi_j \psi_k \psi_l\right]\right). \tag{1.85}$$

Now we want to realize the average over the disorder ensemble for  $J_{ijkl}$ . We will do the so-called annealed average, in which J is treated as a microscopic degree of freedom<sup>7</sup>

Averaging over the couplings means computing

$$\overline{Z} \sim \int dJ_{ijkl} \exp\left(-\sum_{1 \le i < j < k < l \le N} \frac{J_{ijkl}^2}{2\frac{3!J^2}{N^3}}\right) Z(J_{ijkl}). \tag{1.86}$$

The integral can be performed easily as in (1.85) the coupling appears linearly

$$\overline{Z} \sim \int D\psi_i \exp\left(-\int d\tau \frac{1}{2} \sum_i \psi_i \partial_\tau \psi_i + \sum_{1 \le i \le k \le l \le N} \frac{3J^2}{N^3} \int \int d\tau d\tau' (\psi_i \psi_j \psi_k \psi_l)(\tau) (\psi_i \psi_j \psi_k \psi_l)(\tau')\right).$$
(1.87)

Now we can write the sums in an alternative way:  $\sum_{1 \leq i < j < k < l \leq N} = \frac{1}{4!} \sum_{i \neq j \neq k \neq l}$ . Using this and the fact that in the path integral the Grassmannian variables satisfy  $\psi_i(\tau)^2 = 0$ , we can decouple the sums

$$\sum_{1 \le i < j < k < l \le N} (\psi_i \psi_j \psi_k \psi_l)(\tau)(\psi_i \psi_j \psi_k \psi_l)(\tau') = \frac{1}{4!} \left[ \sum_i \psi_i(\tau) \psi_i(\tau') \right]^4. \tag{1.88}$$

The next step is to insert into the path integral the following identity

$$1 = \int DG\delta(NG(\tau, \tau') - \sum_{i} \psi_{i}(\tau)\psi_{i}(\tau'))$$

$$\sim \int DGD\Sigma \exp\left(-\frac{N}{2} \int \int d\tau d\tau' \Sigma (G - \frac{1}{N} \sum_{i} \psi_{i}\psi_{i})\right). \tag{1.89}$$

The field G is just the fermion bilinear, while  $\Sigma$  is a Lagrange multiplier enforcing the delta

<sup>&</sup>lt;sup>7</sup>There is another, quenched average which one could perform but in this case it leads to the same results [10]. In this approach one averages the free energy and uses the replica trick to obtain the partition function:  $\log Z = \lim_{n\to 0} \partial_n Z^n$ , and then analytically continues to non-integer n

constraint. In this way we can write

$$\overline{Z} \sim \int D\psi_i DGD\Sigma \exp\left(-\int \frac{1}{2} \sum_i \psi_i \partial_\tau \psi_i - \frac{1}{2} \int \int N\Sigma (G - \frac{1}{N} \sum_i \psi_i \psi_i)\right) + \frac{J^2 N}{2 \cdot 4} \int \int G^4 .$$
(1.90)

The goal of this computation was to obtain an exponential that is bilinear in the fermion variables  $\psi_i$ , so that we can do the Gaussian Berezin integral

$$\overline{Z} \sim \int DGD\Sigma \left[ \det(\partial_{\tau} - \Sigma) \right]^{\frac{N}{2}} \exp\left( -\frac{N}{2} \int \int \left( \Sigma G - \frac{1}{4} J^{2} G^{4} \right) \right) 
= \int DGD\Sigma e^{-NI[G,\Sigma]},$$
(1.91)

with

$$I[G,\Sigma] = -\frac{1}{2}\log\det(\partial_{\tau} - \Sigma) + \frac{1}{2}\int\int\left(\Sigma G - \frac{1}{4}J^{2}G^{4}\right). \tag{1.92}$$

Crucially, an N factor appears in front of the action in the second line of (1.91), implying that the large N limit is a classical one. For the generalized model with q-body interactions, this action takes the form

$$I[G, \Sigma] = -\frac{1}{2}\log\det(\partial_{\tau} - \Sigma) + \frac{1}{2}\int\int\left(\Sigma G - \frac{1}{q}J^{2}G^{q}\right). \tag{1.93}$$

The classical equations of motion can be derived by looking for extrema of this action. It is easy to show that these are identical to the Schwinger-Dyson equations (1.71).

## 1.4.2 Schwarzian theory

The presence of the inverse tree-level propagator in (1.72) breaks the reparametrization invariance of the SD equation (1.78). This breaking deserves some careful attention, and for that it is convenient to make the change  $\Sigma \to \Sigma - G_0^{-1}$  in the effective action and separate the conformally-invariant and non-invariant parts  $I_{\text{eff}} = I_{CFT} + I_S$ :

$$\frac{I_{CFT}}{N} = -\frac{1}{2}\log\det\left(-\Sigma(\tau,\tau')\right) + \frac{1}{2}\int d\tau d\tau' \left(\Sigma(\tau,\tau')G(\tau,\tau') - \frac{J^2}{4}G(\tau,\tau')^4\right),\tag{1.94}$$

$$\frac{I_S}{N} = -\frac{1}{2} \int d\tau d\tau' G_0^{-1}(\tau, \tau') G(\tau, \tau'). \tag{1.95}$$

From here we can see that the conformal part  $I_{CFT}$  reproduces the SD equation (1.75) or (1.77), which is invariant with respect to reparametrizations  $\tau \to f(\tau)$ ,  $f'(\tau) > 0$ . Note that the delta-function in  $G_0^{-1}(\tau, \tau')$  picks up small time differences  $|\tau - \tau'| \ll J^{-1}$  and can be neglected in the IR limit. Hence, conformal invariance emerges in the deep IR limit and is broken as one moves away from it.

To study the effect of the non-invariant part of the effective action, let us to move away from the IR limit and estimate how the action (1.95) changes under the conformal transformations (1.78). Consider first the zero temperature case ( $\beta = \infty$ ). First we expand

$$G_c(\tau_1, \tau_2) \to G_c[f(\tau_1), f(\tau_2)] \approx \frac{\operatorname{sgn}(\tau_1 - \tau_2)}{(4\pi)^{\frac{1}{4}} J^{2\Delta}} \frac{f'(\tau_1)^{\Delta} f'(\tau_2)^{\Delta}}{|f(\tau_1) - f(\tau_2)|^{2\Delta}},$$
 (1.96)

near  $\tau = \frac{\tau_1 + \tau_2}{2}$  in powers of  $\tau_{12} = \tau_1 - \tau_2$  (the delta-function from  $G_0^{-1}(\tau_1, \tau_2)$  in (1.95) selects values around  $\tau_{12} \approx 0$ )

$$G(\tau_1, \tau_2) = G_c(\tau_1, \tau_2) \left( 1 + \frac{\Delta}{6} \tau_{12}^2 \operatorname{Sch} \left[ f(\tau), \tau \right] + \mathcal{O}(\tau_{12}^3) \right), \tag{1.97}$$

where  $Sch(f(\tau),\tau) \equiv \frac{f'''}{f'} - \frac{3}{2} \left(\frac{f''}{f'}\right)^2$  is the Schwarzian derivative. Plugging this into the action (1.95) leads to

$$\frac{I_S}{N} = -\frac{1}{2} \langle G_0^{-1} | \delta G \rangle = -\frac{1}{2} \int d\tau d\tau_{12} G_0^{-1}(\tau_{12}) \tilde{G}(\tau_{12}) \left[ \frac{\Delta}{6} \tau_{12}^2 \operatorname{Sch} \left[ f(\tau), \tau \right] + \mathcal{O}(\tau_{12}^3) \right] \approx 
\approx -\frac{\Delta}{12} \int d\tau_{12} \delta(\tau_{12}) \partial_{\tau_{12}} \left( \tau_{12}^2 \tilde{G}(\tau_{12}) \right) \int d\tau \operatorname{Sch} \left[ f(\tau), \tau \right] = 
= -\frac{1}{J} \underbrace{\frac{\Delta}{12} \int d\eta \delta(\eta) \partial_{\eta} \left( \eta^2 \tilde{G}(\eta) \right)}_{G} \int d\tau \operatorname{Sch} \left[ f(\tau), \tau \right] , \tag{1.98}$$

where we have made a change to the dimensionless variable  $\eta = J\tau_{12}$ . It was shown in [101] that  $C \approx 0.48 \times \frac{\Delta}{12} > 0$ . In summary, for the zero-temperature theory we obtain

$$\frac{I_S}{N} \approx -\frac{C}{I} \int_{-\infty}^{\infty} \operatorname{Sch}\left[f(\tau), \tau\right] d\tau. \tag{1.99}$$

The finite-temperature version of (1.99) can be obtained using the map (1.53):

$$\frac{I_S}{N} = -\frac{C}{J} \int_{-\frac{\beta}{2}}^{\frac{\beta}{2}} \operatorname{Sch}\left[\tan\frac{\pi\varphi(\tau)}{\beta}, \tau\right] d\tau. \tag{1.100}$$

In this case the saddle point values of the effective action are parametrized by the function  $\varphi(\tau)$ , which maps the time circle to itself and preserves its orientation.

### 1.4.3 Four-point functions and the OTOC

Let us consider the following four-point correlation function

$$\frac{1}{N^{2}} \sum_{i,j=1}^{N} \langle \mathcal{T}\psi_{i}(\tau_{1})\psi_{i}(\tau_{2})\psi_{j}(\tau_{3})\psi_{j}(\tau_{4}) \rangle = 
= \frac{1}{Z} \int \mathcal{D}G\mathcal{D}\Sigma \left[ G(\tau_{1},\tau_{2})G(\tau_{3},\tau_{4}) + \frac{1}{N} \left( G(\tau_{1},\tau_{4})G(\tau_{2},\tau_{3}) - G(\tau_{1},\tau_{3})G(\tau_{2},\tau_{4}) \right) \right] e^{-I_{\text{eff}}[G,\Sigma]},$$
(1.101)

where we have used the approach we took when deriving the effective action to go from the functional integrals over  $\mathcal{D}\psi_i$  on the LHS to those over  $\mathcal{D}G$  and  $\mathcal{D}\Sigma$  on the RHS. We work in the limit  $J\tau\gg 1$ ,  $N\gg 1$  and keep the leading quantum correction  $(\sim \frac{1}{N})$  to the classical expression

$$\mathcal{F}(\tau_1, \tau_2, \tau_3, \tau_4) = \frac{1}{N^2} \sum_{i,j=1}^{N} \langle \mathcal{T}\psi_i(\tau_1)\psi_i(\tau_2)\psi_j(\tau_3)\psi_j(\tau_4) \rangle - \tilde{G}(\tau_1, \tau_2)\tilde{G}(\tau_3, \tau_4), \qquad (1.102)$$

where  $\tilde{G}$  denotes the saddle point value of the effective action, which in the IR limit can be approximated by the conformal propagator (1.83).

Due to the anticommutativity of the fermions, we can restrict ourselves to the region  $\tau_1 > \tau_2$ ,  $\tau_3 > \tau_4$  and  $\tau_1 > \tau_3$  without loss of generality. For concreteness, we will now study the theory at finite temperature, i.e.  $\tau_{1,2,3,4} \in \left[-\frac{\beta}{2}, \frac{\beta}{2}\right]$ .

It is convenient to separate conformally-invariant  $(\delta G^{\parallel})$  and non-invariant fluctuations  $(\delta G^{\perp})$  near the saddle point value  $\tilde{G}$ . The fluctuations  $\delta G^{\parallel}$  are defined in such way that the function  $G_c + \delta G^{\parallel}$  solves the conformal DS equation (1.76), and the subspace of non-invariant fluctuations  $\delta G^{\perp}$  is the orthogonal complement to the subspace of conformally-invariant fluctuations. Note that due to the symmetry (1.78) all conformal fluctuations can

be parametrized by the function  $\varphi(\tau)$ , which maps the time circle into itself:

$$\delta G_{\varphi}^{\parallel}(\tau_1, \tau_2) = G_c^{\beta} \left[ \varphi(\tau_1), \varphi(\tau_2) \right] - G_c^{\beta}(\tau_1, \tau_2), \quad \text{for some reparametrisation} \quad \tau \to \varphi(\tau).$$
(1.103)

In these notations the functional integral for the four-point function looks as follows

$$\mathcal{F} \approx \mathcal{F}_{0} + \frac{1}{Z} \int \mathcal{D}\delta G^{\parallel} \mathcal{D}\delta G^{\perp} \mathcal{D}\Sigma \left(\delta G^{\parallel}(\tau_{1}, \tau_{2}) + \delta G^{\perp}(\tau_{1}, \tau_{2})\right) \left(\delta G^{\parallel}(\tau_{3}, \tau_{4}) + \delta G^{\perp}(\tau_{3}, \tau_{4})\right) e^{-I_{CFT} - I_{S}}$$

$$= \mathcal{F}_{0} + \mathcal{F}_{S} + \mathcal{F}_{CFT} + \mathcal{O}\left(\frac{1}{N^{2}}\right), \tag{1.104}$$

where we expanded the integrand near the saddle point and introduced the following expectation values

$$\mathcal{F}_0 \equiv \frac{1}{N} \left( \tilde{G}(\tau_1, \tau_4) \tilde{G}(\tau_2, \tau_3) - \tilde{G}(\tau_1, \tau_3) \tilde{G}(\tau_2, \tau_4) \right), \tag{1.105}$$

$$\mathcal{F}_{S} \equiv \left\langle \delta G^{\parallel}(\tau_{1}, \tau_{2}) \delta G^{\parallel}(\tau_{3}, \tau_{4}) \right\rangle_{S} = \frac{\int \mathcal{D}\varphi \, \delta G_{\varphi}^{\parallel}(\tau_{1}, \tau_{2}) G_{\varphi}^{\parallel}(\tau_{3}, \tau_{4}) e^{-I_{S}[\varphi]}}{\int \mathcal{D}\varphi \, e^{-I_{S}[\varphi]}}, \tag{1.106}$$

$$\mathcal{F}_{CFT} \equiv \left\langle \delta G^{\perp}(\tau_1, \tau_2) \delta G^{\perp}(\tau_3, \tau_4) \right\rangle_{CFT} = \frac{\int \mathcal{D} \delta G^{\perp} \delta G^{\perp}(\tau_1, \tau_2) G^{\perp}(\tau_3, \tau_4) e^{-I_{\text{eff}}[\delta G^{\perp}]}}{\int \mathcal{D} \delta G^{\perp} e^{-I_{\text{eff}}[\delta G^{\perp}]}}. \tag{1.107}$$

To obtain the average (1.106), we use that the Jacobian

$$J = \left[\frac{\mathcal{D}G_{\varphi}^{\parallel}}{\mathcal{D}\varphi}\right]_{\varphi(\tau) = \frac{2\pi\tau}{\beta}} \tag{1.108}$$

is constant and non-zero, because for reparametrisations which are infinitesimally close to the identity,  $\varphi(\tau) = \frac{2\pi\tau}{\beta} + \delta\varphi(\tau)$ , fluctuations  $\delta G_{\varphi}^{\parallel}$  depend only on  $\delta\varphi$  The integral  $\int \mathcal{D}\delta G^{\perp}\mathcal{D}\Sigma e^{-I_{CFT}}$  in the numerator and denominator of (1.106) is also constant and non-zero.

The contributions from the conformally-invariant and non-invariant parts are both of order  $\mathcal{O}\left(\frac{1}{N}\right)$ . However, for  $\beta J \gg 1$  the leading contribution to the correlation function comes from the Schwarzian action – soft modes are easier to excite due to the additional small  $\left(\frac{1}{\beta J}\right)$  prefactor present in the latter.

Of particular relevance is the case  $\tau_1 = \frac{\beta}{4} + it$ ,  $\tau_2 = -\frac{\beta}{4} + it$ ,  $\tau_3 = 0$ ,  $\tau_4 = -\frac{\beta}{2}$  for  $t = -i\Delta\tau \gg 1$ 

 $J^{-1}$ , as it describes the regularized out-of-time-ordered correlation function [27]

$$\begin{aligned}
\text{OTOC}(t) &\equiv \frac{1}{N^2} \sum_{i,j=1}^{N} \text{tr} \left[ \rho^{\frac{1}{4}} \chi_i(t) \rho^{\frac{1}{4}} \chi_j(0) \rho^{\frac{1}{4}} \chi_i(t) \rho^{\frac{1}{4}} \chi_j(0) \right] = \\
&= \tilde{G} \left( \frac{\beta}{2} \right) \tilde{G} \left( \frac{\beta}{2} \right) + \mathcal{F} \left( \frac{\beta}{4} + it, -\frac{\beta}{4} + it, 0, -\frac{\beta}{2} \right) = \\
&= \tilde{G} \tilde{G} + \mathcal{F}_S + \mathcal{F}_{CFT} + \mathcal{F}_0 + \mathcal{O} \left( \frac{1}{N^2} \right),
\end{aligned} \tag{1.109}$$

where  $\rho = \frac{1}{Z}e^{-\beta H}$  is the density matrix. A detailed derivation of these results goes beyond the scope of our review. We will limit ourselves to quoting the final form of the OTOC in the SYK model as computed by Kitaev and reviewed by Maldacena and Stanford in [11]:

OTOC(t) 
$$\approx$$
 OTOC<sub>S</sub>(t) +  $\delta$ OTOC(t)  $\approx \frac{\sqrt{\pi}}{2\beta J} \left[ 1 - \text{const} \frac{\beta J}{N} e^{\lambda_L t} \right], \quad \text{for} \quad \beta \ll t \ll \beta \log \frac{N}{\beta J},$ 
(1.110)

where OTOC<sub>S</sub> and  $\delta$ OTOC denote the Schwarzian and conformal contributions, respectively. Here "const" is an  $\mathcal{O}(1)$  number and  $\lambda_L$  is the Lyapunov exponent

$$\lambda_L \approx \frac{2\pi}{\beta} \left( 1 - \frac{6.05}{\beta J} + \cdots \right). \tag{1.111}$$

where the first one is the contribution from the Schwarzian action and the second one is a correction coming from the conformally invariant action. We see that the in the large  $\beta J$  limit the SYK model saturates the bound on chaos.

The fact that the SYK model is maximally chaotic and solvable in the large N limit made of it an extremely useful ground to investigate quantum dynamics in general and its holographic implications in particular. In the remaining of this thesis, we will present various results pertaining to the applicability of ETH in this model as well its quantum chaotic behavior in pure states.

## ETH in the SYK model: a numerical study

In this Chapter, based on [45], we show that the SYK model satisfies the eigenstate thermalization hypothesis by solving the system in exact diagonalization. Using these results we also study the behavior, in eigenstates, of various measures of thermalization and scrambling of information. We establish that two-point functions in finite-energy eigenstates approximate closely their thermal counterparts and that information is scrambled in individual eigenstates. We study both the eigenstates of a single random realization of the model, as well as the model obtained after averaging of the random disordered couplings. We use our results to comment on the implications for thermal states of a putative dual theory, i.e. the AdS<sub>2</sub> black hole.

## 2.1 Summary of results

First and foremost, in this Chapter we establish, by exactly diagonalizing the complex SYK Hamiltonian for up to 17 sites, that expectation values of non-extensive – that is those involving a few sites only – operators are to a very good approximation thermal. In particular their matrix elements take on the expected form encapsulated in the eigenstate thermalization hypothesis. This has interesting ramifications for the holographic dual, and we address some of these in the discussion section.

By studying off-diagonal matrix elements of non-extensive operators we establish that the

SYK model behaves like a random-matrix theory (RMT) for a certain range of energies, but more generally deviates from such RMT behavior. By analogy with the theory of disordered conductors we refer to the energy scale at which deviations from RMT are observed as the Thouless energy  $E_T$ . We find that the Thouless energy is controlled by the coupling as  $E_T \sim J^2$ . The more strongly coupled the system, the larger the energy range for which it exhibits RMT behavior.

Having established that eigenstates behave thermally we compare correlation functions of non-extensive operators in eigenstates with their corresponding thermal expectation values. We find that two-point and four-point correlation functions in eigenstates are qualitatively similar to thermal averages, but do differ in their detailed structure. We also study correlations in large superpositions of eigenstates which approximate thermal averages with respect to a canonical density matrix. To the extent that we can extrapolate these results to large values of N this suggests that individual eigenstates can in some sense be considered to be dual to the black-hole geometry in the putative dual, although we make no statement about its interior (see discussion section).

This motivates us to consider measures of scrambling in eigenstates, which we find to behave in accordance with expectations from combining known results in the canonical ensemble with our results on eigenstate thermalization. We therefore expect that there is a large-N eigenstate equivalent of the maximal scrambling exponent satisfied by the SYK model, as detailed in (2.8) below.

## 2.2 The complex SYK model

In the previous Chapter we introduced the SYK model in its standard version, namely in terms of Majorana fermions. For reasons that will become apparent, in the present Chapter we work with a version that involves complex spinless fermions subject to the Hamiltonian [10,46]

$$H = \sum_{i,j,k,l}^{N} J_{ijkl} c_i^{\dagger} c_j^{\dagger} c_k c_l \tag{2.1}$$

with complex coupling parameters  $J_{ijkl}$ . We define a set of fermion creation and annilihation operators, satisfying

$$\{c_i, c_j^{\dagger}\} = \delta_{ij}, \qquad \{c_i, c_j\} = \{c_i^{\dagger}, c_j^{\dagger}\} = 0.$$
 (2.2)

Antisymmetry of the fermions as well as Hermiticity of the Hamiltonian impose the constraints

$$J_{ijkl} = -J_{jikl}, \quad J_{ijkl} = -J_{ijlk}, \quad J_{ijkl} = J_{klij}^*.$$

$$(2.3)$$

The remaining independent coupling constants in  $J_{ijkl}$  are drawn from a Gaussian distribution with zero mean. The variance

$$\overline{\left|J_{ijkl}\right|^2} = \frac{3!J^2}{N^3} \tag{2.4}$$

sets the average strength of the coupling, which has to scale with the number of sites N as shown to ensure a well-behaved large-N limit. We will keep this normalization despite the fact that we always work at strictly finite N. The Hamiltonian, as written above (2.1) does not respect particle-hole symmetry. However, the particle-hole violating effects come from terms where two indices of  $J_{ijkl}$  take the same value and so they are suppressed by powers of 1/N. One could add a chemical potential that restores particle hole symmetry at any N, as in [46]. Since both versions connect to the same large-N limit we have chosen here instead to work with the simpler Hamiltonian (2.1).

### Properties

The Hamiltionian (2.1) is a variant of a set of models considered previously in the context of quantum spin glasses [13], but crucially does not itself have a spin-glass phase. A closely related model has recently been proposed by Kitaev in terms of Majorana fermions at N sites [9].

As we saw in section 1.4, the model is solvable<sup>1</sup> at large-N and can be shown to exhibit a number of striking properties [9,11,14], chiefly among them the fact that it exhibits maximal

 $<sup>^{1}</sup>$ So far, expressions have been obtained for the two-point, four-point and six-point functions [10, 13, 14, 47-51].

chaos, in the sense that an appropriately defined (see section 2.4.3) out of time order fourpoint function (OTOC) decays exponentially for times up to the scrambling time,

$$\langle A(t)B(0)A(t)B(0)\rangle_{\beta} \sim 1 - \alpha e^{\lambda_L t}, \qquad (2.5)$$

where  $\alpha$  is a coefficient, e.g.  $\alpha \sim \beta J/N$  for the large-N limit of SYK [11]. This defines a quantum version of a Lyapunov exponent. The average is taken in the thermal state, as indicated. This Lyapunov exponent takes the maximal [15] value  $2\pi/\beta$  in the SYK model, which is the same as that of a Schwarzschild black hole in Einstein gravity [9,52]. Here we provide numerical evidence that this Lyapunov exponent can also be extracted by considering instead energy eigenstates, that is to say correlation functions of the form

$$\langle E|A(t)B(0)A(t)B(0)|E\rangle \sim 1 - \alpha e^{\lambda_L t}. \tag{2.6}$$

The value of  $\lambda_L$  in eigenstates can be meaningfully compared with the thermal value by appealing to the eigenstate thermalization hypothesis in order to associate a temperature  $T = \beta^{-1}$  to the individual eigenstate  $|E\rangle$ . To this end one may follow [53] and associate an effective temperature  $\beta^{-1}$  with energy E via the canonical average

$$E(\beta) = \frac{1}{Z} \text{Tr} \left[ e^{-\beta H} H \right]. \tag{2.7}$$

Alternatively, for many of our computations, we determine all thermodynamic quantities in a microcanonical ensemble centered at the average energy  $\overline{E} = (E_n + E_m)/2$  for ease of comparison with the ETH ansatz.

Here we study (2.6) using exact diagonalization. Our work can be viewed as motivating the conjecture that  $\lambda_L$ , defined in terms of eigenstates as in (2.6) will satisfy

$$\lambda_L = 2\pi/\beta(\bar{E}) \tag{2.8}$$

when evaluated at large  $N \gg 1$  and large coupling  $\beta J \gg 1$ , where  $\beta$  is defined as the inverse of the map (2.7) above. Let us now move on to a discussion of the methods and results of this Chapter.

# 2.3 One point functions and eigenstate thermalization

The main analysis technique in this work is numerical diagonalization of the many-body Hamiltonian. For most applications we numerically diagonalize the Hamiltonian (2.1) for up to 17 sites<sup>2</sup>. This allows us to explicitly calculate the matrix elements of non-extensive operators made up of creation and annihilation operators involving a small number of sites.

It is easily seen that total the fermion number

$$\hat{n}_{\rm F} = \sum_{i}^{N} c_i^{\dagger} c_i \tag{2.9}$$

commutes with the Hamiltonian

$$[H, \hat{n}_{\rm F}] = 0,$$
 (2.10)

allowing us to work in sectors of fixed fermion number  $n_{\rm F}$ , denoting the filling fraction  $\nu = \frac{n_F}{N}$ . This is useful numerically as it allows us to cut down the effective matrix sizes in the actual diagonalization process, and is the reason why we work in this Chapter with the complex instead of the Majorana version of the model. For the most part we will work in the half-filling sector  $\nu = \frac{1}{2}$ . If the number of sites N is odd, we mean  $\nu = \frac{N+1}{2N}$  when we refer to 'half-filling'.

### 2.3.1 On-diagonal terms are thermal

According to the ETH ansatz (1.27), diagonal matrix elements  $\mathcal{O}_{nn} = \langle n|\mathcal{O}|n\rangle$  are smooth functions of the average energy  $\bar{E}$ , while off-diagonal elements are suppressed by the entropic factor  $e^{-S/2}$ .

We start by illustrating this exponential suppression in Figure (2.1), where it is easily seen that only the diagonal entries of the matrix are appreciable. We illustrate this behavior for N = 10 in Figure (2.1), but have checked it extensively for other accessible values of

<sup>&</sup>lt;sup>2</sup>We emphasize that this corresponds to a Hilbert space dimension  $2^N = 2^{17}$  which is the same as that of the Majorana SYK model with M = 34 sites, corresponding to a Hilbert space dimension of  $2^{M/2}$ .

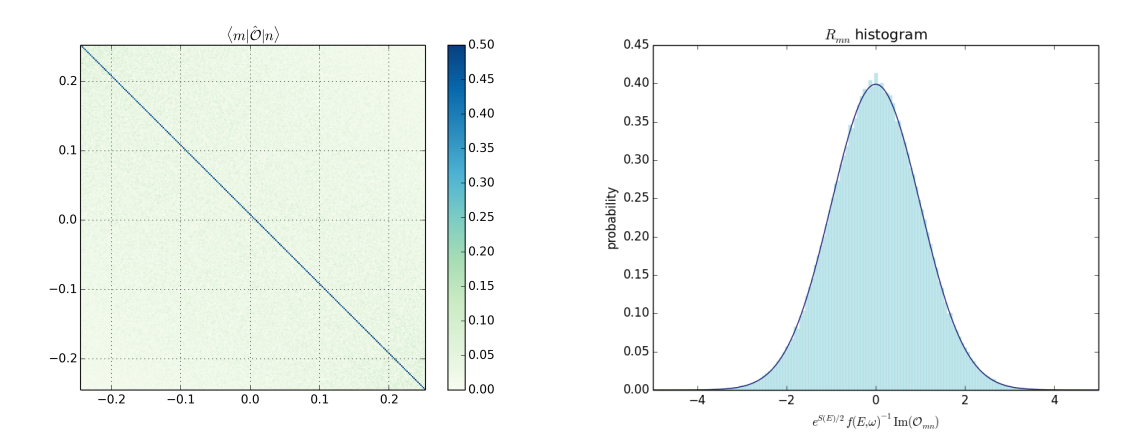


Figure 2.1: Absolute values of matrix elements  $|\mathcal{O}_{nm}| = |\langle n|\mathcal{O}|m\rangle|$  for the single-site number operator  $\mathcal{O} = \hat{n}_N$  at half filling  $\nu = \frac{1}{2}$ . **Left panel**: we show the absolute values of matrix elements against their energies  $E_n/J$  labelled along horizontal and vertical axes for a single realization at N = 10. We have checked this behavior for higher values of N, and found excellent agreement with ETH expectations. **Right panel**: Histogram of the remainders  $R_{mn}$  for 1000 realizations at N = 12. As we see these are accurately fit by a unit width Gaussian with zero mean confirming the ETH ansatz (1.27). Again we have verified this for other accessible values of N. Similar results are obtained for models with short-range interactions in [54].

N finding excellent agreement with ETH expectations. For N=10, one can make out the fluctuating nature of the off-diagonal matrix elements, which we will characterise precisely in section 2.3.2 below. Of course so far this is at the level of qualitative observation and we will turn to a more quantitive analysis of the off-diagonal matrix elements below.

Before we do so, let us analyse the on-diagonal matrix elements,  $\mathcal{O}_{nn}\left(\bar{E}\right)$  in detail. The expectation for finite values of N is that the diagonal matrix elements condense more and more tightly onto a limiting smooth curve  $\overline{\mathcal{O}(\bar{E})}$  which is defined by extrapolation to the thermodynamic limit  $N \to \infty$ . This is illustrated in Figure 2.2. As mentioned before, for a model that involves a disorder average, such as SYK, we should distinguish between what happens in an individual realization, and what happens in the ensemble. The convergence towards a limiting curve for a single realization is shown in the top panel of Figure 2.2, while the convergence due to disorder averaging is shown in the bottom two panels of that same Figure. If a certain property is satisfied in both senses, i.e. for a single realization as well as in the disorder averaged theory, this property is said to be self-averaging. Here we confirm that

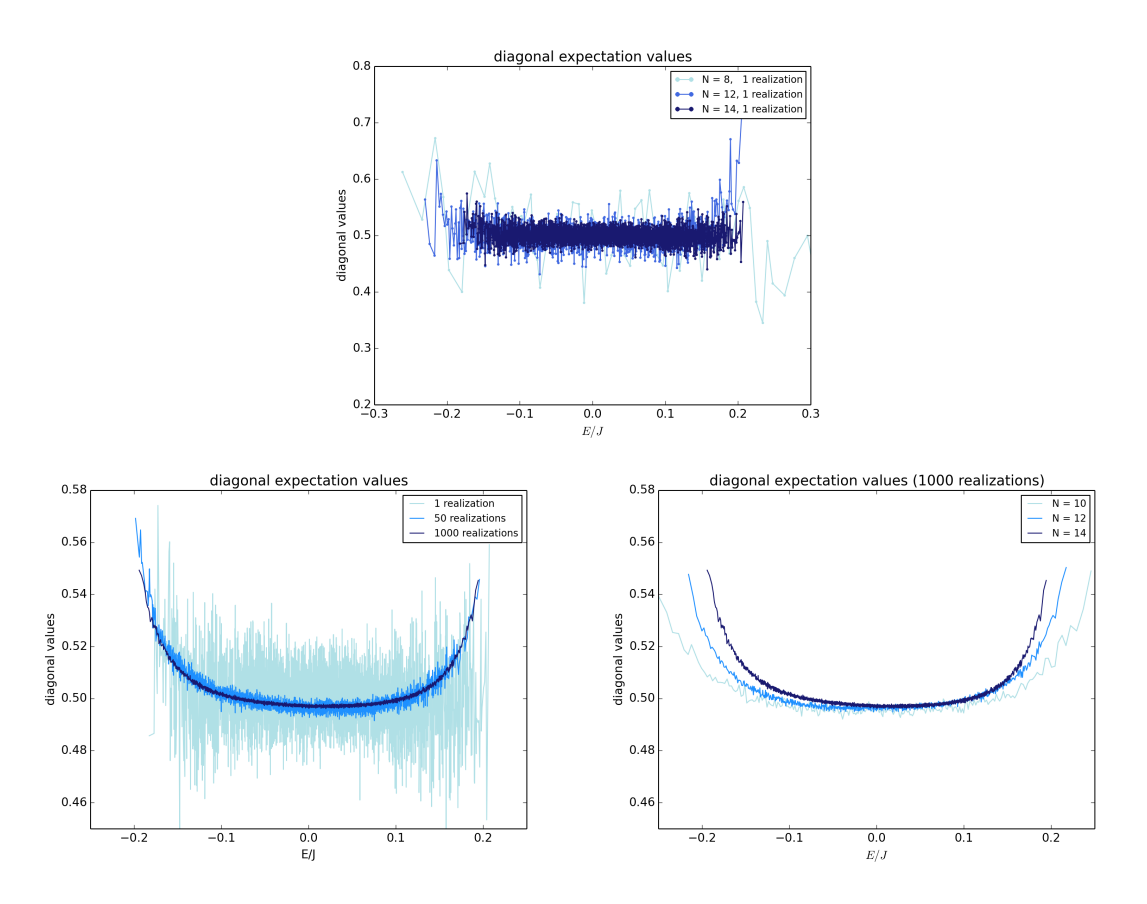


Figure 2.2: Diagonal expectation values for the single-site number operator at site N, that is  $\hat{n}_N$  at half filling  $\nu = \frac{1}{2}$ . **Top panel**: we show a single random realization for increasing Hilbert space dimension corresponding to N=8,12,14. We see that the on-diagonal expectation values of a single realization approach closer and closer to a smooth curve. **Left panel**: we show the effect of averaging of the random couplings at given fixed Hilbert space dimension, N=14. As expected the on-diagonal values of the ensemble approach closer and closer to a smooth curve. **Right panel**: we show the limiting curves for the model with fixed Hilbert space dimension corresponding to N=10,12,14, averaged over 1000 realizations.

the diagonal part of the ETH ansatz in the SYK model is satisfied both in a single realization and in the disordered theory. Of course this is only true for sufficiently large Hilbert space dimension.

We have further verified this property for a number of different non-extensive operators over a range of filling fractions. We show a representative selection of these results for the hopping operator for two fixed sites  $h_{ik} = c_i^{\dagger} c_k + c_k^{\dagger} c_i$  for different values of N in Appendix 2.A.2.

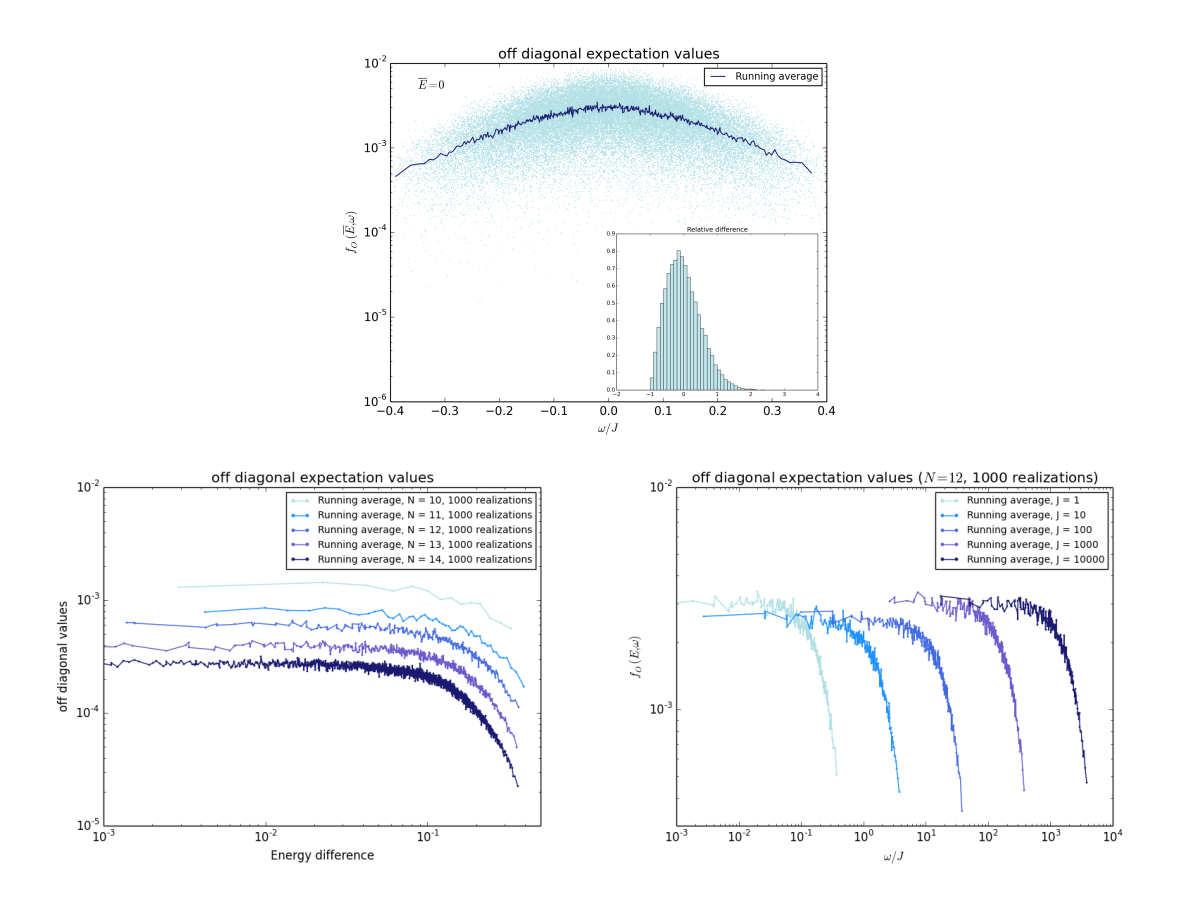


Figure 2.3: Off-diagonal values of matrix elements  $\mathcal{O}_{nm} = |\langle n|\mathcal{O}|m\rangle|$  for the single-site number operator  $\mathcal{O} = \hat{n}_N$  at half filling  $\nu = \frac{1}{2}$ . We show the off-diagonal matrix elements against their energies  $E_n/J$ . **Top panel**: N = 14 with raw data in light blue and the running average in dark blue. The inset shows a histogram of relative error between raw data and running average. We see that the histogram is peaked around zero. **Left panel**: the function  $f_{\mathcal{O}}(\bar{E},\omega)$  (we show the running average) for varying Hilbert space dimension corresponding to N = 10, 11, 12, 13, 14. The cross-over from constant to non-constant behavior is identified with the Thouless energy  $E_T$ . **Right panel**: scaling of the Thouless energy with average coupling strength J. A simple fit gives  $E_T \propto J^2$ .

## 2.3.2 Off-diagonal terms

Moving on to the off-diagonal terms of the matrix elements we demonstrate that the remainder terms are indeed well described by a Gaussian random distribution with zero mean and unit variance, in other words

$$\langle m|\hat{\mathcal{O}}|n\rangle = e^{-S(\bar{E})/2} f_{\mathcal{O}}(\bar{E},\omega) R_{mn}, \qquad n \neq m$$
 (2.11)

In Figure 2.1 we show a histogram of  $R_{mn}$  together with a fit to a Gaussian distribution for the single-site number operator. Since the matrix elements are in general complex, both real and imaginary part should be Gaussian distributed and we show a histogram for the imaginary part.

### The function $f_{\mathcal{O}}(\bar{E},\omega)$

However, we can go further and calculate the function  $f_{\mathcal{O}}(E,\omega)$  itself. This captures more detailed physics and allows, for example, to diagnose for what energy ranges the SYK model behaves like a random matrix ensemble, and for what energy ranges it deviates from such behavior. In RMT the function  $f_{\mathcal{O}}(\bar{E},\omega)$  is a constant function of  $\omega$  at fixed  $\bar{E}$  (see Figure 2.10 in Appendix 2.B), while deviations become apparent whenever  $f_{\mathcal{O}}(E,\omega)$  is a non-trivial function of  $\omega$ . We show the result of this calculation in Figure 2.3, with a cross-over between RMT and non-RMT behavior at a characteristic energy  $E_T$ , set by the coupling strength J. Despite the lack of spatial diffusion in the model we refer to this energy as the Thouless energy  $E_T$ . Due to this lack of spatial structure (SYK is effectively a zero-dimensional model), the Thouless energy cannot be set by a diffusion time, and it is thus natural that it be set instead by the coupling strength J (at fixed energy E). The uppermost panel of Figure 2.3 shows a comparison of the raw data with a running average, which is taken over 100 matrix elements. The resulting smooth curve is then shown in the left bottom panel for a number of different Hilbert space dimensions, as a function of eigenenergy difference  $\omega = E_m - E_n$ . We can discern a regime over which  $f_{\mathcal{O}}(E,\omega)$  is almost constant as a function of  $\omega$ , indicative of RMT like behavior. At a characteristic energy scale  $E_T$  this then gives way to non-constant, i.e. non-RMT behavior. In higher dimensional local models this energy is often associated with the diffusive Thouless energy, but, as indicated before, such a physics interpretation appears not to be available in the zero-dimensional SYK case. We note that this corresponds well with the observations of [55], who previously presented evidence for  $E_T$  in the Majorana model. We have shown that the scale  $E_T$  is set by average strength of the random coupling, J, at fixed average energy  $\bar{E}$ , in other words it is controlled by the dimensionless coupling j = J/E. It should be noted that this is the natural pure-state version of the coupling  $\beta J$  which was used in previous studies of the SYK model. We have thus shown that for stronger coupling  $j \gg 1$  the range of energies  $\omega$  for which the system behaves chaotically (i.e. like RMT) is also increased (see right bottom panel of Figure 2.3). This accords well with intuition as well as previous results in the thermal ensemble indicating chaotic properties to be most pronounced in the strong-coupling regime. Let us now discuss further chaotic aspects of the model.

### 2.4 Correlation functions and chaotic behavior

In section 2.3 we established the applicability of the ETH ansatz by studying one point functions of nonextensive operators in the complex SYK model. We will now study higher-point correlations in order to elucidate dynamical aspects of the model related to quantum chaos. We will explore how correlation functions in pure states can approximate those in thermal states, relying both on numerics and analytics based on the ETH form on eigenstates. Many of these measures have already been studied in the thermal ensemble<sup>3</sup>, whereas our focus here is on studying them in pure states. From the holographic dual point of view we are thus investigating the question of how well the correlation functions computed in a blackhole background are approximated by correlations in pure states, in particular in individual eigenstates.

Again, it is interesting to compare the behavior in a single random realization of the model versus the behavior of the same quantity after averaging over a large number of realizations. We shall start, however, with the spectral form factor where the distinction between pure states and the thermal ensemble is meaningless, as can be seen from its definition in terms of an analytically continued partition function. One may also construct the spectral form factor as the fidelity of a certain pure state [58].

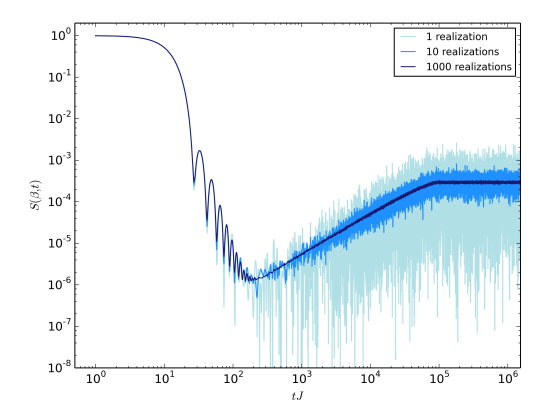
## 2.4.1 The spectral form factor

The spectral form factor is a well studied quantity in random matrix theory (see e.g. [59]) as it gives a clean probe of the eigenspectrum of a model. In particular its late-time behavior is sensitive to the discreteness of the spectrum as well as level statistics. The spectral form factor is most conveniently defined in terms of the analytically continued partition function,

$$S(\beta, t) := \frac{Z(\beta + it)Z(\beta - it)}{Z(\beta)^2}. \tag{2.12}$$

In Figure 2.4 we show  $S(\beta,t)$  for the spinless Fermion SYK model both as a function of  $\beta$  and how it approaches its limiting form as one averages over the random couplings  $J_{ijkl}$ .

<sup>&</sup>lt;sup>3</sup>Where applicable. Of course the spectral form factor, which we study in section 2.4.1 makes no reference to any state or ensemble. At any rate this quantity has already been studied in [56] for the Majorana model and in [57] for the spinless Fermion case.



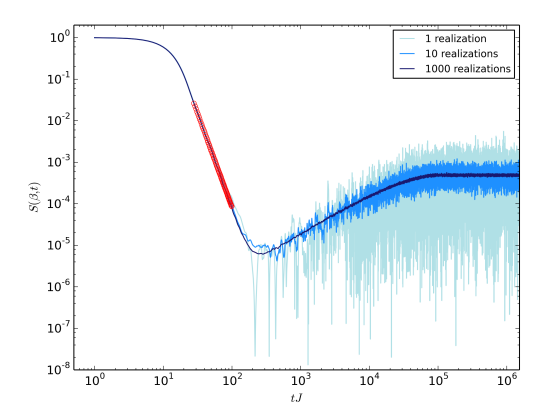


Figure 2.4: Spectral form factor at half filling  $\nu = \frac{1}{2}$  for varying number of realizations and two different temperatures at N=14. In both cases we see the characteristic decay followed by linear ramp and plateau behavior. **Left panel:**  $\beta = 1$ . One sees several partial revivals in the decaying region with a power-law envelope. **Right panel:**  $\beta = 10$ . The red markers show points we used for a fit in the slope region, where we find a decay of  $\propto t^{-4.53...}$ , which is consistent with the value reported in [57].

Interestingly we see a  $t^{-4.5}$  falloff before the dip time. The fit is shown in red in the right panel of Figure 2.4 and the exponent is of course not understood to be exact, depending both on numerical accuracy and the exact choice of the window over which we fit. This does not correspond to the power-law expected from a Wigner edge  $\rho(E) \sim \sqrt{E}$  of the spectral density [56]. It is easy to show [58] that a power law  $\mathcal{S} \sim t^{-2(k+1)}$  in the slope region corresponds to a spectral density  $\rho(E) \sim E^k$ . At high temperature (left panel) this power law is to be understood as the envelope of an oscillatory decay. Such power laws arise quite generally in computations of survival probabilities of many-body quantum systems [60]. We also see the characteristic ramp and plateau behavior [56,58] at late times which, once more, looks qualitatively like RMT. The difference between RMT and the SYK model is to be found in the precise timescales of dip and plateau times [56]. For completeness and ease of comparison we discuss the RMT spectral form factor in some detail in Appendix 2.B.

## 2.4.2 The two-point function

Let us now turn to the study of correlation functions of non-extensive operators. Here we work with the two-site hopping operator  $h_{ij}$  whose one-point functions are studied in Appendix

2.A. The operator is defined as follows: pick two arbitrary sites i and j and write

$$\mathcal{O} = h_{ij} = c_i^{\dagger} c_j + c_i^{\dagger} c_i \,. \tag{2.13}$$

We have also verified that analogous results hold for the connected and full correlation functions of the on-site number operator  $n_i$ .

### **Eigenstates**

We now study correlation functions of the hopping operator in energy eigenstates. For definiteness we will take sites i = N - 1 and j = N, but any two sites will give essentially the same answer. We consider the two point function of the hopping operator,

$$G^{n}(t) = \langle h_{ij}(t)h_{ij}\rangle_{E_{n}} := \langle n|e^{iHt}h_{ij}e^{-iHt}h_{ij}|n\rangle$$
(2.14)

for some excited eigenstate  $|n\rangle$  with energy  $E_n$ , as well as its connected cousin

$$G_c^n(t) = \langle h_{ij}(t)h_{ij}\rangle_{E_n} - \langle h_{ij}\rangle\langle h_{ij}\rangle_{E_n}. \tag{2.15}$$

We find that the connected correlation function in eigenstates quickly decays and subsequently oscillates around zero as shown in Figure 2.5. This latter fact is easily established by averaging over time. One finds

$$\overline{G^n(t)} = \lim_{T \to \infty} \frac{1}{T} \int_0^T \sum_m e^{i(E_n - E_m)t} |\mathcal{O}_{nm}|^2 dt = |\mathcal{O}_{nn}|^2,$$
 (2.16)

where we temporarily denoted the Hermitian operator  $h_{ij}$  by  $\mathcal{O}$  to avoid too much index clutter. It follows that the connected eigenstate correlation function averages to zero,  $\overline{G_c^n(t)} = 0$ , at late times. The typical size of the late-time fluctuations follows from eigenstate thermalization, (1.27), to be  $\sim e^{-S/2}$ . We show explicit computations of  $G_c^n(t)$  for different values of N in Figure 2.5 (top left).

As implied by (1.27), the behavior of the two-point function in eigenstates approximates very closely the corresponding microcanonical quantities. This agreement is expected to be perfect in the thermodynamic limit  $N \to \infty$ . By a microcanonical two point function of an

operator  $\mathcal{O}$  we mean the quantity

$$G^{\bar{E}}(t) = \frac{1}{\mathcal{N}_{\bar{E}}} \sum_{n} \langle n | \mathcal{O}(t) \mathcal{O} | n \rangle, \qquad \overline{G^{\bar{E}}(t)} = \frac{1}{\mathcal{N}_{\bar{E}}} \sum_{n} |\mathcal{O}_{nn}|^2, \qquad (2.17)$$

where  $\mathcal{N}_E$  is the number of states in a window of energies of given width  $\Delta E$  around the average energy  $\bar{E}$  and the sum over n runs over exactly those states. This agreement is illustrated in Figure 2.5 (top right). As a basic check one can convince oneself that (1.27) implies that its long time average gives exactly (2.16), which is also borne out in Figure 2.5 (top right). We conclude therefore that two-point functions in the disorder-averaged theory become arbitrarily close to their thermal (microcanonical) averages. This agreement is perhaps not surprising if one realizes that averaging the correlation function over couplings is operationally similar to a microcanonical average in the first place.

However, we now want to compare the behavior of  $G^n$  and  $G_c^n$ , to the corresponding thermal correlation functions with respect to the canonical density matrix  $\rho = e^{-\beta H}$ , at energy  $E(\beta)$ , determined by the map (2.7), that is

$$G^{\beta}(t) = \frac{1}{Z(\beta)} \operatorname{Tr} \left[ e^{-\beta H} h_{ij}(t) h_{ij} \right]$$
 (2.18)

and its connected cousin

$$G_c^{\beta}(t) = G^{\beta}(t) - \frac{1}{Z(\beta)^2} \left( \text{Tr} \left[ e^{-\beta H} h_{ij} \right] \right)^2, \qquad (2.19)$$

where again  $h_{ij}(t)$  is the hopping operator in the Heisenberg picture at time t. Generally speaking all these correlation functions show the expected behavior, namely an early time exponential decay, followed by intermediate-time power law decay, further followed by a late time ramp to a very late time plateau. The plateau value may be zero, or non-zero depending on which operator and which correlation function one considers.

As illustrated in Figure 2.5 (bottom left) we find that the full correlation function  $G^n(t)$  in eigenstates at energy  $E_n(\beta)$  starts to approximate the corresponding thermal one  $G^{\beta}(t)$  at early time and at late times. Here  $E(\beta)$  is the energy corresponding to the inverse temperature  $\beta$  via the map (2.7), while at intermediate times (during the ramp),  $G^n(t)$  and  $G^{\beta}(t)$ 

can differ.

The connected correlation function  $G_c^n(t)$  in eigenstates oscillates around zero at late times, unlike its thermal equivalent  $G_c^{\beta}(t)$ , which oscillates around a non-zero average value as seen in Figure 2.5 (bottom right). These differences are subleading in the size of the Hilbert space and are expected to become negligible in the  $N \to \infty$  limit. The latter limit is of special interest for a putative gravitational dual as it corresponds to the semi-classical regime where a geometric description should become possible.

As a side comment, in the limit  $\beta \to \infty$ , the thermal expectation value starts approximating the eigenstate one arbitrarily closely. This, of course, has nothing to do with thermalization, as it corresponds to the zero-temperature limit, where the 'thermal' average projects on the ground state, and is thus manifestly equal to the eigenstate correlation function. In conclusion then we find that the two-point function in individual eigenstates of the disorder-averaged theory behaves thermally, showing the most precise match with the microcanonical average of the correlation function. Since we work at finite N the different statistical ensembles need not give the same answers, and indeed subtle differences are seen between canonical and eigenstate correlation functions. These differences are expected to disappear in the thermodynamic limit. We can already appreciate the convergence of the different ensembles for N = 6 versus N = 10 by comparing Fig. 2.5 (bottom right) with its inset.

#### Superposition states

Up to this point we have considered mostly eigenstates. From what we have found one can conclude also that arbitrary pure states with narrow support in energy thermalize to microcanonical averages at late times, consistent with eigenstate thermalization. However, thermalization of states with broad support in energy do not thermalize in this way. We will next consider pure states, closely related to the ones considered in [61], with very broad spread over the energy spectrum<sup>4</sup> and demonstrate that they nevertheless thermalize, but more precisely to canonical averages. Note, again, that at finite N microcanonical and canonical averages do not have to exactly agree, and consequently one or the other may be a better approximation to a thermalizing pure state correlation function.

<sup>&</sup>lt;sup>4</sup>For a discussion of similar states in the context of tensor models, see [62]

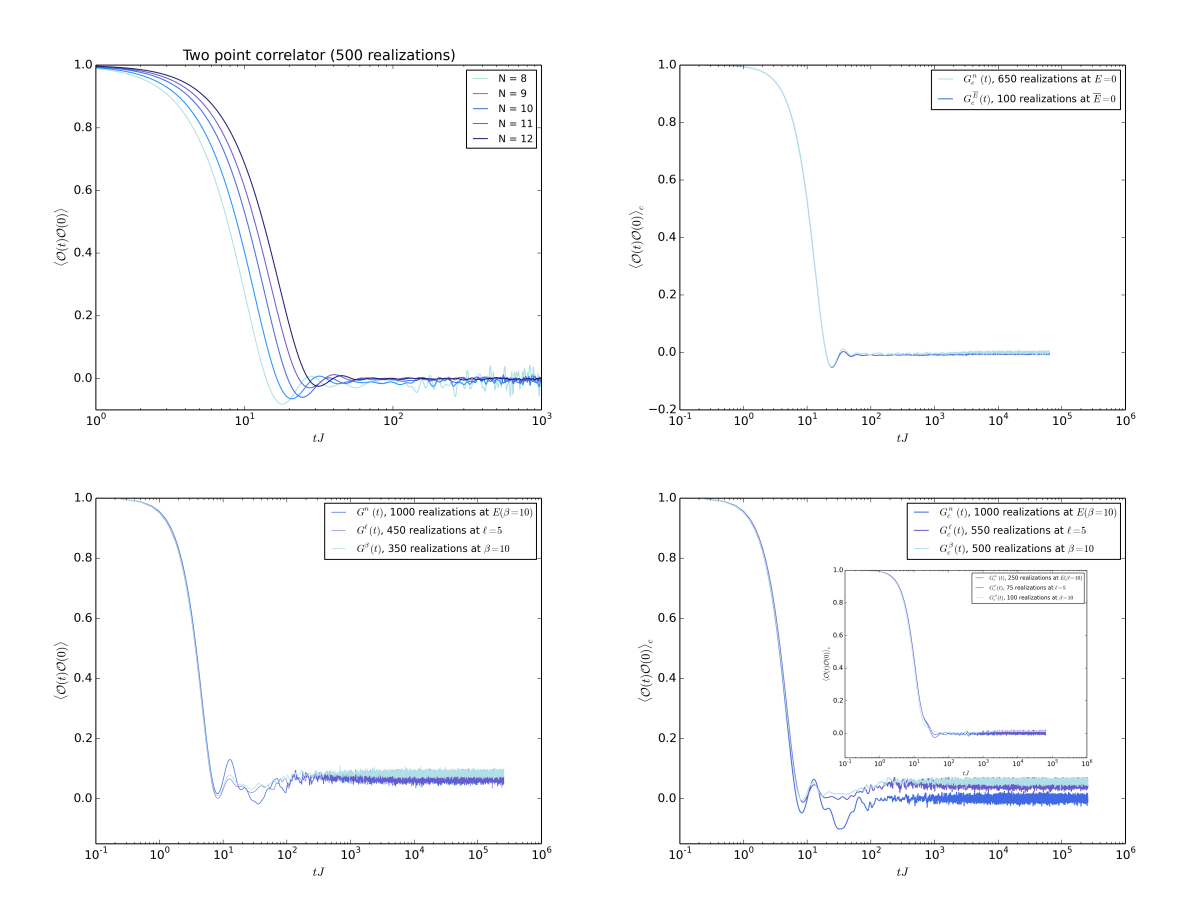


Figure 2.5: Two-point function of the hopping operator at half filling  $\nu = \frac{1}{2}$ . **Top left panel:** Two-point correlation function,  $G_c^n(t)$ , in one eigenstate for N=8,9,10,11,12. The initial decay is followed by late time fluctuations around zero of typical size  $\sim e^{-S/2}$ . **Top right panel:** Comparison of microcanonical  $G_c^{\bar{E}}(t)$  with eigenstate  $G_c^n(t)$  at the same energy for N=10. One can appreciate the excellent agreement, which would only become better as the number of realizations is increased. **Bottom left panel:** Comparison of  $G^{\beta}(t), G^n(t), G^{\ell}(t)$  with parameters  $\beta, E(\beta)$  and  $2\ell = \beta$  at N=6. **Bottom right panel:** Comparison of  $G_c^{\beta}(t), G_c^n(t), G_c^{\ell}(t)$  with parameters  $\beta, E(\beta)$  and  $2\ell = \beta$  at N=6 (inset N=10).

We consider pure states which are superpositions of eigenstates, as one would obtain, e.g. as a result of a sudden quench. An interesting class of such pure states can be constructed as follows. Let  $|\mathcal{C}\rangle$  be a canonical state at half filling. Select a set of  $N_{\mathcal{C}}$  creation operators  $S_{\mathcal{C}} = \left\{c_a^{\dagger}\right\}_{a=1}^{N_{\mathcal{C}}}$ . Then let

$$|\mathcal{C}\rangle = \prod_{i \in S_{\mathcal{C}}} c_i^{\dagger} |\Omega\rangle ,$$
 (2.20)

where  $|\Omega\rangle$  is the state with no fermions. We assumed that N is even and we work at half filling

 $\nu = \frac{N_C}{N} = \frac{1}{2}$ , but such states can be constructed also for odd N and other filling fractions. What is important is that we think of these states at large N as being finitely excited, i.e.  $\nu$  is held fixed as  $N \to \infty$ . Now we define a one-parameter family of pure states via Euclidean evolution of the canonical state,

$$|\ell\rangle = e^{-\ell H}|\mathcal{C}\rangle. \tag{2.21}$$

Such a state can be expanded in the eigenbasis

$$|\ell\rangle = \sum_{\alpha} e^{-\ell E_{\alpha}} c_{\alpha} |E_{\alpha}\rangle$$
 (2.22)

where, according to ETH, the coefficients  $c_{\alpha}$  are Gaussian distributed complex random variables [4]. We expect these states to behave approximately thermally at a temperature  $\beta^{-1}$  that we can determine by the map (2.7), together with the fact that the eigenstates satisfy (1.27). To this end we compute

$$\langle \ell | H | \ell \rangle = \sum_{\alpha,\beta} c_{\alpha}^* c_{\beta} e^{-\ell (E_{\alpha} + E_{\beta})} E_{\alpha} . \tag{2.23}$$

The random nature of the coefficients  $c_{\alpha}$  ensures that this expectation value behaves like a thermal average. We can make this more precise by averaging the expansion coefficients over the eigenstate ensemble [4], using

$$\left[c_{\alpha}^* c_{\beta}\right] = \frac{1}{N_C} \delta_{\alpha\beta} \,. \tag{2.24}$$

With the help of this expression, we find

$$\frac{\langle \ell | H | \ell \rangle}{\langle \ell | \ell \rangle} \longrightarrow \frac{1}{Z(2\ell)} \sum_{\alpha} e^{-2\ell E_{\alpha}} E_{\alpha} , \qquad (2.25)$$

where we have averaged numerator and denominator independently. This quantity is equivalent to the thermal expectation value  $\langle E \rangle_{\beta=2\ell}$  since the state  $|\mathcal{C}\rangle$  typically has support over the whole spectrum. It is thus natural to compare expectation values in  $|\mathcal{C}\rangle$  with thermal expectation values in the canonical ensemble at  $\beta = 2\ell$ . The behavior of these states in a sense is similar to the thermofield double state, with the role of the trace over the second

copy taken over by the random distribution of expansion coefficients. In Fig (2.5) we show the correlation function

$$G^{\ell}(t) = \langle \ell | h_{ij}(t) h_{ij} | \ell \rangle \tag{2.26}$$

and its connected version  $G_c^{\ell}(t)$ , defined in the obvious way, in comparison with the analogous canonical averages. We see that in fact they are rather close to their thermal counterparts at inverse temperature  $\beta = 2\ell$  as expected. Let us next move on to four-point functions, an in particular the issue of chaos in eigenstates.

### 2.4.3 The four-point function

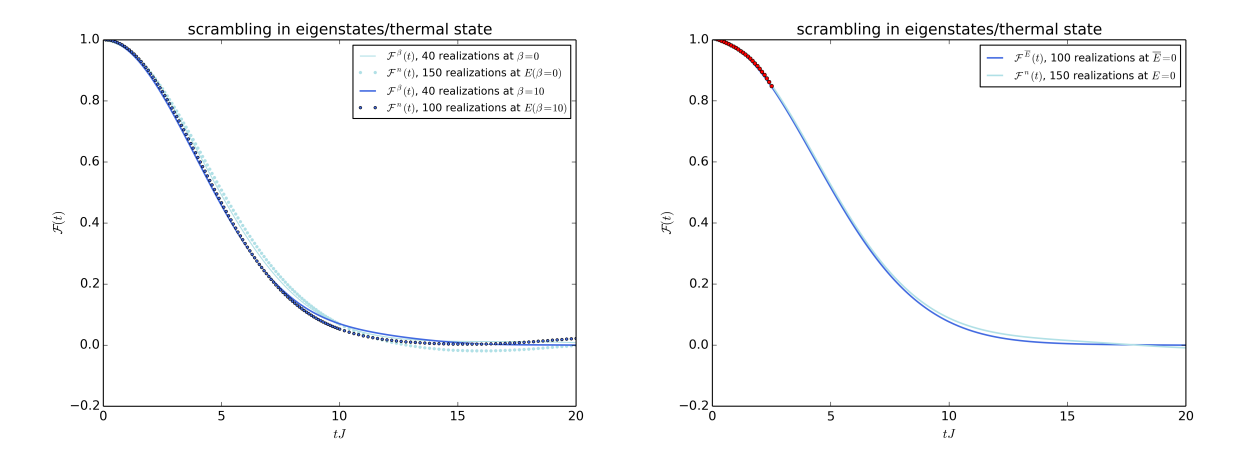


Figure 2.6: Four-point out-of-time order (OTO) correlation function of the hopping operator. **Left panel:** Four-point OTO correlation function in individual eigenstates vs. thermal OTO correlation function at temperature  $\beta(E) = 0,10$  (for N=7). **Right panel:** Four-point OTO correlation function in individual eigenstate  $|n\rangle$  vs. thermal OTO correlation function in the microcanonical ensemble at energy  $\bar{E} = E_n$  (for N=7) with a fit to the functional form (2.8,2.29) for  $\alpha = 0.033...$  and  $\lambda = 0.69...$ .

We now finally turn to studying the four-point function<sup>5</sup> which serves to characterize early time chaos via the Lyapunov exponent  $\lambda_L$  defined in equation (2.6). Again we emphasize that this has been studied extensively in the thermal ensemble [9,11,15,46], while here our main focus is to study it in eigenstates.

<sup>&</sup>lt;sup>5</sup>The results in this section were obtained in collaboration with Jérémie Francfort.

2.5 Discussion 59

We again focus on the two-site hopping operator  $h_{ij}$ . For an SYK model on a grid of size N, let us define two operators

$$W = h_{N-1,N} \qquad V = h_{N-3,N-2} \tag{2.27}$$

together with their out-of-time-order four-point function

$$\mathcal{F}(t) = \frac{\langle W(t)V(0)W(t)V(0)\rangle + \langle V(t)W(0)V(t)W(0)\rangle}{2\langle W(0)W(0)V(0)V(0)\rangle}.$$
 (2.28)

The expectation value is taken, as before, in a finite-energy eigenstate, denoted  $\mathcal{F}^n(t)$ , or for comparison in the (micro-)canonical ensemble, denoted  $\mathcal{F}^{\bar{E}}(t)$ ,  $\mathcal{F}^{\beta}(t)$ , respectively. The expected form (see (2.8)) of this function at times up to the scrambling time is

$$\mathcal{F}(t) = \mathcal{F}_0 - \alpha e^{\lambda t},\tag{2.29}$$

where the coefficient  $\alpha = \beta J/N$  in the canonical ensemble, at strong coupling and large N [15], the same circumstances under which the Lyapunov exponent takes its maximal value  $\lambda = 2\pi/\beta$  [9,15]. For our OTO correlation functions  $\mathcal{F}^{\bar{E}}(t)$ , which well approximates that in the corresponding eigenstate, we show a fit to the form (2.29) in Figure 2.6. Our results here are consistent with those of [46] who considered  $\mathcal{F}^{\beta}(t)$  in exact diagonalization and concluded that at finite N, the Lyapunov exponent is not maximal and does not vary inversely with  $\beta$ , but rather that the parameter governing  $\lambda$  is the coupling J. The behavior of the OTO correlator in eigenstates thus accords very well with expectations from eigenstate thermalization. In particular the early-time physics, including the scrambling time, of this correlator in eigenstates coincide to numerical accuracy with the thermal results. This suggests that the large-N OTO correlator in eigenstates  $\mathcal{F}^{n}(t)$  will also take the form (2.29) with Lyapunov exponent given by (2.8).

### 2.5 Discussion

In the work described in this Chapter we have endeavoured to establish the mechanism of thermalization in the complex spinless SYK model, as a toy model of a strongly correlated quantum system with a holographic dual<sup>6</sup>. We focused on the complex model but, as we will motivate *analytically* in the coming Chapters, the Majorana model exhibits qualitatively similar behavior, that is to say it also satisfies eigenstate thermalization.

We were careful to establish eigenstate thermalization both for an individual random realization - with increasing accuracy as the Hilbert space dimension  $2^N$  is increased – as well as for a fixed Hilbert space dimension at moderate N – with increasing accuracy as one averages over more and more realizations.

We have also studied the extent to which two-point and four point correlations in finite-energy pure states approximate those in the thermal ensemble at the corresponding temperature. Our results support the conclusion that individual eigenstates in the SYK model behave thermally. We established that the agreement between pure and thermal expectation values becomes better for a single realization of the model as N is increased and for a fixed finite N, as we average over a larger and larger ensemble of Hamiltonians. However, consistent with earlier findings [56] we observe that correlation functions are self-averaging at early times, but lose this property at late times. This property is shared by the spectral form factor. Herein lies an important subtlety: a bulk dual<sup>7</sup> of SYK has been proposed for the disorder averaged theory, which means that any bulk solution is strictly dual to an ensemble of boundary Hamiltonians. One should therefore not associate a single eigenstate of an individual realization of the boundary theory with the late-time behavior of a bulk solution. This point does not apply to the tensor models of [23–25]. It should, however, be kept in mind during the rest of the discussion section.

# 2.5.1 Comments on putative bulk dual

Let us now address the question of the interpretation of our results in terms of a putative holographic dual, keeping in mind our previous comments on the status of such a dual. A crucial issue in the holographic description of black holes is the representation of their interior from the boundary theory point of view [71]. One application of our results in this

<sup>&</sup>lt;sup>6</sup>To the extent that such a dual has been established. See [11,12,63–69] for extensive discussions and results on this issue, including an explicit brane construction whose spectrum contains the exact SYK spectrum [69].

<sup>&</sup>lt;sup>7</sup>See previous footnote.

2.5 Discussion 61

respect concerns the relationship between entanglement and geometry [72,73] (see also [74,75] for a world-sheet analog). One may appeal to the approach of [76] to argue that a typical highly entangled eigenstate of the SYK model does not have a dual with a smooth geometrical connection. The argument of [76] uses eigenstate thermalization as a hypothesis to roughly reason as follows. We note that a typical two-sided correlation function in the eternal black hole geometry will be of order  $e^{S}$  at early times, coming from the wormhole connecting the two boundaries [72,73]. One then appeals to the eigenstate expectation values of the form (1.27) to argue that the same operator in a generic highly entangled finite energy state does not have the required  $e^S$  correlations at early time, in fact it is exponentially suppressed. This way one arrives at a contradiction with the assumption that the correlator can be computed in a smooth geometry with a wormhole connection between the two boundaries. Closely related ideas have been advanced in [77]. By establishing eigenstate thermalization in the SYK/NAdS<sub>2</sub> context, one important implication of our work is that a generic highly entangled state of the SYK model either does not have a smooth geometric dual, or that entanglement does not generically correspond to having a geometrical wormhole in the putative bulk dual of SYK. However, without entering into the details, if one allows the state-dependent construction of interior operators by [78], smooth black hole interiors may be constructed.

Of course more directly eigenstate thermalization tells us that one-sided correlation functions look thermal even in eigenstates. This means that correlations in individual eigenstates are well approximated by dual computations in the black hole geometry. Similar results apply in AdS<sub>3</sub>/CFT<sub>2</sub> see e.g. [5,79], where two-point functions of light operators in states created by heavy primary operators were shown to be well approximated by the corresponding results in the BTZ black hole and non-equilibrium initial states thermalize exactly to this state [7,8].

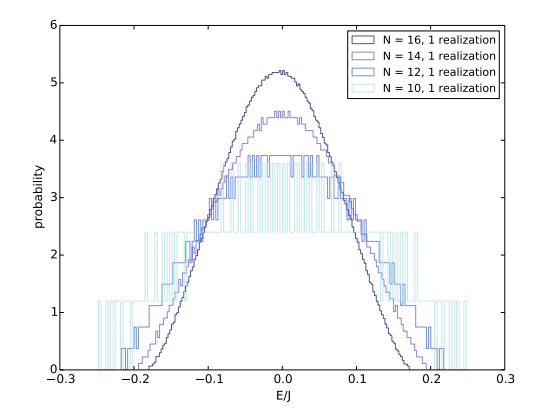
As already alluded, eigenstate thermalization has been discussed also as the mechanism of thermalization in two-dimensional CFT [5,79–81] as well has higher-dimensional cases [80]. In higher dimensions a direct approach, such as in this Chapter, seems out of reach. It would therefore be interesting to gain a more analytical understanding of our results, and we take on this issue in the coming Chapters. It will be interesting to try and carry our results over into a more widely applicable picture of thermalization in theories with holographic duals.

In this respect it may be interesting to map out the applicability of eigenstate thermalization in more SYK-like models, such as [82–85]. Conversely, if one instead accepts that eigenstate thermalization should hold in theories with holographic duals, one might hope to use the constraints on matrix elements due to eigenstate thermalization, in order to further refine the requirements on CFTs with a well-behaved holographic dual.

It is to be expected that the detailed study of thermalization via eigenstates in SYK, both numerically and analytically, gives us a concrete opportunity to better understand the physics of quantum black holes, at least at the level of toy models. We will continue our studies of all these issues in the coming Chapters.

# 2.A Full spectrum & ETH for other operators

This appendix is concerned with filling in some details on the spectrum of the model, as well as to supply more details on eigenstates thermlization for a different non-extensive operator, namely the hopping operator. A careful analysis of the spectral properties of the SYK model



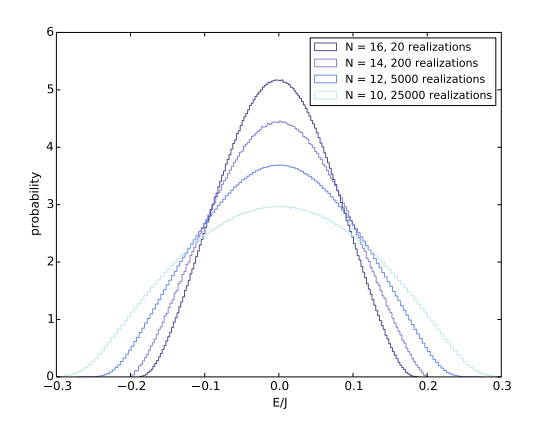


Figure 2.7: Unit normalized histogram of energy eigenvalues (in units of J) in the SYK model for N = 10, 12, 14, 16 sites. This converges to the continuum probability density  $\rho(E)$ . Left panel: spectrum for a single realization. Right panel: spectrum averaged over disorder realizations. We see that already for N = 16 the spectrum for a single realization is essentially indistinguishable from the ensemble average.

was carried out in [?,11,14,55,56]. Here we present some essential features on the complex-spinless case, to set the context, and also to benchmark our numerics. More details are presented in the aforementioned references.

# 2.A.1 Density of states

The full spectrum of the model is most efficiently computed by considering each allowed filling fraction  $\nu$  separately. It is both of interest to consider the spectrum of a single randomly chosen realization as well as averaged over a large number of realizations (see. Figure 2.7). As has been observed before, for the Majorana model, the spectrum self averages very well even for moderate values of N as can be surmised from comparing left and right panels of Figure 2.7.

### 2.A.2 ETH for the hopping operator

Everything we said about thermalization in eigenstates should hold for any non-extensive operator in SYK model. In order to illustrate that this is indeed the case, we collect here some illustrative results for an operator which differs considerably from the on-site number operator, namely the two-site hopping operator.

A further Hermitian operator of interest is the two-site hopping operator  $h_{ij}$ . It is defined by fixing two arbitrary sites i and j and then writing

$$h_{ij} = c_i^{\dagger} c_j + c_j^{\dagger} c_i \,. \tag{2.30}$$

One might think that the simpler operator  $c_i^{\dagger} + c_i$  would also have been a possible choice, but it is easy to see that does not conserve fermion number and so its matrix elements vanish in a fixed fermion sector as considered in this work.

We have extensively studied the matrix elements of the hopping operator, finding that they also satisfy the ETH ansatz. Fig 2.8 illustrates the exponential suppression of off-diagonal matrix elements by an entropy factor. The subtlety for the hopping operator is that its thermal value, i.e. its on-diagonal matrix elements, is actually zero. This is shown in Figure 2.9. As before we carefully distinguish between the behavior of a single randomly chosen SYK Hamiltonian (left panel) and the average over a large number of realizations (right panel).

# 2.B Random matrix theory

In this appendix we collect some results on random matrix theory, which have been referred to occasionally in the main text. These serve as a reference for the behavior of the complex spinless SYK model, which, as we explained, shows RMT-like behavior for some parameter and energy ranges. The RMT results also served as helpful test cases to verify our algorithm with the aid of known results.

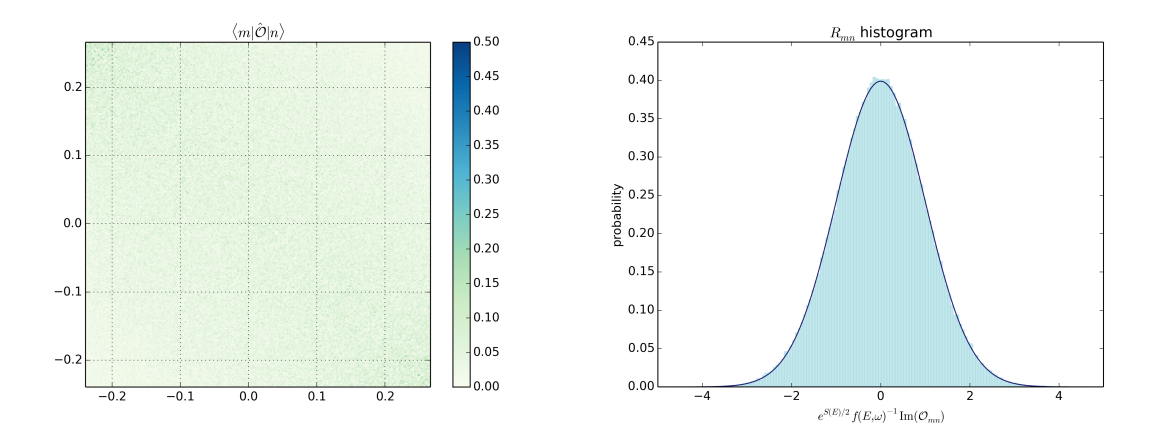


Figure 2.8: Absolute values of matrix elements  $|Q_{nm}| = |\langle n|Q|m\rangle|$  for the two-site hopping operator  $Q = \hat{h}_{N-1,N}$  at half filling  $\nu = \frac{1}{2}$  for a single realization. **Left panel**: we show the absolute values of matrix elements against their energies  $E_n/J$  for N=10, labelled along horizontal and vertical axes. The reason one sees no clear structure along the diagonal is that the thermal expectation value  $\overline{Q}(\overline{E}) \approx 0$  for almost all energies as illustrated below in Figure 2.9. **Right panel**: Histogram of the remainders  $R_{mn}$  for 1000 realizations at N=12. As we see these are accurately fit by a unit width Gaussian with zero mean confirming the ETH ansatz (1.27). Again we have verified this for other accessible values of N.

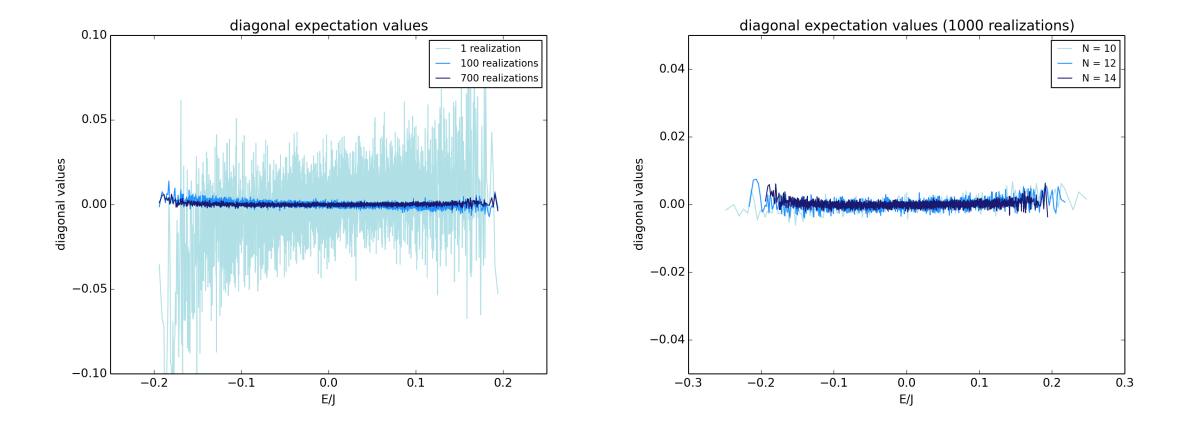
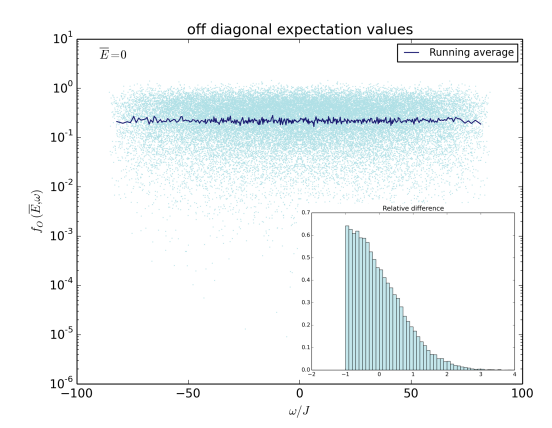


Figure 2.9: Diagonal expectation values for the two-site hopping operator  $h_{N-1,N}$ , at half filling  $\nu = \frac{1}{2}$ . **Left panel**: the effect of averaging of the random couplings at given fixed Hilbert space dimension, N = 14. As expected the on-diagonal values of the ensemble approach closer and closer to a smooth curve. **Right panel**: a single random realization for increasing Hilbert space dimension corresponding to N = 12, N = 14, N = 16. We see that the on-diagonal expectation values of a single realization approaches closer and closer to a smooth curve.



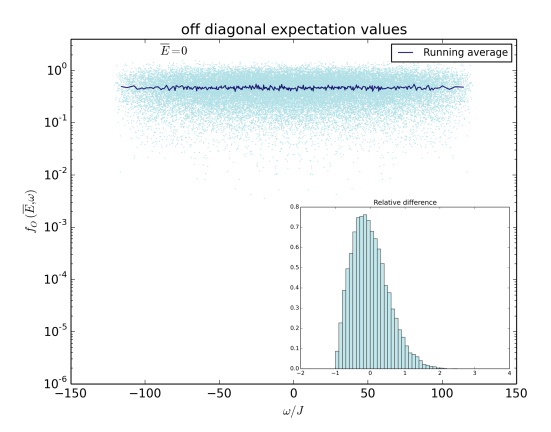


Figure 2.10: Off-diagonal values of matrix elements  $\mathcal{O}_{nm} = |\langle n|\mathcal{O}|m\rangle|$  for a randomly chosen operator  $\mathcal{O}$  in random matrix theory (a GOE matrix on the left and a GUE matrix on the right) averaged over 1000 realizations. The inset shows a histogram of relative differences between raw data and running average (within a selected energy window) **Left panel:** the function  $f_{\mathcal{O}}(\bar{E},\omega)$  (we show the running average in dark blue and the raw data in light blue) in the GOE for Hilbert space dimension  $\dim(\mathcal{H}) = 2^{12}$ . One clearly sees the constancy of  $f_{\mathcal{O}}(\bar{E},\omega)$  in RMT. **Right panel:** the function  $f_{\mathcal{O}}(\bar{E},\omega)$  (we show the running average in dark blue and the raw data in light blue) in the GOE for Hilbert space dimension  $\dim(\mathcal{H}) = 2^{12}$ . One clearly sees the constancy of  $f_{\mathcal{O}}(\bar{E},\omega)$  in RMT.

### 2.B.1 Off-diagonal matrix elements

Let us begin by studying the off-diagonal matrix elements

$$\mathcal{O}_{mn} = \langle m|\mathcal{O}|n\rangle, \qquad m \neq n,$$
 (2.31)

where  $\{|n\rangle\}$  is the set of eigenstates of the RMT Hamiltonian and  $\mathcal{O}$  is itself a randomly selected Hermitian operator. Of course we average all quantities over the RMT ensemble, in practice by taking the average over a large number of individual draws from the ensemble.

# 2.B.2 Spectral form factor

The RMT spectral form factor has recently been studied by various groups [?, 56, 58] as a reference and illustration for certain aspects of the SYK case, which are qualitatively well captured in RMT. For convenience we also present this quantity here, focusing on the GUE.

In RMT, more specifically the GUE, it is actually possible to analytically calculate the

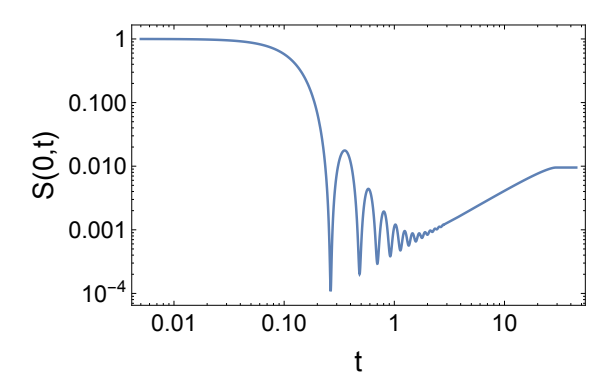


Figure 2.11: Spectral form factor in the GUE of size L = 105 at  $\beta = 0$ . The figure shows a plot of the analytic function (2.33).

spectral form factor [58,59] using the method of orthogonal polynomials. Let L be the Hilbert space dimension, that is to say we consider the ensemble of  $L \times L$  Hermitian matrices. For SYK the Hilbert space dimension was  $2^N$  so, when comparing the two one should obviously set  $2^N = L$ . If we define  $\nu = \beta + it$ , the answer takes the form [58]

$$S(\beta, t) = \frac{g(\beta, t)}{Z(\beta)^2} \tag{2.32}$$

with

$$g(\beta, t) = e^{\frac{1}{4}(\nu^2 + \bar{\nu}^2)} \left( g_c(\beta, t) + g_d(\beta, t) \right) + Z(2\beta). \tag{2.33}$$

The connected part is compactly expressed as

$$g_c(\beta, t) = \sum_{j,k}^{L-1} \left(\frac{\nu}{\bar{\nu}}\right)^{k-j} \left| \psi_{jk} \left( -\frac{\nu^2}{2} \right) \right|^2$$
 (2.34)

with  $\psi_{ij}(x)$  is given in terms of an associated Laguerre polynomial  $\mathsf{L}_i^{j-i}(x)$ 

$$\psi_{ij}(x) = \frac{\Gamma(i+1)}{\Gamma(j+1)} \mathsf{L}_i^{j-i}(x) \tag{2.35}$$

and the disconnected part as

$$g_d(\beta, t) = \left| \mathsf{L}_{L-1}^1 \left( -\frac{\nu^2}{2} \right) \right|^2$$
 (2.36)

in terms of the associated Laguerre polynomial  $\mathsf{L}^1_{L-1}(x)$ . We show a plot of the function

(2.33) in Figure 2.11. One can clearly appreciate the qualitative ressemblance to the SYK case. A detailed discussion of time scales and various power laws can be found in [58].

# ETH in the conformal SYK model

We now present an analytical treatment of some of the questions addressed numerically in the previous Chapter. The material presented here first appeard in [88] and was done in collaboration with Julian Sonner and Pranjal Nayak. We study a version of the SYK model which preserves the reparametrization symmetry at all length scales. We analyze the heavy-light correlation functions of the operators in the conformal spectrum of the theory. The three point functions of such operators allow us to demonstrate that matrix elements of primaries  $\mathcal{O}_n$  of the CFT<sub>1</sub> take the form postulated by the Eigenstate Thermalization Hypothesis. We also discuss the implications of these results for the states in AdS<sub>2</sub> gravity dual.

### 3.1 Introduction

The SYK model, and the tensor-models that have a similar large N behaviour, have an emergent reparametrization symmetry in the infrared limit, [11,14,23-25,48,104]. This emergent symmetry along with the chaotic behaviour of these models has motivated a study of a simpler version of AdS/CFT correspondence between a 1-dimensional quantum mechanical theory and a 2-dimensional theory of gravity that goes by the name  $nAdS_2/nCFT_1$  correspondence, [12,66,67,89,90,104]. There is by now a large corpus of work which studies this class of models, and which applies them: see [28,44] (and the references therein) for recent reviews. A better understanding of the  $nAdS_2/nCFT_1$  duality is important not only as a useful testing grounds to improve our understanding of the AdS/CFT correspondence and, by extension,

quantum gravity in higher dimensions, it also describes the physics of near-extremal black holes in higher dimensions that have a near horizon  $AdS_2$  geometry, [65, 91–97]. A major attraction of the SYK model (and its various cousins) is the ability to solve it analytically<sup>1</sup>, especially in the infrared limit. This offers an opportunity to study the emergence of thermal behaviour in this system analytically.

As we saw in section 1.2.1, the eigenstate thermalization hypothesis provides a way to explain thermalization in a quantum system from a microscopic point of view, [130]. It states that with respect to a 'typical' observable, individual eigenstates already contain all the information of the thermal ensemble. ETH can be encoded in terms of the matrix elements of a 'typical' operator in the energy eigenbasis,

$$\langle m | \mathcal{O} | n \rangle = \bar{\mathcal{O}}_{mc} \left( \bar{E} \right) \delta_{mn} + e^{-S(\bar{E})/2} f(\bar{E}, \omega) R_{mn} \tag{3.1}$$

Here,  $\bar{\mathcal{O}}_{mc}(\bar{E})$  is the expectation value of the operator  $\mathcal{O}$  in a microcanonical ensemble with average energy  $\bar{E}$ ;  $S(\bar{E})$  is the corresponding microcanonical entropy of states with energy  $\bar{E}$ . Therefore, ETH requires that a typical operator be diagonal in the energy eigenbasis in the thermodynamic limit, while the off-diagonal terms are exponentially suppressed. In Random Matrix Theory (RMT), the canonical model of chaos and thermalization in quantum mechanical systems, the off-diagonal matrix elements,  $R_{mn}$ , are randomly chosen from an ensemble with zero mean and unit variance. However, for a more general theory, that is not necessary and could hold a key to understanding how the spectrum of different systems differs from that of RMT, [99].

In the IR limit, where the SYK model can be treated exactly and analytically, a reparametrization symmetry emerges which is broken explicitly by the low-energy modes (pseudo-Nambu-Goldstones) of the model that are popularly known as *Schwarzian modes*. The action for these modes is given in terms of the Schwarzian action,

$$\frac{\alpha}{J} \int d\tau \operatorname{Sch} \left( f(\tau); t \right) , \qquad (3.2)$$

<sup>&</sup>lt;sup>1</sup>The simplicity of the model has also allowed a number of experimental proposals that aim to realise this holographic system in the lab, starting with [18,19]. See also this review [98].

<sup>&</sup>lt;sup>2</sup>In the notation of (3.1) this means  $f_{\text{RMT}}(\bar{E},\omega) = 1$ 

3.1 Introduction 71

where,  $Sch(f(\tau);t)$  denotes the Schwarzian derivative of the function  $f(\tau)$ ,

$$\operatorname{Sch}(f(\tau);t) = \frac{f'''(\tau)}{f'(\tau)} - \frac{3}{2} \left(\frac{f''(\tau)}{f'(\tau)}\right)^2.$$

It is this part of the full SYK action that breaks the reparametrization symmetry explicitly. In this Chapter, we study the correlation functions without the contribution of these low energy modes, whence the correlation functions are the conformal correlation functions. Through the operator-state correspondence a three-point function is related to an operator expectation value measured in energy eigenstates, see section 3.3.1, and can be used to study eigenstate thermalization.

### Summary of results

We find through a study of the three-point functions that the conformal sector of the SYK model thermalizes via the mechanism of ETH. While what we describe here might look like an approximate computation in the SYK theory, a model where this is an exact computation of the correlation functions was discussed in [100]. The corresponding two-dimensional dual theory is a quantum field theory of infinitely many massive scalar fields on the curved AdS<sub>2</sub> manifold. Since such a two-dimensional theory seems to lack gravitational modes, one might not expect to observe black hole formation. However, the observed thermalization we find in our work leads to an interesting question of black hole formation in 2d gravity.

We also discuss the relation of the conformal sector of the SYK model to a generalized free theory (GFT) in one dimension and how our results on eigenstate thermalization in the conformal sector of the SYK model also indicate the same in this GFT. This is a surprising result which we discuss in more detail in section 3.3.3.

In the next Chapter we will study detailed aspects of eigenstate thermalization with the inclusion of the Schwarzian modes.

# Outline of this Chapter

In section 3.2 we revisit the properties of the SYK model that are relevant for our current discussion, summarizing some key properties that we require in this Chapter while referring

the reader to relevant papers or sections within this thesis for details. In section 3.3, we start with a discussion of the spectrum of primary operators in the conformal limit of the SYK model. Then we describe the state-operator correspondence in a 1-dimensional theory and use it to define eigenstates created by insertion of primary operators. Thereby, we study the OPE coefficients in this theory, which are related to matrix elements of a light primary operator in the basis of eigenstates. In the appropriate limit, these OPE coefficients describe eigenstate thermalization in SYK. Later in subsection 3.3.3 we discuss eigenstate thermalization in a generalized free theory in 1-dimensions. We conclude the Chapter with a summary and a plausible bulk interpretation of our results in section 3.4. The appendices contain some supplementary details of the calculations.

# 3.2 Relevant Properties of the SYK system

In this section we summarize the main features of the Sachdev-Ye-Kitaev model relevant for our current analysis. Much of this material is by now well known and was partially introduced in the previous Chapters, but we wish to draw the reader's attention to specific technical aspects we shall make use of later on. We work mainly with the Majorana version of the model generalized to q-body interactions<sup>3</sup>,

$$H = i^{q/2} \sum_{i_1 < i_2 < \dots < i_q \le N} J_{i_1 \dots i_q} \psi_{i_1} \psi_{i_2} \dots \psi_{i_q}.$$
(3.3)

As before, we will focus our attention on the disorder-averaged theory, where the couplings  $J_{i_1...i_q}$  are averaged over a Gaussian random ensemble, with vanishing mean coupling and variance  $\overline{J_{i_1...i_q}^2} = J^2(q-1)!/N^{q-1}$ . The disorder average gives rise to an O(N) invariant theory, where the original q-Fermi interaction is squared to give an invariant 2q-Fermi interaction with coupling strength  $J^2$ ,

$$S = \int \mathcal{D}\psi \mathcal{D}G\mathcal{D}\Sigma \ e^{-S[\psi_i, G, \Sigma]} \,, \tag{3.4}$$

<sup>&</sup>lt;sup>3</sup>Our results apply equally to the complex 'Dirac' model [10] introduced in Chapter 2.

with the averaged action S written in terms of the original fermions, as well as two bilocal fields  $G(\tau, \tau')$  and  $\Sigma(\tau', \tau)$  whose role will become clear shortly,

$$S = \frac{1}{2} \sum_{i} \int d\tau \, \psi_{i}(\tau) \, \frac{\partial}{\partial \tau} \psi_{i}(\tau) - \frac{J^{2}N}{2q} \int d\tau d\tau' \, |G(\tau, \tau')|^{q}$$

$$+ \frac{1}{2} \int d\tau d\tau' \, \Sigma(\tau', \tau) \left( NG(\tau, \tau') - \sum_{i} \psi_{i}(\tau) \psi_{i}(\tau') \right), \qquad (3.5)$$

The Lagrange multiplier field  $\Sigma$  simply imposes the relation

$$G(\tau, \tau') = \frac{1}{N} \sum_{i=1}^{N} \psi_i(\tau) \psi_i(\tau').$$
 (3.6)

The above action arises for the replica diagonal and the replica symmetric solution of the saddle point, [?]. Alternatively, in the large N limit, it can also be obtained by replacing the quenched disorder by an annealed disordered coupling, [11,104]. In the subsequent discussion, we restrict ourselves to replica diagonal and symmetric ansatz which has the dominant contribution, [102].

As we saw in 1.4, this action is quadratic in the fermions, so that we can integrate them out to give rise to the usual Tr log in the action. The result is an action written solely in terms of the bilocal collective fields G and  $\Sigma$ , generating a vertex expansion that can be used to calculate the non-vanishing even-point functions of the fundamental fermions, via the relation (3.6). Note that both the collective fields are anti-symmetric under exchange of the time coordinates,

$$G(\tau, \tau') = -G(\tau', \tau), \qquad \Sigma(\tau, \tau') = -\Sigma(\tau', \tau) . \tag{3.7}$$

### 3.2.1 Vertex expansion

Applying this procedure we obtain the collective field action<sup>4</sup>

$$-\frac{S_{\text{col}}}{N} = \log \operatorname{Pf} \left[ \delta(\tau - \tau') \partial_{\tau} + \Sigma(\tau', \tau) \right] + \frac{J^{2}}{2q} \int d\tau d\tau' |G(\tau, \tau')|^{q} - \frac{1}{2} \int d\tau d\tau' \; \Sigma(\tau', \tau) G(\tau, \tau') \,. \tag{3.8}$$

<sup>&</sup>lt;sup>4</sup>We work in Euclidean signature.

$$\tau_1$$
 $\tau_2$ 
 $\tau_3$ 
 $\tau_4$ 
 $\tau_2$ 
 $\tau_4$ 
 $\tau_4$ 
 $\tau_5$ 
 $\tau_4$ 
 $\tau_5$ 
 $\tau_6$ 
 $\tau_7$ 
 $\tau_7$ 
 $\tau_8$ 
 $\tau_8$ 
 $\tau_9$ 
 $\tau_9$ 

Figure 3.1: Schwinger-Dyson equation for the exact propagator  $\mathcal{G}(\tau_1, \tau_2; \tau_3, \tau_4)$ . For the theory formulated in terms of Majorana fermions this is a four-point function.

The utility of this formulation is that it systematically determines integral (Schwinger-Dyson or 'SD') equations for the 2n-point functions of the fermions, order by order in a 1/N expansion. To this end, let us note that this theory has a semi-classical limit as  $N \to \infty$ , governed by the saddle-point equations

$$\delta(\tau - \tau')\partial_{\tau} + \Sigma(\tau', \tau) - G^{-1}(\tau, \tau') = 0 \tag{3.9a}$$

$$J^{2}G^{q-1}(\tau,\tau') - \Sigma(\tau',\tau) = 0 \tag{3.9b}$$

In order to generate the vertices relevant for the computation of fermion four- and six-point functions, we expand this action around the leading-order solution up to third order in the collective fields

$$\frac{S_{\text{col}}}{N} = S_{(0)} + \frac{1}{N}S_{(2)} + \frac{1}{N^{3/2}}S_{(3)} + \cdots, \tag{3.10}$$

where the term  $S_{(2)}$  contains the two-point vertices in the collective fields and  $S_{(3)}$  the three-point vertices, relevant for four- and six-point functions of the fundamental fermions respectively. More concretely, we follow a two-step procedure. We start by solving the first of the two SD equations to obtain

$$\Sigma(\tau',\tau) = -\delta(\tau - \tau')\partial_{\tau} + G^{-1}(\tau,\tau')$$
(3.11)

which we substitute back into the action to obtain

$$-\frac{S_{\text{col}}}{N} = \log \Pr\left[G(\tau, \tau')\right] + \frac{1}{2} \int d\tau \, \partial_{\tau} G(\tau, \tau') \Big|_{\tau' \to \tau} + \frac{J^2}{2q} \int d\tau d\tau' \, |G(\tau, \tau')|^q \tag{3.12}$$

up to a constant which we have discarded. We then expand  $G = G_0 + \sqrt{\frac{2}{N}} g(\tau, \tau')$  to find the

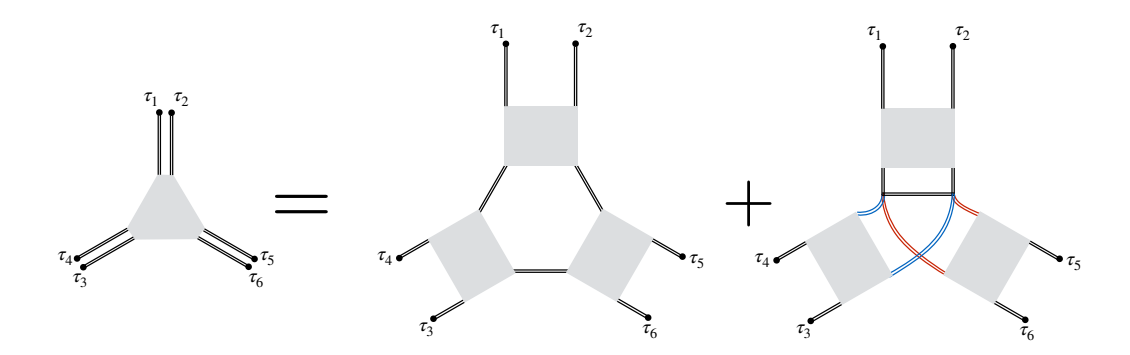


Figure 3.2: Schwinger-Dyson equation determining the three-point vertex  $\mathcal{V}_{(3)}$ . We note that there are two kinds of contributions on the right-hand side, planar ones and non-planar ones. For the theory formulated in terms of Majorana fermions this is a six-point function.

two and three-point vertices, starting with

$$S_{(2)} = \int d\tau_1 d\tau_2 d\tau_3 d\tau_4 \ g(\tau_1, \tau_2) \mathcal{K}_{(2)}(\tau_1, \tau_2; \tau_3, \tau_4) g(\tau_3, \tau_4) \ , \tag{3.13}$$

allowing us to deduce the propagator for the bilocal field

$$\mathcal{G}(\tau_1, \tau_2; \tau_3, \tau_4) = \int_{\tau_2}^{\tau_1} \int_{\tau_4}^{\tau_3} . \tag{3.14}$$

and the Schwinger-Dyson equation shown in Figure 3.1. At the next order we find the three-point vertex

$$S_{(3)} = \int \prod_{i=1}^{6} d\tau_i \, \mathcal{V}_{(3)}(\tau_1, \dots \tau_6) \, g(\tau_1, \tau_2) g(\tau_3, \tau_4) g(\tau_5, \tau_6) \,, \tag{3.15}$$

where, once again the vertex succinctly encodes the Schwinger-Dyson equation shown in Figure 3.2, receiving both planar and non-planar contributions. The precise mathematical expressions for these vertices are somewhat complicated and were originally computed in the papers [48,50,103], and are reproduced in section 3.A. Note that the notation  $\mathcal{K}_{(2)}$  and  $\mathcal{V}_{(3)}$  is supposed to illustrate the fact that we should think of (the inverse of)  $\mathcal{K}$  as a propagator for bilocal fields, while  $\mathcal{V}_{(3)}$  gives a non-trivial three-point interaction vertex between bilocal collective fields.

### 3.2.2 The IR theory & Schwarzian contribution

The discussion of the previous section is correct in the large N limit, for all values of the coupling constant J. However the exact computation of the vertices requires the knowledge of the saddle point solution,  $G_0$  (see (3.46) and (3.48)). The Schwinger-Dyson equations, (3.9), are solvable in the deep infrared limit,  $|\tau|J\gg 1$ , [11,14,48,104]. In this limit, the derivative terms in the action (3.8) and the SD equations (3.9) can be dropped. The resulting effective action (3.8) has a reparametrization (1D conformal) invariance under  $\tau \to f(\tau)$  provided one transforms

$$G(\tau_1, \tau_2) \rightarrow f'(\tau_1)^{\Delta} f'(\tau_2)^{\Delta} G(f(\tau_1), f(\tau_2)) ,$$
  
$$\Sigma(\tau_2, \tau_1) \rightarrow f'(\tau_1)^{1-\Delta} f'(\tau_2)^{1-\Delta} \Sigma(f(\tau_1), f(\tau_2)) .$$
(3.16)

Crucially this is not an invariance of the full action; working perturbatively around the IR limit, the leading action cost associated with a reparametrization  $f(\tau)$  can be determined most efficiently by expanding (3.12) around the IR

$$\frac{1}{2} \int d\tau \, \partial_{\tau} G(\tau, \tau')|_{\tau' \to \tau} = \frac{\alpha}{J} \int \operatorname{Sch} \left( f(\tau); \tau \right) d\tau + \cdots, \tag{3.17}$$

where  $\alpha$  is a coefficient that must be determined by solving the full Schwinger-Dyson equation (3.9), which is typically done numerically, [11,104]. Since this is the leading-order IR effect of breaking reparametrizations, we also refer to the Schwarzian contribution as the soft-mode action. In the current Chapter, we do not consider the effect of this soft-mode action on the correlation functions, which is discussed in next Chapter ??. The exclusion of the Schwarzian modes leads to an exact conformal field theory. A modified version of the SYK model which has an exact conformal symmetry is discussed in [100] and the results we present here are applicable to this modified model as well. In the deep IR limit, where the SYK model has the approximate reparametrization symmetry, its spectrum has a discrete tower of operators that are approximate Conformal Primaries of  $SL(2,\mathbb{R})$ . We discuss the properties and correlation functions of the these operators in the next section. Our discussion follows the earlier work of [48,49,105].

# 3.3 Heavy States in Conformal Three-point Correlators

### 3.3.1 Operators and states

If we exclude the contribution of the Schwarzian mode we obtain an exact conformal field theory whose correlation functions obey the usual constraints imposed by  $SL(2,\mathbb{R})$ . Let us introduce the primary operators

$$\mathcal{O}_{n}(\tau_{1}) = \lim_{\tau_{2} \to \tau_{1}} \frac{1}{\sqrt{N}} \left[ \sum_{k=0}^{2n+1} \sum_{i=1}^{N} d_{nk} \partial^{k} \psi_{i}(\tau_{1}) \partial^{2n+1-k} \psi_{i}(\tau_{2}) \right], \tag{3.18}$$

which obey

$$\langle \mathcal{O}_{m} \mathcal{O}_{n} \rangle = \frac{\delta_{mn}}{|\tau_{n} - \tau_{m}|^{2h}},$$

$$\langle \mathcal{O}_{m} \mathcal{O}_{k} \mathcal{O}_{n} \rangle = \frac{1}{\sqrt{N}} \frac{c_{mkn}}{|\tau_{mk}|^{h_{m} + h_{k} - h_{n}} |\tau_{mn}|^{h_{m} + k_{n} - h_{k}} |\tau_{nk}|^{h_{n} + h_{k} - h_{m}}}$$
(3.19)

with conformal dimensions

$$h_n = 2n + 1 + 2\epsilon_n$$
  $\epsilon_n = \frac{1}{q} \frac{2n^2 + n + 1}{2n^2 + n - 1}$ ,  $n \ge 1$ ,  $q \gg 1$ . (3.20)

Using the 1D version of the operator-state correspondence, about which we have more to say below, we can evaluate the matrix element of an operator  $\mathcal{O}_k$  as a limit of the three-point function,

$$\langle E_m | \mathcal{O}_k | E_n \rangle = \langle \mathcal{O}_m(0) \mathcal{O}(1)_k \mathcal{O}(\infty)_n \rangle = c_{mkn}.$$
 (3.21)

This allows us to focus, as shown, on the OPE coefficient  $c_{mkn}$ . In the limit  $m, n \gg k$ , that is when the operators  $\mathcal{O}_{m,n}$  create heavier states compared to the contribution of the probe operator  $\mathcal{O}_k$ , the OPE coefficients should satisfy the ETH relation, [80],

$$c_{mkn} = f_k(\overline{E})\delta_{mn} + \mathcal{O}\left[e^{-S(\overline{E})/2}\right], \qquad (3.22)$$

<sup>&</sup>lt;sup>5</sup>see the discussion below for the precise notion of heaviness.

where  $f_k(\overline{E})$  is a smooth function of its argument  $\overline{E} = \frac{E_m + E_n}{2}$  and the off-diagonal elements are suppressed by an entropic factor. Our objective is thus to compute the OPE coefficients using the bilocal action introduced above. This will evidently involve the computation of sixpoint functions of the fermions. Before embarking on the computation, we want to emphasize that the operators with  $m, n \gg k$  are not heavy operators in the conventional sense. Usually the term 'heavy' is used to denote the operators whose dimension scales with the number of degrees of freedom of the theory (N for vector theories and  $N^2$  for matrix-like theories). This is consistent with the putative bulk dual description, where only fields massive enough to back-react on the geometry are expected to form black holes. However, the operators that we discuss in this work do not fall in this category. We consider operators whose conformal dimension approaches infinity but does not scale with N. We call these middleweight operators. In higher-dimensional examples of the AdS/CFT correspondence such operators are dual to bulk fields that can be studied in the geodesic approximation, [106, 107], but would not by themselves, lead to the formation of a black hole. In the field theory description, that would mean that the states created by such operators do not thermalize. That we find any form of thermalization for such operators is surprising.

In the following section, we discuss our understanding of the state-operator correspondence in 1-dimension more precisely.

#### Comments on operator-state correspondence

In dimensions  $d \geq 2$  the operator state correspondence relies on the fact that we may conformally map the sphere  $S^d$  to the cylinder  $\mathbb{R} \times S^{d-1}$ , so that asymptotic states at  $\tau = \pm \infty$  on the cylinder map to operator insertions at the north and south poles of the sphere, or equivalently to the origin and the point at infinity of the plane  $\mathbb{R}^d$ . In one dimension this is more subtle, as the analogous map is one between  $S^1$  and  $\mathbb{R} \times S^0$ , which corresponds to the geometry  $\mathbb{R} \times \{0, -\pi\}$ , i.e. two disjoint copies of the real line. This map is realized by setting [?]

$$\sigma + i\tau = 2 \arctan \tanh \left(\frac{i\theta}{2}\right)$$
 (3.23)

so that the two points  $\theta = \pm \pi/2$  are mapped to  $\tau = \pm \infty$ . The segment  $-\pi/2 < \theta < \pi/2$  is mapped to a copy of  $\mathbb R$  at  $\sigma = 0$ , while the remaining half circle  $\pi/2 < \theta < 3\pi/2$  is mapped

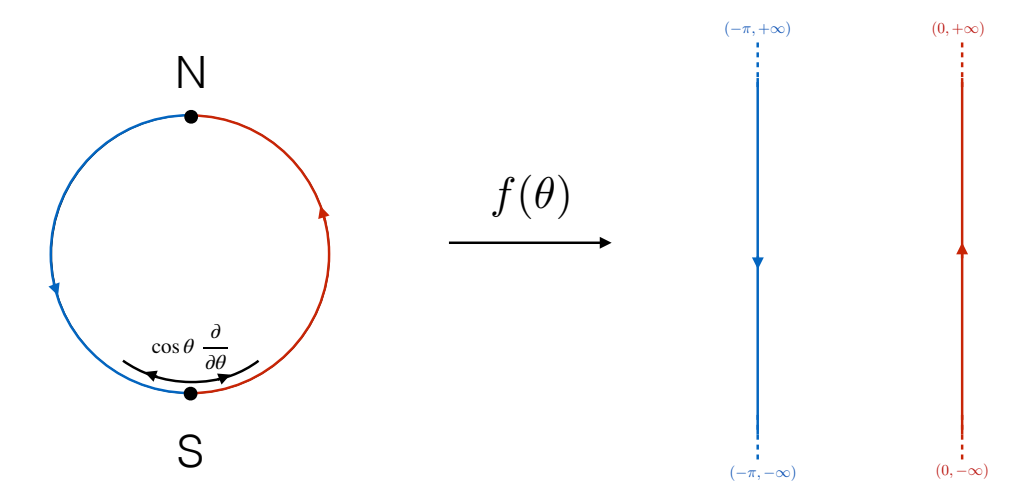


Figure 3.3: The operator-state map in 1D CFT proceeds via the map  $S^1 \to S^0 \times \mathbb{R}$  introduced in Eq. (3.23). The semi circle in red is mapped to one copy of  $\mathbb{R}$  shown in red, situated at  $\sigma = 0$ , while the blue semi-circle is mapped to the blue copy of  $\mathbb{R}$ , situated at  $\sigma = -\pi$ . The Hamiltonian  $\frac{\partial}{\partial \tau}$  is mapped to  $\cos \theta \frac{\partial}{\partial \theta}$  and thus generates radial evolution as shown around the south pole. Modulo the subtlety of mapping to the disconnected  $S^0 \times \mathbb{R}$  this is the analog of radial quantization in higher dimensional CFT.

to a second copy of  $\mathbb{R}$  at  $\sigma = -\pi$ . The generator of time translations is mapped to  $\partial_{\tau} = \cos\theta\partial_{\theta}$ , which corresponds to 1D radial evolution as shown in Figure 3.3. In this way, a correlation function of the type (3.21) creates and probes a state in the doubled Hilbert space  $\mathcal{H}_{\text{CFT}} \otimes \mathcal{H}_{\text{CFT}}$ . This has its manifestation on the bulk side where  $AdS_2$  has a boundary consisting of two disconnected copies of the real line with time running in the same direction on both components.

### 3.3.2 Fermion six-point functions and OPE coefficients

In section 3.2.1 we explained how to generate the Schwinger-Dyson equation determining the six-point function of fermions from the bilocal action. We now proceed to actually evaluate the diagrams in the appropriate limit. As can be seen from Figure 3.2, there are two types of diagrams that contribute, *planar* diagrams and *non-planar* diagrams, also referred to as

contact diagrams. Consequently, also the OPE coefficients can be organized into

$$c_{nkm} = c_{nkm}^{(2)} + c_{nkm}^{(1)}, (3.24)$$

where the first term corresponds to the sum of planar diagrams, and the second to the sum of non-planar diagrams. Consulting the definition of the  $\mathcal{O}_n$  operators (3.18), it becomes clear that the relevant limit of the fermion six-point functions is one where the insertions of the fermions approach each other in pairs. This allows one to use the OPE expansion of the fermions themselves,

$$\frac{1}{N} \sum_{i=1}^{N} \psi_i(\tau_1) \psi_i(\tau_2) \mathcal{O}_m(\tau) = \frac{1}{\sqrt{N}} \sum_{n} c_n \mathcal{C}(\tau_{12}, \partial_{\tau_2}) \mathcal{O}_n(\tau_2) \mathcal{O}_m(\tau), \qquad (3.25)$$

with the result [49]

$$c_{mkn}^{(1)} = c_m c_n c_k b^q (q-1)(q-2) \mathcal{I}_{mkn}^{(1)}$$
(3.26)

$$c_{mkn}^{(2)} = c_m c_n c_k \, \xi_m \xi_n \xi_k \, \mathcal{I}_{mkn}^{(2)} \,. \tag{3.27}$$

Here,  $\mathcal{I}_{mkn}^{(1)}$ ,  $\mathcal{I}_{mkn}^{(2)}$  are certain kinematic integrals arising in evaluating the contact and planar diagrams, respectively. The results of these integrals are given in section 3.C. In the large q limit the  $c_n$  are given by

$$c_n = \epsilon_n \left[ \frac{n(2n+1)}{((2n^2+n+1)(2n^2+n-1))} \frac{\sqrt{\pi}\Gamma(2n_1)}{2^{4n-2}\Gamma(2n+\frac{1}{2})} \right]^{\frac{1}{2}}, \qquad (q \gg 1)$$
 (3.28)

and the  $\xi_n$  are defined as

$$\xi_n = \frac{2n+1}{2n^2+n+1}, \qquad (q \gg 1).$$
 (3.29)

In order to study the thermal properties of middleweight eigenstates, we should take a further limit, this time one where two of the operators, the ones creating the state, are much heavier than the remaining 'probe' operator. We thus want to study the OPE coefficients  $c_{nkm}$  in the limit  $n, m \gg k$ . This will allow us to simplify the corresponding expressions considerably. The first important simplification that occurs is the dominance of planer diagrams over contact diagrams  $c_{nkm}^{(2)} \gg c_{nkm}^{(1)}$ , as we show in detail in section 3.B. We thus focus on  $c_{mkn}^{(2)}$  in the

remainder of this section. For our analysis we find it most convenient to work with the expressions for  $c_{mkn}^{(2)}$  in the large q limit, which was derived in [49], even though more explicit expression have been given later in [105]. The required kinematic integral can be written in the form

$$\mathcal{I}_{mkn}^{(2)} = s_{mkn}^{(2)} \left[ 2 \frac{\epsilon_n^+ + \epsilon_m^-}{\epsilon_n^+ \epsilon_m^-} \frac{\epsilon_m^+ + \epsilon_k^-}{\epsilon_k^+ \epsilon_n^-} \frac{\epsilon_k^+ + \epsilon_n^-}{\epsilon_k^+ \epsilon_n^-} - \frac{1}{\epsilon_m^- \epsilon_k^- \epsilon_n^-} - \frac{1}{\epsilon_m^+ \epsilon_k^+ \epsilon_n^+} \right], \tag{3.30}$$

where  $\epsilon_n^{\pm} = \epsilon_n \pm \Delta$ . Let us further define the variables

$$\sigma = n + m, \qquad d = n - m = \sigma \delta, \tag{3.31}$$

which express the average and difference of energies  $\sigma$  and  $\delta$  in the large m, n limit. Then the expressions for  $s_{mkn}^{(2)}$  take the form of certain, combinatorial coefficients, which for arbitrary k evaluate to

$$s_{mkn}^{(2)} = \mathfrak{g}\left(4k - 2|2k - 2\right) \frac{\Gamma(2\sigma - 1)}{\Gamma(\sigma - d)\Gamma(\sigma + d)},$$
(3.32)

where  $\mathfrak{g}(a|b)$  denotes a rational fraction (of variables  $\sigma, d$ ) of degree a in the numerator and degree b in the denominator. We have tabulated the explicit form of these polynomials for the first few integer values of k in Table 3.1. We next notice that the ratio of Gamma functions is related to a regularized Kronecker delta symbol

$$\mathfrak{b}_{\sigma,\delta} = 2^{-2(\sigma-1)} \sqrt{\pi\sigma} \frac{\Gamma(2\sigma-1)}{\Gamma(\sigma-\sigma\delta)\Gamma(\sigma+\sigma\delta)} \xrightarrow{\sigma \to \infty} \delta_{\delta,0}$$
 (3.33)

The width of the Binomial function, and consequently of the regularized Kronecker delta function<sup>6</sup>, in terms of  $\delta$  is  $1/\sqrt{\sigma}$ , and approaches 0 as  $\sigma \to \infty$ . What this means in terms of the microcanonical ensemble is that we are considering all energy eigenstates within a window  $(\sigma - \sqrt{\sigma}, \sigma + \sqrt{\sigma})$ . Such an interpretation of the microcanonical ensemble is conventional in the literature of Random Matrix theory, see [?]. The limit,  $\sigma \to \infty$  is the right limit to consider for our middleweight operators to be much heavier than the probe operator, and thus it is encouraging to see the Kronecker delta coming out. In fact, as we show now, the off-diagonal elements, corresponding to  $n - m = d \neq 0$ , are suppressed by a factor  $e^{-\sigma \ln 2}$ . In order to extract the on- and off-diagonal functions in the ETH form of the matrix elements (3.21), we

<sup>&</sup>lt;sup>6</sup>See section 3.D for a more in-depth discussion of the regularized Kronecker delta.

$$\begin{array}{c|c} k & s_{mkn}^{(2)} \\ \hline 1 & 2\left(d^2+\sigma^2+\sigma-1\right)\frac{\Gamma(2\sigma-1)}{\Gamma(\sigma-d)\Gamma(\sigma+d)} \\ \hline 2 & \frac{1}{3(2s-2)(2s-3)} \bigg[7d^6+d^4\Big(9\sigma^2+9\sigma-53\Big)+d^2\Big(9\sigma(\sigma+1)\left(\sigma^2+\sigma-7\right)+118\Big) \\ & +(\sigma-1)(\sigma+2)\Big((\sigma^2+\sigma)(7\sigma^2+7\sigma-36)+36\Big)\bigg] \times \frac{\Gamma(2\sigma-1)}{\Gamma(\sigma-d)\Gamma(\sigma+d)} \\ \hline 3 & \bigg[3d^{10}+45d^8\left(\sigma^2+\sigma-17\right)+d^6\Big(10(\sigma^2+\sigma)(5\sigma^2+5\sigma-103)+6459\Big) \\ & +5d^4\left((\sigma^2+\sigma)\left(10\sigma^2+10\sigma\left(\sigma^2+\sigma-22\right)+1681\right)-4887\Big) \\ & +d^2\Big(5(\sigma^2+\sigma)\Big((\sigma^2+\sigma)\left((\sigma^2+\sigma)(9\sigma^2+9\sigma-202)+1638\right)-5804\Big)+40308\Big) \\ & +3(\sigma-2)(\sigma-1)(\sigma+2)(\sigma+3)\Big((\sigma^2+\sigma)\left((\sigma^2+\sigma)(11\sigma^2+11\sigma-157)+600\right)-600\Big)\bigg] \\ & \frac{1}{30(2\sigma-2)(2\sigma-3)(2\sigma-4)(2\sigma-5)} \times \frac{\Gamma(2\sigma-1)}{\Gamma(\sigma-d)\Gamma(\sigma+d)} \\ \vdots & \vdots \end{array}$$

Table 3.1: Table of  $s_{mkn}^{(2)}$  evaluated for some small values of k

may separate out the regularized Kronecker delta from the functions  $c_{nkm}^{(2)}$ , to obtain

$$c_{mkn}^{(2)} = f_{mkn} \mathfrak{b}_{\sigma,d}.$$
 (3.34)

We have now assembled all the ingredients that go into the evaluation of  $f_{mkn}$ . Of course we are only interested in this quantity in the middleweight limit, which allows us to simplify the full expression with the result

$$\lim_{\sigma \to \infty} c_{mkn}^{(2)} = \frac{\Gamma(2k)}{2\sqrt{\Gamma(4k)}} \frac{k}{2k^2 + 2k + 1} \left[ \frac{(2k+1)(2k^2 + k + 1)}{(2k-1)(k+1)} \right]^{3/2} p_k \sigma^{2k} \delta_{m,n} + e^{-\sigma \ln 2} R(\sigma, \delta) .$$
(3.35)

Here  $p_k$  takes values  $\{2, \frac{7}{12}, \frac{33}{480}, \frac{715}{161280}, \ldots\}$ , which are the leading coefficients in Table 3.2. This should be compared to the ansatz (3.22). The result we have just found is precisely of the form appearing in the statement of eigenstate thermalization, with a smooth function depending on the average energy on the diagonal and exponentially suppressed off-diagonal matrix elements depending smoothly on both the average energy as well as the difference.

Isolating the diagonal contribution we find the expression

$$f_k(\overline{E}) = \frac{\Gamma(2k)}{2\sqrt{\Gamma(4k)}} \frac{k}{2k^2 + 2k + 1} \left[ \frac{(2k+1)(2k^2 + k + 1)}{(2k-1)(k+1)} \right]^{3/2} p_k(2E)^{2k}$$
(3.36)

where we have defined the average energy  $\overline{E} = \frac{m+n}{2}$ . We can also use Equation (3.35) in order to obtain an explicit expression for the off-diagonal matrix elements

$$R(\sigma, \delta) = \frac{1}{2} \left( 1 - \delta^2 \right)^{\frac{1}{4}} \frac{\Gamma(2k)}{\sqrt{\Gamma(4k)}} \frac{k}{k^2 + 2k + 1} \left[ \frac{(2k+1)(2k^2 + k + 1)}{(2k-1)(k+1)} \right]^{\frac{3}{2}} \lim_{\sigma \to \infty} \mathfrak{g}(4k - 2|2k - 2)$$
(3.37)

where we show the appropriate  $\lim_{\sigma \to \infty} \mathfrak{g}(4k-2|2k-2)$  in Table 3.2.

k	$\lim_{\sigma \to \infty} \mathfrak{g}\left(4k - 2 2k - 2\right)$
1	$2\sigma^2\left(1+\delta^2\right)$
2	$\frac{1}{12}\sigma^4\left(7\delta^6 + 9\delta^4 + 9\delta^2 + 7\right)$
3	$\frac{1}{480}\sigma^6 \left(33\delta^{10} + 45\delta^8 + 50\delta^6 + 50\delta^4 + 45\delta^2 + 33\right)$
4	$\frac{1}{161280}\sigma^{8}(715\delta^{14} + 1001\delta^{12} + 1155\delta^{10} + 1225\delta^{8} + 1225\delta^{6} + 1155\delta^{4} + 1001\delta^{2} + 715)$
:	:

Table 3.2: Behaviour of  $\mathfrak{g}(4k-2|2k-2)$  in the  $\sigma \to \infty$  limit

Lastly, in the above discussion we showed that the off-diagonal matrix elements of the operator,  $\mathcal{O}_k$ , are suppressed with respect to the diagonal elements by a factor of  $e^{-\sigma \ln 2}$ . In the eigenstate thermalization *hypothesis*, the off-diagonal elements are suppressed exponentially by the microcanonical entropy at the average energy of the ensemble,  $e^{-S(\bar{E})/2}$ . A naive counting of the number of states with energies between  $\left(\bar{E} - \sqrt{\bar{E}}, \bar{E} + \sqrt{\bar{E}}\right)$  gives  $S(\bar{E}) \sim \sqrt{\bar{E}} + \ln(\bar{E})$ . Thus, we find that the observed suppression in the SYK model is stronger than what is required by ETH, together with our estimate  $S(\bar{E})$ . Our suppression although stronger than what is required according to the standard definition of ETH, does not violate the lower bound stemming from the requirement of  $\mathcal{O}(1)$  fluctuations around the thermal value.<sup>7</sup>

<sup>&</sup>lt;sup>7</sup>Requiring typical fluctuations of simple operators to be  $\mathcal{O}(1)$ , off-diagonal terms contribute a sum

### Summary

In this section, we have shown that the states created by the conformal primaries in the IR limit of the SYK model, and more appropriately, in the cSYK model show Eigenstate Thermalization. This result may appear surprising from two different points of view. Firstly, the dimensions of these operators do not scale with the degrees of freedom, N, in our theory (middleweight operators). From the bulk perspective these operators are dual to some fields that are not massive enough to back-react on the  $AdS_2$ , and yet the observed thermalization would suggest that their insertion creates something like a blackhole microstate. It would also be interesting to obtain the exact behaviour for truly heavy operators, i.e. ones that scale with N, whose insertion should change the leading saddle point in the bilocal collective field action (3.12). Note that the result is rather surprising given that the OPE coefficients  $c_{nkm}$  are dominated by the planar contribution, which can be shown to be closely related to those of a Generalized Free Theory. This point merits a more in-depth discussion which we now address.

### 3.3.3 Thermalization in a generalized free theory?

While it is satisfying to have explicitly established the thermality of eigenstates in the conformal sector of the SYK model at large N, our result is puzzling, seeing as it can be reproduced from a certain Generalized Free Theory (GFT). Following [49] let us define the following GFT:

$$S = \frac{1}{2} \sum_{i=1}^{N} \int \frac{d\omega}{2\pi} \chi_i(-\omega) G_{(0)}(\omega)^{-1} \chi_i(\omega) , \qquad (3.38)$$

where  $G_{(0)}(\omega)$  is the Fourier transform of the leading IR solution to the Schwinger-Dyson Equation (3.9),

$$G_{(0)}(\omega) = i\cos(\pi\Delta)\Gamma(1-2\Delta)|\omega|^{2\Delta-1}\operatorname{sgn}(\omega)$$
(3.39)

This theory is free, in the sense that all correlation functions can be obtained simply by Wick contractions, but it has a non-trivial propagator, given by (3.39), and its primaries are given by the same expression (3.18), now written in terms of the generalized free fermions  $\chi_i$ . One over  $e^S$  terms, where  $e^S$  is the dimension of the Hilbert space. Thus each term in the sum is at least  $\mathcal{O}(e^{-S})$ .

can thus obtain the three-point functions of  $\mathcal{O}_n$  operators simply by repeatedly acting with derivatives as specified in the definition (3.18) and then taking the short-time limit. This results in the expression [49]

$$\langle \mathcal{O}_{m} \mathcal{O}_{k} \mathcal{O}_{n} \rangle = \lim_{\tau_{5} \to \tau_{6}} \lim_{\tau_{3} \to \tau_{4} \tau_{1} \to \tau_{2}} \frac{1}{\sqrt{N}} \sum_{r=0}^{2n+1} \sum_{s=0}^{2m+1} \sum_{t=0}^{2m+1} d_{nr} d_{ms} d_{kt} \partial_{1}^{r} \partial_{2}^{2n+1-r}$$

$$\partial_{3}^{s} \partial_{4}^{2m+1-s} \partial_{5}^{t} \partial_{6}^{2k+1-t} \Big[ G(\tau_{1}, \tau_{6}) G(\tau_{2}, \tau_{3}) G(\tau_{4}, \tau_{5}) + \text{perm} \Big]$$

$$= \frac{1}{\sqrt{N}} \frac{c_{mkn}^{free}}{|\tau_{mk}|^{h_{m}+h_{k}-h_{n}} |\tau_{mn}|^{h_{m}+k_{n}-h_{k}} |\tau_{nk}|^{h_{n}+h_{k}-h_{m}}}$$
(3.40)

from which we can extract the OPE coefficients themselves

$$c_{mkn}^{free} = \frac{8 s_{nmk}^{(2)}}{N_n^{free} N_m^{free} N_k^{free}}$$
where,  $(N_n^{free})^2 = \frac{2^{4n+1}}{(2n+1)} \frac{\Gamma(2n+\frac{1}{2})}{\sqrt{\pi} \Gamma(2n)}$ . (3.41)

In the middleweight limit we are interested in, we can determine the ratio of the OPE coefficients in GFT and the SYK model,

$$\lim_{m,n\gg k} \frac{c_{mkn}^{\text{SYK}}}{c_{mkn}^{\text{free}}} = \lim_{m,n\gg k} \left[ 2\left(1 + \frac{\epsilon_m^-}{\epsilon_n^+}\right) \left(1 + \frac{\epsilon_k^-}{\epsilon_m^+}\right) \left(1 + \frac{\epsilon_n^-}{\epsilon_k^+}\right) - 1 - \frac{\epsilon_n^- \epsilon_m^- \epsilon_k^-}{\epsilon_n^+ \epsilon_m^+ \epsilon_k^+} \right]$$

$$= \frac{2k^2 + k + 1}{2k^2 + k - 1} . \tag{3.42}$$

This tells us that our analysis, establishing that the SYK OPE coefficients take a form compatible with the eigenstate thermalization hypothesis, also applies to the OPE coefficients of the GFT. On the face of it, this is very surprising; we usually do not think of free theories with correlation functions given in terms of Wick contractions as resulting in any kind of thermalization. For the specific GFT under consideration here, however, this thermal behaviour results from the interplay of the non-trivial propagator and the combinatorics of the derivatives acting on the simple Wick-type six-point functions of the  $\chi_i$  fermions. A similar analysis for a similar class of operators that were studied in [108] for a 2-dimensional CFT is discussed section 3.E. In that study of the OPE coefficients we find lack of ETH like behaviour. The ETH behaviour for the generalized free theory described above is in some

sense reminiscent of the thermal (chaotic) looking physics of the D1-D5 CFT at the orbifold point [109], which is a free theory, albeit one with a complicated spectrum of operators. As a sanity check, one can quickly convince oneself that the limit in which the GFT actually becomes the theory of free fermions ( $\Delta = 0$ ), gives a vanishing three-point function, so we are saved from the conclusion that a theory of free fermions shows ETH itself.

# 3.4 Summary and Discussion

We have studied here the 3-point correlation functions of the 'excited' operators, given by (3.18), that arise in the IR limit of the SYK model. In our analysis, we did not consider the contribution of the pseudo-Nambu-Goldstone (Schwarzian) modes to these correlation functions. We argued that through a state-operator correspondence in a 1-dimensional theory, the OPE coefficients that appear in the three point function can be interpreted as matrix elements of an operator in the energy eigenbasis. By comparing these matrix elements in the thermodynamic limit with the expected behaviour (3.1), we showed that in this sector (without the contribution of the Schwarzian modes) the model shows eigenstate thermalization. This is apparent from (3.35), where the expectation value of operator  $\langle m | \mathcal{O}_k | n \rangle$  was studied in high-energy states,  $m, n \gg k \sim \mathcal{O}(1)$  and it was argued that the operator becomes diagonal in this limit. We also computed the exponential suppression of the off-diagonal terms. While our naive counting of microcanonical entropy at energy  $\bar{E}$  gives  $S(\bar{E}) \sim \sqrt{\bar{E}} + \ln(\bar{E})$ , we find a suppression by a factor of  $\sim e^{-\bar{E}}$  which is stronger than  $e^{-S(\bar{E})}$ . This suggests that our estimate of the microcanonical entropy might be too naive, or that the off-diagonal terms are indeed more strongly suppressed than is required for ETH. In any case, we do not expect the microcanonical entropy to grow faster than E.

### Perspectives

Our current investigation has left us with some open questions that ask for a better understanding. Above, we have discussed our lack of understanding of the density of middleweight states. This is important to understand the suppression of the off-diagonal terms compared to the diagonal terms. A better understanding of these terms would be useful in understanding

the departure of the model from the RMT behaviour, [99].

It would be interesting to study the correlation functions of the truly 'heavy' operators (whose conformal dimension scales with N) in the conformal sector of the theory. Explicit computations involving such operators are often hard from the field theory point of view, and very little is known about such operators even in  $\mathcal{N}=4$  super-Yang-Mills (sYM) theory. It might be possible that correlation functions of such operators are computable in the SYK model, having the potential to shed some light on tools that could be used to do a similar computation for  $\mathcal{N}=4$  sYM.

In this Chapter we focused on the field theoretic study the SYK model in the conformal limit of the theory. The 2-dimensional dual, without the inclusion of the Schwarzian modes, is a theory of massive scalars on AdS<sub>2</sub> background. It would be interesting to understand this observed thermalization from the bulk perspective in this non-gravitating theory of 2-dimensional gravity. A related question is to understand the chaotic behaviour of correlation functions in the cSYK theory, both from the field theoretic as well as the gravitational point of view. In the current understanding, the origin of chaotic behaviour in SYK model lies in the exchange of Schwarzian modes, [11, 104], which we will now study in our next Chapter.

### 3.A Collective field action

In this section we discuss the collective field action, (3.10). We derive the vertices of this action in an 1/N expansion around the solution of the replica diagonal and replica symmetric solution,  $G_0(\tau_1, \tau_2)$ , of the saddle point equations, (3.9).<sup>8</sup> Using the expansion,

$$G(\tau_1, \tau_2) = G_0(\tau_1, \tau_2) + \sqrt{\frac{2}{N}}g(\tau_1, \tau_2) ,$$
 (3.43)

in (3.12),

$$-\frac{S_{\text{col}}}{N} = \log \Pr\left[G(\tau, \tau')\right] + \frac{1}{2} \int d\tau \, \partial_{\tau} G(\tau, \tau') \Big|_{\tau' \to \tau} + \frac{J^2}{2q} \int d\tau d\tau' \, |G(\tau, \tau')|^q \tag{3.44}$$

we get,

$$S_{(2)} = \frac{1}{2} \int d\tau_1 d\tau_2 d\tau_3 d\tau_4 \ g(\tau_1, \tau_2) \left[ G_0^{-1}(\tau_1, \tau_3) G_0^{-1}(\tau_2, \tau_4) -3J^2 G_0^2(\tau_1, \tau_2) \delta(\tau_3 - \tau_1) \delta(\tau_2 - \tau_4) \right] g(\tau_3, \tau_4) \ . \tag{3.45}$$

Comparing it with, (3.13), we get,

$$\mathcal{K}_{(2)}(\tau_1, \tau_2; \tau_3, \tau_4) = G_0^{-1}(\tau_1, \tau_3)G_0^{-1}(\tau_2, \tau_4) - 3J^2G_0^2(\tau_1, \tau_2)\delta(\tau_3 - \tau_1)\delta(\tau_2 - \tau_4) . \tag{3.46}$$

Similarly, studying the fluctuations to the next order in 1/N, one can compute the cubic interactions in the action,

$$S_{(3)} = \sqrt{2} \int d\tau_1 \dots d\tau_6 \ g(\tau_1, \tau_2) g(\tau_3, \tau_4) g(\tau_5, \tau_6) \left[ -\frac{1}{3} G_0^{-1}(\tau_6, \tau_1) G_0^{-1}(\tau_2, \tau_3) G_0^{-1}(\tau_4, \tau_5) -J^2 G_0(\tau_1, \tau_2) \delta(\tau_3 - \tau_1) \delta(\tau_4 - \tau_2) \delta(\tau_5 - \tau_1) \delta(\tau_6 - \tau_2) \right]. (3.47)$$

<sup>&</sup>lt;sup>8</sup>In addition to the replica diagonal saddle point solutions, we are also considering replica diagonal and symmetric fluctuations which are known to contribute dominantly, [102].

Once again, comparing with (3.15) gives us,

$$\mathcal{V}_{(3)}(\tau_1, \dots, \tau_6) = -\sqrt{2} \left[ \frac{1}{3} G_0^{-1}(\tau_6, \tau_1) G_0^{-1}(\tau_2, \tau_3) G_0^{-1}(\tau_4, \tau_5) + J^2 G_0(\tau_1, \tau_2) \delta(\tau_3 - \tau_1) \delta(\tau_4 - \tau_2) \delta(\tau_5 - \tau_1) \delta(\tau_6 - \tau_2) \right]. \tag{3.48}$$

# 3.B Dominance of Planar diagrams

In this section we demonstrate the dominance of planar diagrams over the contact diagrams in the limit in which two of the three insertions are much heavier than the third one. In Figure 3.4 we plot the OPE coefficients,  $c_{mkn}^{(1)}$  and  $c_{mkn}^{(2)}$ , ((3.26), (3.27)) for m = n, and some small values of k to demonstrate this dominance.

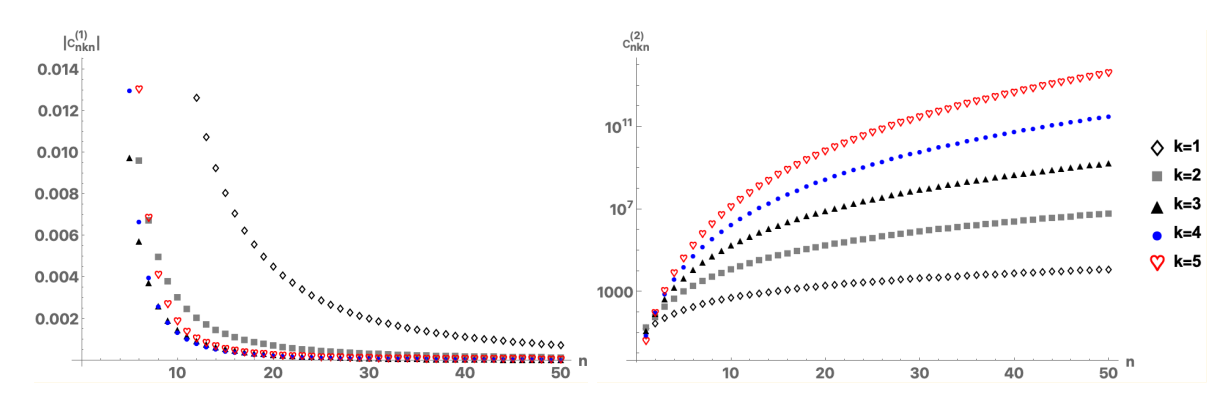


Figure 3.4: **Left:** Diagonal values of the OPE coefficients  $c_{mkn}^{(1)}$  become smaller as we take the limit  $m, n \gg k$ . **Right:** Diagonal values of the OPE coefficients  $c_{mkn}^{(2)}$  become larger as we take the limit  $m, n \gg k$ , thereby demonstrating the dominance of contact diagrams over the planar diagrams in this limit. Note that the y-axis of the right figure is plotted on a logarithmic scale.

In Figure 3.5, we plot the ratio of the coefficients,  $|c_{m1n}^{(1)}|/c_{m1n}^{(2)}$ . This ratio is sufficiently small even for finite m, n. This plot also shows the suppression of the off-diagonal OPE coefficients corresponding to contact diagrams.

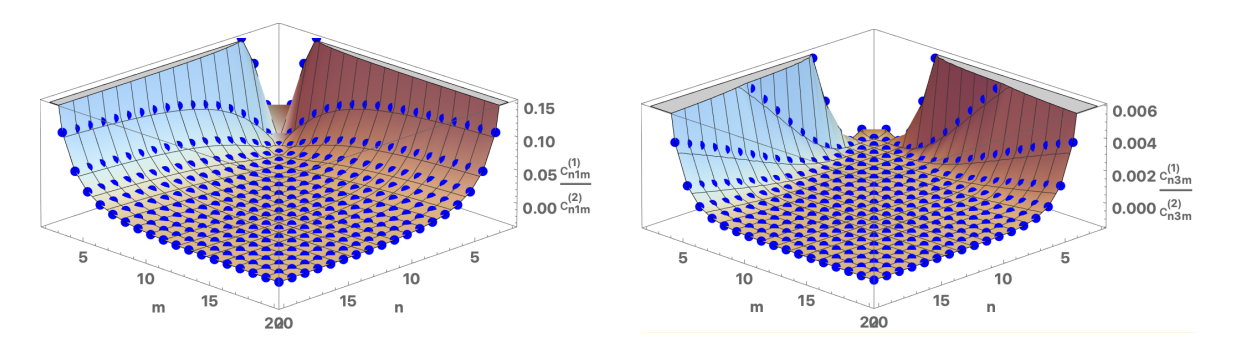


Figure 3.5: **Left:** The ratio  $\left|c_{m1n}^{(1)}\right|/c_{m1n}^{(2)}$  is largely suppressed even for k=1 as m or n are increased. **Right:** Increasing k accentuates the supression even further (here k=3).

# 3.C Expressions for $\mathcal{I}_{mkn}^{(1)}$ and $\mathcal{I}_{mkn}^{(2)}$

The exact expressions for  $\mathcal{I}_{mkn}^{(1)}$  and  $\mathcal{I}_{mkn}^{(2)}$  were derived in [105]. However, to avoid clutter and for the sake of intuition, we work with the corresponding expressions in the  $q \gg 1$  limit. In what follows, the notation  $\mathcal{I}_{123}$  is used to refer to the term arising from a three-point function of operators of dimension  $h_1, h_2$  and  $h_3$ , i.e.  $\mathcal{I}_{123} \equiv \mathcal{I}_{h_1h_2h_3} \neq \mathcal{I}_{m=1,k=2,n=3}$ .

For  $q \gg 1$ , the dimensions of the  $\mathcal{O}_n$  approach their free-field values, 2n + 1,

$$h_n = 2n + 1 + 2\epsilon_n$$
,  $\epsilon_n = \frac{1}{q} \frac{2n^2 + n + 1}{2n^2 + n - 1}$ ,  $n \ge 1$ ,  $q \gg 1$ , (3.49)

while the OPE coefficients in the large q limit behave as,

$$c_n^2 = \epsilon_n^2 \frac{n(1+2n)}{(n(1+2n)+1)(n(1+2n)-1)} \frac{\sqrt{\pi}\Gamma(2n+1)}{\Gamma(2n+\frac{1}{2})2^{4n-2}} , \qquad q \gg 1 .$$
 (3.50)

The contact diagram contribution to the three-point function  $\langle \mathcal{O}_1 \mathcal{O}_2 \mathcal{O}_3 \rangle$  has a coefficient that was denoted by  $c_{123}^{(1)}$ , given as  $c_{123}^{(1)} = c_1 c_2 c_3 \mathcal{I}_{123}^{(1)}$  (see (3.26)), where an exact expression for  $\mathcal{I}_{123}^{(1)}$  can be found in [105]. Using (3.49), an expression for  $\mathcal{I}_{123}^{(1)}$  in the  $q \to \infty$  limit is given by, [49],

$$\mathcal{I}_{123}^{(1)} = 2s_{123}^{(1)} \frac{\epsilon_1 + \epsilon_{n_2} + \epsilon_{n_3}}{\epsilon_{n_1} \epsilon_{n_2} \epsilon_{n_3}} , \quad q \gg 1 , \qquad (3.51)$$

where  $s_{123}^{(1)}$  is,

$$s_{123}^{(1)} = (-4)^{n_1 + n_2 + n_3} \frac{\Gamma(\frac{1}{2} + n_2 + n_3 - n_1)\Gamma(\frac{1}{2} + n_1 + n_3 - n_2)\Gamma(\frac{1}{2} + n_1 + n_2 - n_3)\Gamma(1 + n_1 + n_2 + n_3)}{\pi^{\frac{3}{2}}\Gamma(1 + 2n_1)\Gamma(1 + 2n_2)\Gamma(1 + 2n_3)}.$$
(3.52)

The planar diagram contribution to the three-point function has a coefficient that was denoted by  $c_{123}^{(2)}$ , given in (3.27) as  $c_{123}^{(2)} = c_1c_2c_3\xi(h_1)\xi(h_2)\xi(h_3)\mathcal{I}_{123}^{(2)}$ . To avoid clutter, let us define,

$$\epsilon^{\pm} = \epsilon \pm \Delta \quad , \tag{3.53}$$

in terms of which, the factor  $\xi(h_n)$  simplifies to,

$$\xi(h_n) = \frac{\epsilon^-}{\epsilon_n} \left( n + \frac{1}{2} \right) , \qquad q \gg 1 , \qquad (3.54)$$

while the expression for  $\mathcal{I}_{123}^{(2)}$  is the  $q \to \infty$  limit is,

$$\mathcal{I}_{123}^{(2)} = s_{123}^{(2)} \left( 2 \frac{(\epsilon_1^+ + \epsilon_2^-)(\epsilon_2^+ + \epsilon_3^-)(\epsilon_3^+ + \epsilon_1^-)}{\epsilon_1^+ \epsilon_1^- \epsilon_2^+ \epsilon_2^+ \epsilon_3^-} - \frac{1}{\epsilon_1^+ \epsilon_2^+ \epsilon_3^+} - \frac{1}{\epsilon_1^- \epsilon_2^- \epsilon_3^-} \right) , \quad q \gg 1 , \quad (3.55)$$

with  $\epsilon_i \equiv \epsilon_{n_i}$ , and  $s_{123}^{(2)}$  is,

$$s_{123}^{(2)} = \frac{(2n_1 + 2n_2 - 2n_3)!(2n_2 + 2n_3 - 1)!}{(2n_1 - 1)!(2n_2 - 1)!(2n_3 - 1)!(1 + 2n_2 - 2n_3)!} \times {}_{4}F_{3} \begin{bmatrix} 1 - 2n_1 & 2 + 2n_1 & 1 - 2n_3 & -2n_3 \\ 2 & 1 - 2n_2 - 2n_3 & 2 + 2n_2 - 2n_3 \end{bmatrix}; 1 \end{bmatrix},$$
(3.56)

where it is assumed that  $n_1 > n_2 > n_3$ . Using the definition of  ${}_4F_3$ , this may be written as a single finite sum. Equation (3.55) was found by Gross and Rosenhaus in [49] without taking the large q limit of the exact answer, but rather by evaluating the integral  $I_{123}^{(2)}$  to leading order in 1/q. They noted that  $s_{123}^{(2)}$  is the same expression that appears in computing the three-point function in a generalized free field theory with fermions of dimension  $\Delta$ , in the

limit  $\Delta \to 0$ . Specifically,

$$s_{123}^{(2)} = -\sum_{p_1, p_2, p_3} {2n_1 \choose p_1} {2n_2 \choose p_2} {2n_3 \choose p_3} {2n_1 + p_2 - p_1 \choose p_2 + 1} {2n_2 + p_3 - p_2 \choose p_3 + 1} {2n_3 + p_1 - p_3 \choose p_1 + 1} \times \frac{z^{p_1 - p_2 + 2n_2 - 2n_3}}{(-1 - z)^{p_3 - p_2 + 2n_1 - 2n_3}},$$
(3.57)

where z is a cross ratio of times; the answer is independent of z. While it is not manifest that (3.56) and (3.57) are the same, one can verify that they are.

# 3.D Regularised Kronecker delta function

Here, we discuss some of the properties of the regularized Kronecker delta function, in particular the exponential suppression of the off-diagonal components. Recall,

$$\mathfrak{b}_{\sigma,\delta} = 2^{-2(\sigma-1)} \sqrt{\pi\sigma} \frac{\Gamma(2\sigma-1)}{\Gamma(\sigma-d)\Gamma(\sigma+d)} \xrightarrow{\sigma \to \infty} \delta_{d,0} . \tag{3.58}$$

Figure 3.6 shows the behaviour of the function for increasing values of  $\sigma$ , after using (3.31). Notice, that the width of the plot decreases for increasing values of  $\sigma$ . The variable  $\delta \in [-1, 1]$ 

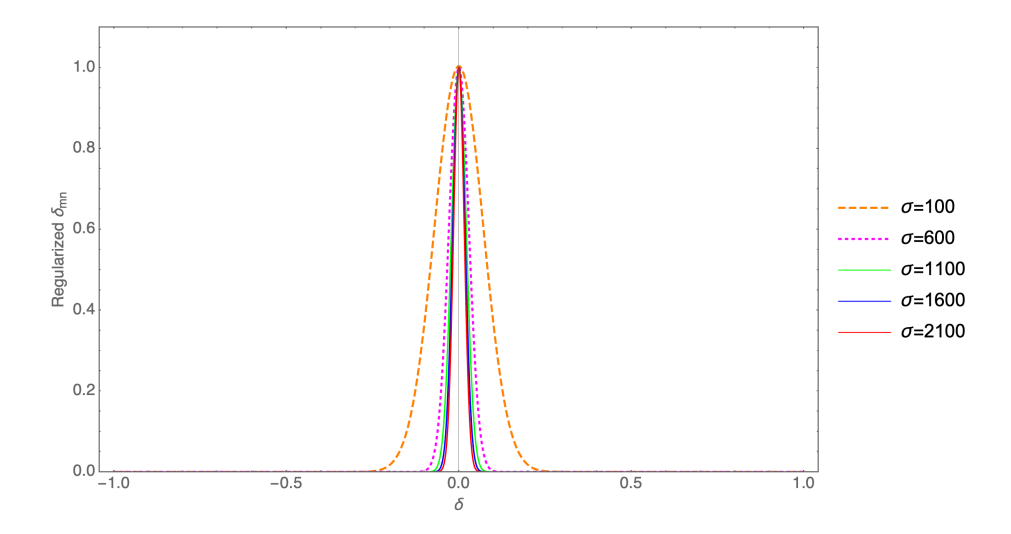


Figure 3.6: The function in (3.58) evaluated for various values of  $\sigma$ .

because the function on the LHS of (3.58),  $\mathfrak{b}_{\sigma,\delta}$ , is not well defined outside this interval.

However, we can define the function to be zero outside this interval. Let us next approximate the value of the function away from the peak. We do this by expanding  $\mathfrak{b}_{\sigma,\delta}$  around,  $\delta = 1$ :

$$\mathfrak{b}_{\sigma,\delta} \sim 4^{-\sigma} \left[ 1 + (\delta - 1)\sigma \left( \log \left( \frac{1 - \delta}{2} \right) - 1 \right) + \mathcal{O} \left( (1 - \delta)^2 \right) \right]$$
 (3.59)

Clearly the value of the function is suppressed exponentially for large values of  $\sigma$ .

### 3.E Lack of ETH in Free fields

In [108], operators of the kind,

$$O_k = \partial^k T \partial^k T : , (3.60)$$

were considered in a 2-dimensional conformal field theory. Here, T is the stress tensor of the theory. The OPE coefficients for operators of this kind were computed there and was found to be,

$$c_{k_1k_2k_3} = \sqrt{8} \frac{(k_1 + k_2 + 3)!(k_2 + k_3 + 3)!(k_3 + k_1 + 3)!}{(2k_1 + 3)!(2k_2 + 3)!(2k_3 + 3)!},$$
(3.61)

where,  $c_{k_1k_2k_3}$  is the OPE coefficient between the operators  $O_{k_1}$ ,  $O_{k_2}$  and  $O_{k_3}$ . To see if this shows ETH behaviour, (3.22), let us factor out the regularised Kronecker  $\delta$ -function, (3.33). Then in the  $k_1, k_3 \to \infty$  limit, we get,

$$c_{k_1 k_2 k_3} \approx \frac{\sqrt{\pi} 2^{-2k_2 - \frac{3}{2}} \left(4 - \delta^2\right)^{k_2} \sigma^{2k_2 + \frac{7}{2}}}{(1 - \delta^2)^{\frac{1}{2}} \Gamma(2k_2 + 4)} \times \left(\frac{\left(1 - \delta^2\right) \left(\frac{1 - \delta}{1 + \delta}\right)^{-\delta} \left(\frac{2 - \delta}{2 + \delta}\right)^{\delta/2}}{4 - \delta^2}\right)^{\sigma} \mathfrak{b}_{\sigma, \delta} . \tag{3.62}$$

Here, once again we have used  $k_1 + k_3 = 2\sigma$  and  $k_3 - k_1 = d = \sigma\delta$ . Note that unlike in (3.35), the function multiplying the regularised Kronecker  $\delta$ -function is exponential in  $\sigma$ . In fact, for diagonal elements corresponding to  $\delta = 0$ , this function is proportional to  $e^{-2\sigma \ln 2}$ . Consequently, as  $\sigma \to \infty$ , the diagonal elements vanish, thereby demonstrating lack of ETH-like behaviour.

# Extended eigenstate Thermalization in the Schwarzian theory

In this Chapter, based on [?], a work done in collaboration with Pranjal Nayak and Julian Sonner, we provide a universal description of the behavior of the basic operators of the Schwarzian theory in pure states. When the pure states are energy eigenstates, expectation values of non-extensive operators are thermal. On the other hand, in coherent pure states, these same operators can exhibit ergodic or non-ergodic behavior, which is characterized by elliptic, parabolic or hyperbolic monodromy of an auxiliary equation; or equivalently, which coadjoint Virasoro orbit the state lies on. These results allow us to establish an extended version of the eigenstate thermalization hypothesis (ETH) in theories with a Schwarzian sector. We also elucidate the role of FZZT-type boundary conditions in the Schwarzian theory, shedding light on the physics of microstates associated with ZZ branes and FZZT branes in low dimensional holography.

## 4.1 Introduction

The Schwarzian theory, namely the theory defined by the path integral

$$\int \mathcal{D}\mu(f)e^{C\int\{f(\tau),\tau\}d\tau} \tag{4.1}$$

where  $\{f;\tau\}^1$  is the Schwarzian derivative and  $\mathcal{D}\mu(f)$  is the appropriate measure on Diff $(S^1)$ , plays a key role in various different developments in low-dimensional holography. It appears as the low-energy description [11] of the SYK model [13,104], as well as related tensor models [23,24,111]. It can also be shown [12,66,67,89] to arise in two-dimensional gravity theories, notably in the JT model [63,64]. Furthermore it allows one to establish results on thermal properties of eigenstates and more general pure states in 2D CFT [7,8,45,112–117]. In all these situations the appearance of the Schwarzian is intimately related to conformal (Virasoro) symmetry and its breaking [11,66,101,104]: an action of the type (4.1) arises as the universal description of such effects in all instances mentioned.

In this final Chapter we provide a universal description of the behavior of the basic operators of the Schwarzian theory in pure states. The philosophy behind our exploration of such effects is again encapsulated in the eigenstate thermalization hypothesis (ETH).

Returning to the case at hand, namely theories of the type (4.1) we find that their basic operators – the bilocals  $\mathcal{O}(\tau_1, \tau_2)$  – can have ergodic and non-ergodic behavior, i.e. they either approximate thermal ensembles well, or fail to thermalize, akin to the known behavior across a chaotic-integrable transition. Which behavior ensues depends on the parameters of the theory as well as the state, but is universally classified by elliptic, parabolic and hyperbolic monodromy, (or equivalently, which coadjoint Virasoro orbit the state lies on).

This allows us to establish an extended version of the eigenstate thermalization hypothesis (ETH) [45,116] which includes the usual notion of ETH for simple operators, and extends it to more complex operators, in particular including out-of-time-order correlation functions (OTOCs)<sup>2</sup>. Our argument proceeds along two closely related lines: firstly we give semiclassical arguments directly in the Schwarzian theory, based on the relationship between (4.4) and the coadjoint orbit theory [120,121]. Secondly we use the relationship between two-dimensional boundary Liouville theory and the Schwarzian theory to provide *exact* results, whose semi-classical expansion coincides with the previous analysis. A crucial novel ingredient in our story is the inclusion of effects of FZZT branes [122,123] in the Liouville description, which descend to certain coherent states in the Schwarzian, as we shall explain. Effects of

<sup>&</sup>lt;sup>1</sup>Note that we have also used the notation  $Sch(f,\tau)$  to denote the same operator.

<sup>&</sup>lt;sup>2</sup>For an argument leading to a similar notion of extended ETH from the point of view of black-hole interiors, see [119].

4.1 Introduction 97

this type have been pointed out to arise in the study of the late-time behavior of a certain matrix model designed as a topological completion of JT gravity [124]. In this context FZZT type states are related to the late-time ramp behavior seen, for example, in the spectral form factor [56,58,125,126]. As we show here, these same effects are also seen to play an important role in understanding ETH in theories of the type (4.1).

This Chapter is structured as follows: the rest of this introduction consists of a summary of the main results presented here. Section 4.2 describes how to construct the Schwarzian path integral from two-dimensional Liouville theory. This kind of construction was previously exploited in [113,127], but we extend it here to include more general boundary conditions that allow us to deal with a general class of pure states. In section 4.3 we then analyze the semiclassical limit of the correlation functions of interest and in particular provide a general proof that the heavy pure states of interest scramble as efficiently as the thermal ensemble, a result we refer to as extended ETH. Finally, section 4.4 makes full use of the construction of the Schwarzian theory in terms of boundary Liouville CFT to write down exact quantum expressions for the various pure-state expectation values considered in section 4.3. We also demonstrate that the exact expressions agree with semiclassics when expanded in that limit. We finally discuss our results and provide a perspective on open issues in the Conclusions section.

## 4.1.1 Summary of results

One of the main goals of the work presented here is to establish results for correlation functions in pure states

$$\operatorname{Tr}\left[\rho_{\Psi} \mathcal{O}_{\ell_{1}}(\tau_{1}, \tau_{1}') \cdots \mathcal{O}_{\ell_{n}}(\tau_{n}, \tau_{n}')\right], \qquad \rho_{\Psi} = |\Psi\rangle\langle\Psi| \tag{4.2}$$

where  $|\Psi\rangle$  is either an eigenstate of the Schwarzian theory

$$H|E(k)\rangle = \frac{k^2}{2C}|E(k)\rangle, \qquad (4.3)$$

or a pure coherent state of the type

$$|E_r\rangle \sim e^{r\mathcal{V}}|E\rangle$$
 (4.4)

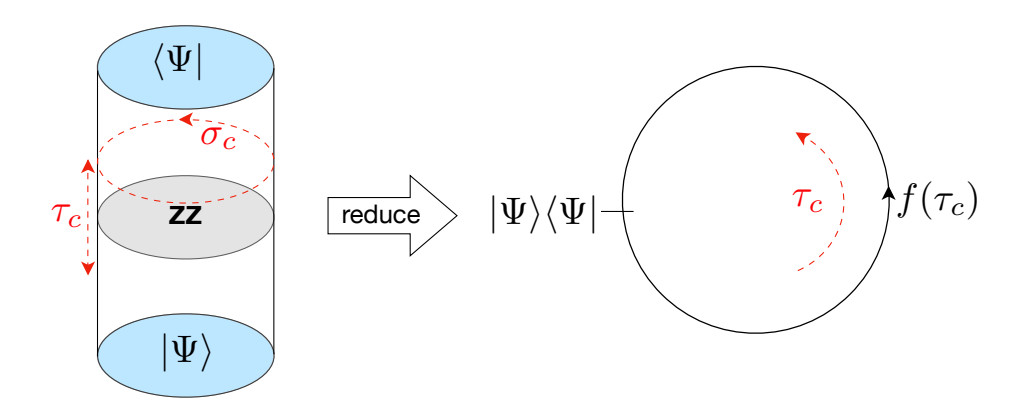


Figure 4.1: We obtain results on Schwarzian correlation functions by taking an appropriate limit of 2D Liouville theory with boundary conditions, or equivalently (as shown on the left) with the corresponding boundary states (details in section 4.2.3). The full cylinder is obtained when we implement the ZZ boundary condition via a doubling trick, allowing us to extend the field periodically. The resulting theory on the torus is then reduced to one dimension and gives rise to correlation functions in the Schwarzian theory with respect to the pure-state density operator  $\rho_{\Psi} = |\Psi\rangle\langle\Psi|$ .

where  $|E\rangle$  is any eigenstate of the theory, including the vacuum  $|0\rangle$ . The operator  $\mathcal{V}$  starts its life in two dimensions as a Liouville vertex operator  $\sim e^{\varphi}$  that upon descent to one dimension corresponds to a bilocal operator insertion in the Schwarzian theory. We establish that for one and two-point functions of bilocal operators these correlation functions become thermal in the semiclassical limit  $(C \to \infty)$  in the sense of eigenstate thermalization and compute the associated ETH temperature  $\beta_{\Psi}$ . By definition, this temperature is also the temperature of a canonical ensemble with temperature chosen in order to reproduce microcanonical averages at energy E. We have written the result (4.2) for the case of an arbitrary number of bilocal insertions. Strictly speaking in the work presented here we only establish the result for up to two bilocals, but our methods can in principle be extended to the most general case (4.2).

We will describe the precise construction in section 4.2, preferring to first summarize the main results in as non-technical a manner as possible.

We prove that both classes of pure states  $|\Psi\rangle$  under consideration behave thermally to leading order in large C. We show both using semiclassical quantization of the appropriate coadjoint orbits of Virasoro as well as via semiclassical expansions of *exact* results in the quantum theory that bilocal one and two-point functions with respect to the eigenstate

4.1 Introduction 99

 $|E(k)\rangle$  appear thermal at temperature  $\pi T_E = \sqrt{E/2}$ , while the coherent states  $|E_r\rangle$  behave thermally at temperature

$$T_{\theta} = \frac{\theta}{\pi} \sqrt{\frac{E}{2}} \,, \tag{4.5}$$

for  $\theta \in \mathbb{R}$ , corresponding to the parameter range  $r < \sqrt{2}$  for the coherent state introduced in (4.4) above.<sup>3</sup> These states behave non-ergodically for the parameter range  $r > \sqrt{2}$ , which formally corresponds to setting  $\theta \in i\mathbb{R}$  in (4.5). In this regime there is no meaningful effective temperature to be associated to the states, but the combination of parameters (4.5) still remains important, appearing for example as an oscillation frequency of OTOCs. In fact, one recovers the result for the eigenstates by setting  $\theta = 1$ , and we explain why in more detail below. Physically, the system shows a phase transition between ergodic and non-ergodic behavior at the critical value  $r = \sqrt{2}$ , very similar to the phenomenon established in [116] for holographic 2D CFT. The resulting phase diagram is shown in Figure 4.2. It is intriguing to see exactly the same mathematical structure at play here, namely the transition between the elliptic and hyperbolic monodromy, or equivalently the co-adjoint orbits of Virasoro. The role of the critical theory is played by the parabolic case and it would be interesting to explore whether the theory of this orbit can serve as a universal description of ergodic to non-ergodic transitions.

Note that we wrote the expectation value (4.2) with Euclidean time insertions, but our results also extend to Lorentzian insertions, and in particular to out-of-time order type correlation functions. Crucially, in this case we are able to prove the conjecture first made in [45] and revisited in Chapter 2, namely that these pure states scramble with the maximally allowed Lyapunov exponent if one were allowed to naively extend the eigenstate thermalization hypothesis to these types of operators. In other words we find that

$$\langle \Psi | \mathcal{O}_{\ell_1}(t,0) \mathcal{O}_{\ell_2}(t,0) | \Psi \rangle_{\text{OTO}} \sim 1 - \frac{\#}{C} e^{\frac{2\pi}{\beta_{\Psi}} t}$$
 (4.6)

up to the scrambling time.<sup>4</sup> This behavior was conjectured in Chapter 2 on the basis of

 $<sup>\</sup>overline{\theta}$  and r both parametrize the states and are related to each other through (4.21).

<sup>&</sup>lt;sup>4</sup>An analogous statement is true in 2D CFT assuming identity block domination [116]. On general grounds, on the second sheet, one would expect contributions from other blocks to potentially spoil this behavior, unless we make further assumptions about the kind of CFT we consider, such as sparse spectrum and large gaps. In the Schwarzian theory the situation seems to be better as the identity

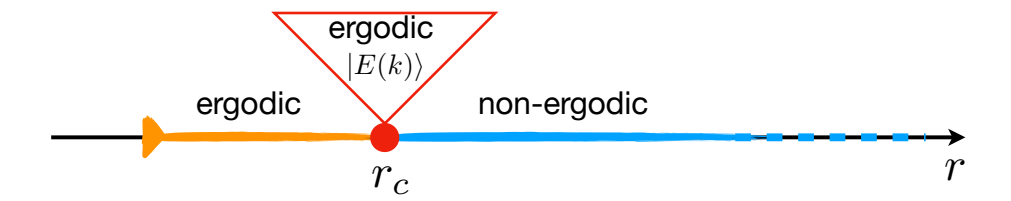


Figure 4.2: Phase diagram of the chaotic properties of the Schwarzian theory. The theory behaves thermally for the parameter range  $-\sqrt{2} < r < r_c$  with  $r_c = \sqrt{2}$ . The range  $r < r_c$  corresponds to elliptic coherent state insertions, while the critical case  $r = r_c$  can also be interpreted as the parabolic orbit corresponding to the eigenstates  $|E(k)\rangle$  of the theory. In the full range  $-\sqrt{2} < r \le r_c$  we find that the model scrambles with the maximal Lyapunov exponent predicted by ETH temperature,  $\lambda = 2\pi T_{\rm ETH}$ . In the hyperbolic range  $r > r_c$  the Schwarzian theory behaves non-ergodically, and in particular its OTOC is oscillatory. See also table 4.8 for more details.

numerical evidence as well as in the works of [119,128] with an eye on the necessary conditions for reconstructing the holographic bulk geometry of pure states. This kind of behavior has already been established analytically in 2D CFT assuming identity block domination in [116] and furthermore shown to be play a crucial role in holographic bulk reconstruction [119,128].

## Extended eigenstate thermalization hypothesis

A physical way to summarize these observations and analytical results, as well as previous evidence presented in Chapters 2 and 3 is the statement that there exist theories satisfying an extended ETH. Let  $\mathscr{A}$  denote the set of operators which satisfy the ETH in its usual form [129, 130]. Then, by extended ETH, we mean that operators in eigenstates such as (4.3) and, as a consequence in pure states such as (4.4), approximate thermal ones in real time, up to exponentially small corrections in entropy, at least until the scrambling time  $t_s$ . Moreover we include in the set  $\mathscr A$  more complex operators, such as the four-point OTO type correlations considered here as well as in Chapter 2 (see also [116].) Furthermore, we suggest that certain theories saturate the bound [15] when the OTOC is evaluated in eigenstates, as was first conjectured in [45] and revisited in Chapter 2, that is they satisfy maximal extended ETH. One interesting class of such theories we have in mind are CFTs with a sparse

4.1 Introduction 101

spectrum and a large gap,  $\Delta_{\rm gap}$ , to higher spins [131–134], in other words theories admitting a semiclassical description in terms of Einstein gravity corrected by higher derivative terms which are suppressed by powers of  $\Delta_{\rm gap}$ . It would clearly be desirable to obtain a better understanding of how far one should be allowed to extend the admissible class operators,  $\mathscr{A}$ , for example by adding successively higher OTOCs [135, 136].

For demonstrating ETH in any system it is crucial that the off-diagonal expectation values of the operators under consideration,  $\mathscr{A}$ , are exponentially suppressed with respect to the diagonal elements. Such off-diagonal terms were studied in Chapters 2 and ??. Here we compute only the diagonal elements while the computation of off-diagonal terms will require generalizing some of the techniques developed below.

#### Comments on ZZ and FZZT branes

An interesting role in our story is played by ZZ and FZZT branes in the Liouville picture and the corresponding boundary conditions these imply for the Schwarzian path integral. A general lesson is that ZZ branes and FZZT branes enter somewhat asymmetrically, in so far as in the Schwarzian picture the ZZ branes give rise to integrals over the density of states, while FZZT branes allow us to consider non-trivial coherent external states with respect to which we compute expectation values. On the other hand, we can recover the ZZ boundary conditions characterized by the continuous parameter r rather simply, by choosing the single value  $r = \sqrt{2}$ , so that in practice all the associated pure states can be treated in a uniform fashion. As we shall see this provides a useful perspective on all these branes and their thermal properties by linking them to the different coadjoint orbits of Virasoro, again parametrized by r, with the critical case  $r_c = \sqrt{2}$  (see, e.g. Fig. 4.2).

Given that these branes and their associated states feature so prominently in the understanding of thermalization in the Schwarzian theory (and by way of establishing this result, also in 2D Liouville theory), a very interesting question would be that of the bulk manifestation<sup>5</sup>. Since thermal ensembles in the boundary are a dual manifestation of bulk black holes, we are thus asking about the relevance of (F)ZZ(T) branes to the general structure of

<sup>&</sup>lt;sup>5</sup>The paper [137] discusses bulk manifestations of different Virasoro orbits, including elliptic, parabolic and hyperbolic, in terms of defect geometries in JT gravity.

black-hole microstates.

In fact, in the context of the 'old'  $c \le 1$  matrix model many results in this direction are known [122, 123, 138, 139] and it would certainly be interesting to flesh out a similar story in the present case. For recent work in this direction see [124].

## 4.2 Pure states in Liouville and the Schwarzian

In this section we describe in detail how to construct expectation values with respect to a density operator  $\rho_{\Psi} = |\Psi\rangle\langle\Psi|$  in the Schwarzian theory. On the way we also explain, in our picture, how to obtain the thermal ensemble  $\rho_{\beta}$ , more commonly encountered in the study of the Schwarzian theory to date. We will adopt the perspective advocated in [127] in order to do this, namely we will start with 2D Liouville theory with appropriate boundary conditions and then descend to the Schwarzian by taking an appropriate limit.

## 4.2.1 Boundary Liouville theory and Schwarzian coherent states

In this section we collect a number of results, most of which are well known, both to prepare the scene, as well as to establish our conventions for what is to come. We review how to descend from Liouville theory in 2D to the Schwarzian path integral (4.1), as well as the broad classification of classical solutions of Liouville according to their monodromy properties. Let us start with the Hamiltonian path integral for boundary Liouville theory on the interval  $I = [0, \beta/2]$ ,

$$\langle \cdot \cdot \rangle_{\rm bc} = \int \mathcal{D}\varphi \mathcal{D}\pi \left( \cdot \right) e^{\int d\tau d\sigma} \frac{\pi \dot{\varphi}}{8\pi b^2} - \mathcal{H}$$
 (4.7)

where 'bc' generically denotes 'boundary conditions' to be imposed on the fields at  $\sigma = 0$  and  $\sigma = \beta/2$ . We shall be interested both in so-called ZZ branes as well as FZZT branes, which correspond to Dirichlet and Neumann conditions, respectively. The Hamiltonian density is

<sup>&</sup>lt;sup>6</sup>While it might seem counter intuitive to call the spatial direction  $\beta$ , the periodicity in this direction will eventually be related to Euclidean 1D time.

given as

$$\mathcal{H} = \frac{1}{8\pi b^2} \left( \frac{\pi^2}{2} + \frac{\varphi_\sigma^2}{2} + e^{\varphi} - 2\varphi_{\sigma\sigma} \right) + H_{\text{boundary}}$$
 (4.8)

with Liouville central charge  $c=1+6\left(b+b^{-1}\right)^2$ . We added the boundary Hamiltonian  $H_{\text{boundary}}$  in order to implement the Dirichlet or Neumann conditions of interest and to be specified shortly. We will ultimately be interested in the limit  $c\to\infty$ , corresponding to taking  $b\to 0$ . The Schwarzian limit is essentially the classical limit of the 2D path integral (4.7) by taking  $c\to\infty$  while at the same time letting  $a\to 0$ , such that  $\frac{ca}{24\pi}\coloneqq C$  remains finite, where a is the size of the Euclidean time coordinate in 2-dimensions. In this limit, the path integral reduces to the zero-mode in time of the fields  $\varphi(\sigma,\tau)$  and  $\pi(\sigma,\tau)$ , i.e. time-independent configurations and may be brought into the form (4.1). A key difference to the treatment in [113,127,140] is that we are especially interested in FZZT type boundary conditions, so we describe in some detail how these are implemented and how they descend to the Schwarzian theory.

Let us thus return to our discussion of boundary Liouville theory. The boundary conditions we would like to impose [122, 123, 141, 142] are most easily stated in terms of the vertex operator

$$\mathcal{V}_{\ell}(w,\bar{w}) = e^{\ell\varphi(w,\bar{w})}, \qquad (w = \tau + i\sigma, \quad \bar{w} = \tau - i\sigma)$$
(4.9)

We also define the exponentiated Liouville field

$$V(w,\bar{w}) = e^{-\frac{1}{2}\varphi} \tag{4.10}$$

for later convenience. The Schwarzian boundary states descend from considering the Liouville theory between branes, so that  $\sigma \in I$ . In order to characterize the branes, we need to specify Dirichlet or Neumann boundary conditions at both ends. The most general case of interest in this Chapter<sup>7</sup> will be a Dirichlet condition at  $\sigma = 0$ , as well as a family of Neumann boundary conditions at  $\sigma = \beta/2$ :

$$V(\tau,\sigma)\Big|_{\sigma=0} = 0, \qquad \partial_{\sigma}V(\tau,\sigma)\Big|_{\sigma=\frac{\beta}{2}} = \frac{r}{2}$$
 (4.11)

<sup>&</sup>lt;sup>7</sup>In section 4.4 we will also give results for Neumann boundary conditions at both ends. We do not currently understand the physical relevance of these states and leave further investigation for future work.

where r is a parameter whose ranges we will specify later. In terms of the field  $\varphi$ , the Neumann boundary condition takes the form

$$\partial_{\sigma}\varphi + re^{\frac{\varphi}{2}}\Big|_{\sigma = \frac{\beta}{2}} = 0 \tag{4.12}$$

and is implemented by adding the boundary action

$$S_{\rm N} = -\frac{r}{4\pi b^2} \int d\tau \, e^{\frac{1}{2}\varphi} \bigg|_{\sigma = \frac{\beta}{2}}$$
 (4.13)

which, inside the path integral, has precisely the interpretation of creating the coherent state (4.4). In preparation for our later analysis of the Schwarzian theory, it will in fact be useful to review the construction of classical solutions of boundary Liouville theory with the specified boundary conditions, and we closely follow the presentation in [142]. The setup here is that of a conformal field theory with a boundary which was first studied in [143] and subsequently in [122, 123, 141, 142, 144] for the Liouville field theory. First, let us perform a conformal transformation that maps the strip,  $\mathbb{R} \times I$ , to upper half plane,  $\mathbb{H}$ ,  $\mathbb{R}$ 

$$z = e^{\frac{2\pi}{\beta}w}, \quad \bar{z} = e^{\frac{2\pi}{\beta}\bar{w}} . \tag{4.14}$$

We will see below that this map naturally helps us to define a theory at finite temperature after the dimensional reduction (see the discussion following (4.28) below), although we will often be interested in taking the zero-temperature limit and instead work with individual pure states. Under such an exponential map, the boundaries  $\sigma = 0, \beta/2$  are mapped to the real line, Im(z) = 0. The stress tensor on the plane is,

$$T = \frac{\partial_z^2 V}{V} + \frac{1}{4z^2}, \qquad \bar{T} = \frac{\partial_{\bar{z}}^2 V}{V} + \frac{1}{4\bar{z}^2}.$$
 (4.15)

<sup>&</sup>lt;sup>8</sup>Recall that the Liouville field  $\varphi(w) \to \varphi(z) - \ln \left| \frac{\partial w}{\partial z} \right|^2$  also transforms under conformal transformations.

Conservation of the stress tensor implies holomorphicity and the Neumann boundary conditions naturally provide vanishing energy flux through the boundary, Im(z) = 0,

$$T(z) = \overline{T}(\overline{z})$$
, when  $z = \overline{z}$  (4.16)

For the case of Dirichlet boundary condition, this is imposed as an additional condition which imposes the regularity of the stress tensor on the boundary. The doubling trick on the plane then lets one define the stress tensor on the lower half plane,  $T(z^*) = \bar{T}(\bar{z})$ , [143], thereby making the stress tensor periodic in the original  $\sigma$ -coordinate,

$$T(\sigma + \beta) = T(\sigma)$$
.

Classical solutions of the Liouville equation in the Fuchsian form (4.15) are well studied and are organized by the monodromy of the solutions around the unit circle in the complex plane. To see this, we write the Liouville field as a linear combination of two functions  $\Psi^T = (\psi_1, \psi_2)$  in the form

$$V(z,\bar{z}) = \Psi(\bar{z})^T A \Psi(z), \qquad A \in SL(2,\mathbb{R})$$
(4.17)

where the functions  $\psi_{1,2}$  are defined as the two linearly independent solutions of Hill's equation

$$\psi'' - T\psi = 0 \tag{4.18}$$

with T the Liouville stress tensor introduced above. We then define the monodromy matrix M, via

$$\Psi(e^{2i\pi}z) = M\Psi(z). \tag{4.19}$$

One can show that  $M \in SL(2,\mathbb{R})$ , [145], and that it is in fact defined only up to conjugation  $M \cong S^{-1}MS$  for  $S \in SL(2,\mathbb{R})$ , so that conformally inequivalent solutions are labelled by conjugacy classes of  $SL(2,\mathbb{R})$ , coinciding with the classification of coadjoint orbits of Diff( $S^1$ ) [142,146]. The main tool to classify the different classes of solutions is the monodromy matrix M, which must fall into one of three classes: hyperbolic, parabolic or elliptic, characterized

<sup>&</sup>lt;sup>9</sup>Non-vanishing energy flux for the Dirichlet problem would correspond to singularities on the boundary. See [142] for more discussion. Moreover, this also facilitates the use of doubling trick.

by the trace of the monodromy matrix M. We do this by writing the Neumann boundary condition in terms of  $V(z,\bar{z})$  as,

$$\frac{z\partial V(z,\bar{z}) - \bar{z}\bar{\partial}V(z,\bar{z})}{\sqrt{z\bar{z}}}\Big|_{\bar{z}=z<0} = r/2 . \tag{4.20}$$

With the aid of the Wronskian condition  $\psi_1'\psi_2 - \psi_1\psi_2' = 1$ , this implies that

$$\operatorname{Tr} M = \frac{r}{2} = \frac{\cos(\pi\theta)}{\sqrt{2}}, \qquad (4.21)$$

where the second equality introduces an alternative but standard parametrization of the boundary parameter r. This equation will be our main tool to classify different types of semiclassical solutions of the Schwarzian model. Following the analysis in [142], we have three cases, namely

$$-\sqrt{2} < r < \sqrt{2} \qquad \theta \in \mathbb{R} \qquad \text{elliptic}$$
 
$$r = \pm \sqrt{2} \qquad \theta = 0, \pm 1 \qquad \text{parabolic}$$
 
$$r > \sqrt{2} \qquad \theta \in i\mathbb{R} \qquad \text{hyperbolic} \qquad (4.22)$$

Using the map (4.14), one can write the classical solution for the Liouville theory found in [142] in each of the equivalence classes in terms of a single holomorphic function, F(z),

$$V(z,\bar{z}) = \frac{1}{2\sqrt{2}\theta} \sqrt{\frac{F(z)F(\bar{z})}{F'(z)F'(\bar{z})}} \left[ \left(\frac{F(z)}{F(\bar{z})}\right)^{\theta/2} - \left(\frac{F(\bar{z})}{F(z)}\right)^{\theta/2} \right], \tag{4.23}$$

where  $F(e^{2i\pi}z) = e^{2i\pi}F(z)$ .

A further crucial element of the construction of classical solutions described above is that the stress tensor of any solution of Hill's equation for the theory on  $\mathbb{H}$  falling into these three classes can be brought to the constant form [142]

$$T^{\mathbb{H}} = T_0^{\mathbb{H}}, \quad \text{with} \quad T_0^{\mathbb{H}} = \frac{\theta^2}{4z^2},$$
 (4.24)

via a conformal transformation. This is the stress tensor on the plane. Alternatively, one can

compute the stress tensor on the strip,  $\mathbb{R} \times I$ , where it takes the form

$$T = T_0 = -\frac{\theta^2}{4} \ . \tag{4.25}$$

We refer to  $T_0$  as the constant representative.<sup>10</sup> It is interesting to note that this equation is very reminiscent of the trace of the monodromy matrix appearing in the computation of conformal blocks of 2D CFT at large central charge [7,147,148]. The difference seems to be in that while these references study the monodromy around operator insertions, here we have appropriate boundary conditions along the entire real line in the complex z-plane. However, following [122] one can understand these boundary conditions as insertion of boundary operators and the monodromy under study in the present work is then the monodromy around this boundary operator.

## 4.2.2 Descending to the Schwarzian

Inspired by the non-linear field transformation of Gervais-Neveu, [149, 150], we perform the following field redefinition in the path integral, (4.7). The following derivation becomes more transparent if we use Cartesian coordinates, S and T, parametrising the z-plane instead of the polar coordinates,  $\sigma$  and  $\tau$ . In terms of these Cartesian coordinates, the field redefinitions we need take the form,

$$e^{\varphi} = -8 \frac{\partial_{S} F(z, \bar{z}) \partial_{S} \bar{F}(z, \bar{z})}{\left(F - \bar{F}\right)^{2}}$$

$$\pi = \frac{\partial_{S}^{2} F}{\partial_{S} F} - \frac{\partial_{S}^{2} \bar{F}}{\partial_{S} \bar{F}} - \frac{\partial_{S} F}{F} + \frac{\partial_{S} \bar{F}}{\bar{F}} - \left[\frac{F + \bar{F}}{F - \bar{F}}\right] \left[\frac{\partial_{S} F}{F} + \frac{\partial_{S} \bar{F}}{\bar{F}}\right] .$$

$$(4.26)$$

Under this transformation, <sup>11</sup> the bulk action becomes,

$$S = \frac{1}{4\pi b^2} \int_{\mathbb{H}} d^2 z \left[ \frac{1}{2} \pi [F] \left( S \partial_S + T \partial_T \right) \varphi [F] + \{ F; S \} + \{ \bar{F}; S \} \right]$$
(4.27)

<sup>&</sup>lt;sup>10</sup>We have dropped the Casimir energy part that comes from the quantum corrections since it is not important for identifying the orbits.

<sup>&</sup>lt;sup>11</sup>In these expressions  $F(z,\bar{z}), \bar{F}(z,\bar{z})$  are independent off-shell fields of both the holomorphic and the anti-holomorphic coordinates. We have suppressed the functional dependence to avoid clutter. Also,  $\partial_S := \partial - \bar{\partial}$  and  $\partial_T := \partial + \bar{\partial}$ .

Using the doubling trick to identify  $z^* = \bar{z}$ , we write the action as an integral over the entire complex plane,

$$S[F] = \frac{1}{4\pi b^2} \int_{\mathbb{C}} d^2z \left[ \frac{1}{2} \pi [F] \left( S \partial_S + T \partial_T \right) \varphi[F] + \{F; S\} \right]$$
(4.28)

This path integral should be understood along with the insertion of the appropriate state along the negative real axis, implemented by the boundary term (4.13). Some comments are in order: firstly, recall that the F(z) function is related to the transformations of the strip, I, by,

$$F(z) = e^{\frac{2\pi i}{\beta}f(\sigma)} \tag{4.29}$$

on the  $\tau=0$  slice. The parameter  $\beta$  entering into this transformation is freely tunable and corresponds to the physical (inverse) temperature of the Schwarzian theory in 1D. This is the well known tan-transformation ( $\mathbb{SL}(2,\mathbb{R})$  equivalent thereof) from the study of 1D CFTs, [11,14]. Recall, that the semiclassical limit (of the Liouville theory),  $b \to 0$ , of the path integral localizes on  $\tau$ -independent configurations (radially independent configurations in z-plane) and the first term (the  $\pi \partial_{\tau} \varphi$  term) in the above action drops out. This also means that the S and  $\sigma$  dependence of the functions become equivalent. In this classical limit, around the generic saddle point, (4.23), one reproduces the Schwarzian action,

$$S[f] = -C \int_{-\beta/2}^{\beta/2} d\sigma \left[ \{ f(\sigma); \sigma \} + \frac{2\pi^2 \theta^2}{\beta^2} f'(\sigma)^2 \right]$$
 (4.30)

where

$$C = \frac{a}{4\pi b^2} \tag{4.31}$$

is the overall coefficient in front of the Schwarzian action (4.1). Using the field redefinitions, (4.26), insertion of any vertex operator,  $e^{2\ell\varphi(z,\bar{z})}$ , corresponds to an insertion of the kind,

$$\mathcal{O}_{\ell}(\sigma, -\sigma) = \left(\frac{8\pi^{2}\theta^{2}}{\beta^{2}} \frac{f'(\sigma)f'(-\sigma)}{\sin^{2}\left(\frac{\pi\theta}{\beta}\left(f(\sigma) - f(-\sigma)\right)\right)}\right)^{2\ell}$$
(4.32)

in the classical limit. Similarly, the boundary term (4.13) can we written as,

$$S_N = -\frac{a r \theta}{\sqrt{2} \beta b^2} \frac{f'(\beta/2)}{\sin(\pi \theta)}$$
(4.33)

where, we have used:  $f(\beta/2) - f(-\beta/2) = \beta$ ; and,  $f'(\beta/2) = f'(-\beta/2)$ . From this point of view of obtaining Schwarzian theory as a dimensional reduction of the 2-dimensional Liouville theory, the Dirichlet boundary condition at  $\sigma = 0$  corresponds to an insertion of complete set of states in the Schwarzian theory.<sup>12</sup> Finally, the generic 2-dimensional path integral, (4.7), with operator insertions and Neumann boundary condition on one end and Dirichlet boundary condition on the other after dimensional reduction becomes,

$$\langle \cdot \rangle = \int \frac{\mathcal{D}f}{G} \left( \cdot \right) \exp \left[ -\frac{2\sqrt{2}\pi C \, r \, \theta}{\beta} \, \frac{f'(\beta/2)}{\sin(\pi \, \theta)} - C \int_{-\beta/2}^{\beta/2} d\sigma \left( \{f(\sigma); \sigma\} + \frac{2\pi^2 \theta^2}{\beta^2} f'(\sigma)^2 \right) \right] \, . \quad (4.34)$$

We can alternatively write the above integral in a more symmetric form:

$$\langle \cdot \rangle = \int \frac{\mathcal{D}f}{G} \Big( \cdot \Big) \exp \left[ -\frac{2\sqrt{2}\pi C \, r \, \theta}{\beta} \, \frac{\sqrt{f'(-\beta/2)f'(\beta/2)}}{\sin(\pi \, \theta)} - C \int_{-\beta/2}^{\beta/2} d\sigma \left( \{f(\sigma); \sigma\} + \frac{2\pi^2 \theta^2}{\beta^2} f'(\sigma)^2 \right) \right]$$

$$(4.35)$$

The advantage of this symmetric representation is that we can interpret the operator insertion as the one that creates the FZZT states described in (4.4) and the RHS of the figure 4.1.<sup>13</sup> The Jacobian,  $Pf(\omega)$ , due to the field redefinition from  $\varphi, \pi \to f$  is absorbed in the function integral measure  $\frac{\mathscr{D}f}{G}$  as was shown in [151]. Here  $\omega$  is the Alekseev-Shatasvili symplectic form given by, [120, 142, 144]

$$\omega = \delta T_0 \wedge \int_{-\beta/2}^{\beta/2} d\sigma f'(\sigma) \, \delta f(\sigma) + T_0 \int_{-\beta/2}^{\beta/2} d\sigma \, \delta f'(\sigma) \wedge \delta f(\sigma) + \frac{1}{4} \int_{-\beta/2}^{\beta/2} d\sigma \, \frac{f''(\sigma) \wedge \delta f'(\sigma)}{f'(\sigma)^2} . \tag{4.36}$$

Note that while the Schwarzian action in (4.34) has an  $\mathbb{SL}(2,\mathbb{R})$  symmetry, this is further broken to U(1) due to the presence of the operator insertion at  $\sigma = \beta/2$ . Consequently  $G = \mathbb{SL}(2,\mathbb{R})$  or U(1) depending on which orbit we are integrating over. This also suggests that

<sup>&</sup>lt;sup>12</sup>Precisely because there is no insertion of any operator in the dimensionally reduced theory.

 $<sup>^{13}</sup>$ In this particular case, the eigenstate in (4.4) is the vacuum state.

this operator insertion in (4.34) due to the boundary condition at  $\sigma = \beta/2$  can alternatively be understood as integration over circle diffeomorphisms f with nontrivial monodromy specified by r via the trace relation (4.21).

## 4.2.3 Boundary conditions as States of the theory

Up to this point we presented the ZZ and FZZT branes in terms of boundary conditions for Liouville theory on an interval. In fact, for what is to come below, a more natural way to think about them is in terms of (boundary) states. Within Liouville theory, transitioning between boundary conditions and states is equivalent to transitioning between an open-string and a closed-string perspective. Liouville theory is, in fact, one of the most well understood examples of such an open/closed string duality, [123, 152]. We study the boundary Liouville theory given by the path integral (4.7) at finite temperature, T = 1/a. In general, one can choose arbitrary conformal boundary conditions at the ends of the strip i.e. in the open-string perspective. The case of Dirichlet boundary condition at both ends, also known as (1,1)-Zamolodchikov-Zamolodchikov (ZZ) branes was studied in the context of the Schwarzian theory in [127,140]. The generic partition function,  $Z_{\mathfrak{s},\mathfrak{s}'}\left[i\frac{a}{\beta}\right]$ , between two different branes is given by, [123,152],

$$Z_{\mathfrak{s},\mathfrak{s}'}\left[i\frac{a}{\beta}\right] = \int dP \,\Psi_{\mathfrak{s}}(P)\Psi_{\mathfrak{s}'}(-P) \,\chi_{P}(\tilde{q}) \,,$$
where each of  $\mathfrak{s}$  or  $\mathfrak{s}' = \begin{cases} (m,n) \in (\mathbb{Z},\mathbb{Z}) \text{ for a generalized } (m,n)\text{-ZZ brane} \\ s \in \mathbb{R} \text{ for FZZT brane} \end{cases}$  (4.37)

Here, the modular parameter is  $(i \, a/\beta)$  since the size of our open string is  $\beta/2$  and  $q = \exp\left[-2\pi \times \frac{a}{\beta}\right]$ ,  $\tilde{q} = \exp\left[-2\pi \times \frac{\beta}{a}\right]$ . The particular case of our interest presently is the case where  $\mathfrak{s} = s$  for a FZZT brane and  $\mathfrak{s}' = (1,1)$  for a 'basic' ZZ brane. Finally, the Virasoro character corresponding to a non-degenerate state labelled by P is,

$$\chi_P(q) = \frac{q^{P^2}}{\eta(q)}, \quad \eta(q) = q^{1/24} \prod_{n=1}^{\infty} (1 - q^n) .$$
(4.38)

<sup>&</sup>lt;sup>14</sup>Note that this is the temperature of the 2D Liouville theory. It is not the same as  $1/\beta$  which will emerge as the natural periodicity of the Euclidean time direction of the Schwarzian theory in the end (if the latter is studied in a thermal ensemble).

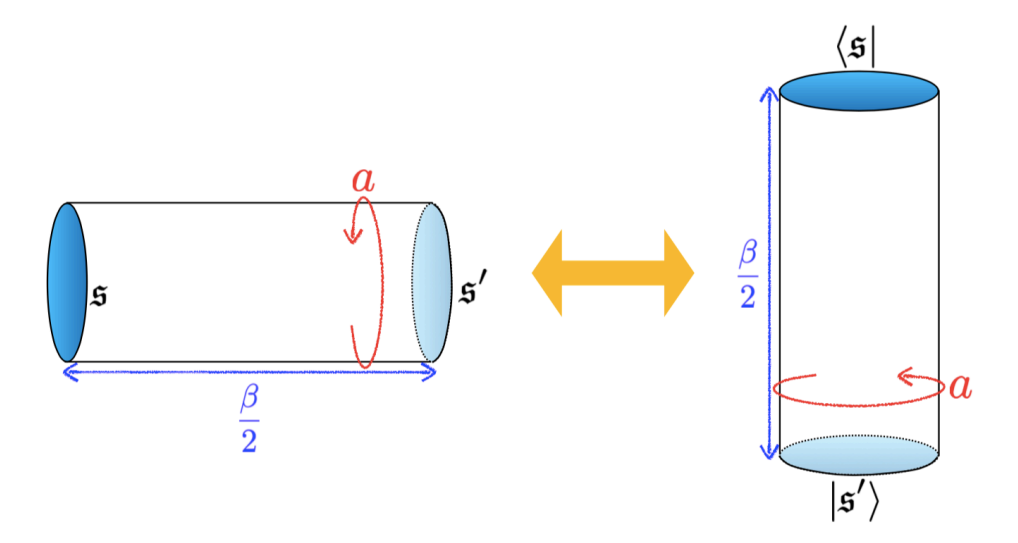


Figure 4.3: An open string Partition function with generic boundary conditions is the same as a closed string amplitude between corresponding boundary states.

While the states given by the wavefunctions  $\Psi_{\mathfrak{s}}(P)$  can be written in terms of the Ishibashi states, [153, 154], <sup>15</sup>

$$\langle \mathfrak{s} | = \int dP \Psi_{\mathfrak{s}}(P) \langle \! \langle P |, \rangle \rangle$$
(4.39)

$$\langle\!\langle P| = \langle \nu_P | \left( 1 + \frac{L_1 \bar{L}_1}{2\Delta_P} + \cdots \right) . \tag{4.40}$$

Here,  $|\nu_P\rangle$  is the state created by the vertex operator  $e^{(Q+2iP)\frac{\varphi}{2b}}$  under the state operator correspondence, with the conformal weight,  $\Delta_P = \frac{Q^2}{4} + P^2$ . Thus the open string partition function between two branes, written as the integral appearing in (4.37), can equivalently be written as an amplitude between two such closed string states,

$$Z_{\mathfrak{s},\mathfrak{s}'}[q] = \langle \mathfrak{s} | \tilde{q}^{L_0/2} | \mathfrak{s}' \rangle . \tag{4.41}$$

The Our Ishibashi states are normalized as,  $\langle P|q^{L_0/2}|P'\rangle = \delta(P-P')\chi_P(q)$ 

The states of importance in this work are,

$$\Psi_{\text{ZZ}}(P) := \Psi_{(1,1)}(P) = 2^{3/4} 2i\pi P \left(\frac{\gamma(b^2)}{8b^2}\right)^{-\frac{iP}{b}} \frac{1}{\Gamma(1 - 2iPb)\Gamma(1 - 2\frac{iP}{b})}$$

$$\Psi_{\text{FZZT}}^{(s)}(P) := \Psi_s(P) = e^{2i\pi Ps} \left[ -\frac{i}{2\pi P} \left(\frac{\gamma(b^2)}{8b^2}\right)^{-\frac{iP}{b}} \Gamma(1 + 2iPb)\Gamma(1 + 2\frac{iP}{b}) \right].$$
(4.42)

Here, for the sake of brevity we have used the standard definition  $\gamma(x) = \Gamma(x)/\Gamma(1-x)$ . This duality needs to be generalized for the case with operator insertions to be useful for our computations. Unnormalized thermal correlation functions can likewise be computed using the open/closed string identity:

$$\operatorname{Tr}_{\mathfrak{s},\mathfrak{s}'}\left[e^{-aH}\mathbb{V}_{n}(w_{n},\bar{w}_{n})\cdots\mathbb{V}_{1}(w_{1},\bar{w}_{1})\right] = \langle\mathfrak{s}|\tilde{q}^{\frac{L_{0}}{2}}e^{\frac{2\pi}{a}\sigma_{n}L_{0}}\mathbb{V}_{n}\cdots\mathbb{V}_{2}e^{-\frac{2\pi}{a}\sigma_{21}L_{0}}\mathbb{V}_{1}e^{-\frac{2\pi}{a}\sigma_{1}L_{0}}|\mathfrak{s}'\rangle \quad (4.43)$$

where, we have used following definitions,

$$\tilde{q}^{L_0} = \exp\left(-2\pi \frac{\beta}{a} L_0\right) = \exp(-\beta H)$$

$$q^{L_0} = \exp\left(-2\pi \frac{a}{\beta} L_0\right) = \exp(-aH)$$

$$w_i = \tau_i + i\sigma_i, \quad \bar{w}_i = \tau_i - i\sigma_i$$

$$\sigma_{ij} = \sigma_i - \sigma_j$$

$$(4.44)$$

and  $V_i$  are the vertex operators of the Liouville theory. We have also used  $\tau_i = 0 \Rightarrow w_i = -\bar{w}_i$ . This choice has been made with eventual dimensional reduction,  $a \to 0$ , in mind.

Finally putting the results from both these perspective together, in the  $b \to 0$  limit, we can equate (4.34) to (4.43),

$$\int \frac{\mathscr{D}f}{G} \left(\cdot\right) \exp\left(S[f] + S_N\right) \sim \left\langle s \middle| e^{-\frac{\beta L_0}{2}} \mathbb{V}_n(\sigma_n, -\sigma_n) \cdots \mathbb{V}_2(\sigma_2, -\sigma_2) \mathbb{V}_1(\sigma_1, -\sigma_1) \middle| (1, 1)\right\rangle \quad (4.45)$$

where, S[f],  $S_N$  are the actions introduced in (4.30) and (4.33); and, (·) corresponds to the insertion of the bilocal operators given by (4.32),  $\mathcal{O}_i(\sigma_i, -\sigma_i)$ , in the Schwarzian theory. Also

the parameter r on the LHS is related to the parameter s of the FZZT state by,

$$\cosh^{2}(\pi bs) = \frac{r^{2}}{2\pi b^{2}}\sin(\pi b^{2}) = \cos^{2}(\pi \theta)\frac{\sin(\pi b^{2})}{\pi b^{2}}$$
(4.46)

For the case of the unperturbed ('standard') Schwarzian theory, we have,

$$\int \frac{\mathcal{D}f}{G} \left(\cdot\right) \exp\left(S[f]\right) \sim \langle (1,1)|e^{-\frac{\beta L_0}{2}} \mathbb{V}_n(\sigma_n, -\sigma_n) \cdots \mathbb{V}_2(\sigma_2, -\sigma_2) \mathbb{V}_1(\sigma_1, -\sigma_1)|(1,1)\rangle \tag{4.47}$$

The tilde in the equations above emphasizes the fact that on both sides of these equations we are computing unnormalized correlation functions. Since we are interested in time-dependent behavior of these correlation functions we will not be careful about the overall time-independent normalizations. Note that in the large central charge limit,  $c \to \infty \equiv b \to 0$ , the Ishibashi states in (4.40),  $\langle P| \to \langle \nu_P|$ , so that in our case they can always be replaced simply with the primary states, which simplifies our task considerably. Also,  $\theta = \pm 1 \Leftrightarrow r^2 = 2 \Leftrightarrow s = \pm i$  corresponds to (1,1)-ZZ state. This is consistent with our previous observation that  $\theta = \pm 1$  corresponds to the standard Schwarzian action in (4.28). In all the subsequent sections, we work only with ZZ-branes of the type (1,1) and therefore we refer to them as  $|ZZ\rangle$  instead of  $|(1,1)\rangle$ . In our notations  $|FZZT\rangle$  denotes a general FZZT brane and the parameter s is suppressed.

This concludes our introduction relating the 1-dimensional Schwarzian theory to boundary Liouville theory in 2-dimensions. We also related the boundary states of the Liouville theory with different states of the Schwarzian theory. We will now use this setup to compute the correlation functions of the 1-dimensional theory with an aim to unravel their thermal behaviour. Before we proceed to do the exact computations in section 4.4, we derive some of these results using semiclassical analysis in section 4.3.

## 4.3 Semiclassical results

In this section we make use of the natural symplectic structure on the coadjoint orbits of Virasoro to extract the scrambling exponent in pure states. The logic is as follows: first we establish the effective temperature (the 'ETH temperature') we should assign to our pure states, including the actual eigenstates of the Schwarzian model. This can be done by studying the one-point functions of bilocal operators  $\mathcal{O}_{\ell}$ . We then go on to the corresponding two-point function of  $\mathcal{O}'_{\ell}s$  and determine the Lyapunov exponent whenever appropriate. In all cases where the one-point function is thermal we find the maximally allowed Lyapunov exponent predicted by taking the ETH temperature seriously. On the other hand, we also establish a phase transition between this ergodic behavior and a non-ergodic phase in which the one-point functions are not periodic in Euclidean time and the corresponding OTOC does not exhibit scrambling behavior. The resulting phase diagram is summarized in Figures 4.2.

## 4.3.1 One-point function and effective temperature

We start our exploration of the semi-classical correlators of the model (4.1) with the simplest example, namely the one-point function of the bilocal operator

$$\mathcal{O}_{\ell}(\sigma_1, \sigma_2) \coloneqq e^{2\ell\varphi(\sigma_1, -\sigma_2)} \tag{4.48}$$

where we have emphasized that the operators in the Schwarzian theory descend from the zero-mode of the primary operator of weight  $\ell$  in the Liouville picture. This will turn out to be convenient for our next step, when we exploit this connection in order to construct the saddle-point solutions of the Schwarzian path integral with ZZ and FZZT boundary conditions. Later, in section 4.4, we will recover these expressions from a semi-classical expansion of the exact answer for the correlation functions.

#### ZZ branes: Dirichlet condition and energy eigenstates in the Schwarzian

Here we are interested in the semi-classical answer for the correlation function

$$\langle E|\mathcal{O}_{\ell}(\sigma_1,\sigma_2)|E\rangle$$
, (4.49)

where  $|E\rangle$  is an eigenstate of energy E. Note that the energy can be defined as the expectation value of the Schwarzian 'operator' in the energy eigenstate, [17, 102, 127, 140]:

$$E := \langle E | \{ F(\sigma), \sigma \} | E \rangle$$
,

with the background temperature,  $1/\beta = 0$ . Semiclassical limit of this equation corresponds to, <sup>16</sup>

$$\{F(\sigma);\sigma\} = \frac{4\pi^2 E}{C} , \qquad (4.50)$$

and, the saddle point solution is given by,

$$F(\sigma) = \tan\left(\pi\sqrt{\frac{2E}{C}}\sigma\right) \tag{4.51}$$

Recall, in the zero temperature limit the parabolic orbit,  $Diff(S^1)/SL(2,\mathbb{R})$ , that is relevant for this case is characterized by the following operator (see also (4.32)),

$$\mathcal{O}_{\ell}^{1}(\sigma_{1}, \sigma_{2}) = \left(\frac{F'(\sigma_{1})F'(\sigma_{2})}{\left(F(\sigma_{1}) - F(\sigma_{2})\right)^{2}}\right)^{2\ell}.$$

$$(4.52)$$

The reason for the superscript '1' in the above equations will become clear once we understand the analogous solutions corresponding to Neumann boundary conditions (FZZT branes). The path integral expression that we are interested in involves an integration over the  $F(\sigma)$  modes, <sup>17</sup>

$$\int \frac{\mathscr{D}F}{\mathrm{SL}(2,\mathbb{R})} \mathcal{O}_{\ell}^{1}(\sigma_{1},\sigma_{2}) e^{C \int d\sigma \{F(\sigma);\sigma\}}. \tag{4.53}$$

However, in the semiclassical limit it can be evaluated at the above saddle point solution, (4.51),

$$\langle E|\mathcal{O}_{\ell}^{1}(\sigma_{1},\sigma_{2})|E\rangle \approx \left(\frac{\pi^{2}}{\beta_{E}^{2}} \frac{1}{\sin^{2}\left(\frac{\pi}{\beta_{E}}\sigma_{12}\right)}\right)^{2\ell} , \qquad 1/\beta_{E} = T_{E} = \sqrt{\frac{2E}{C}}$$

$$(4.54)$$

This is the same as the thermal correlation function at an effective temperature,  $T_E$ . Later in section 4.4 we obtain the same result using the exact methods described in the previous section.

 $<sup>^{16}</sup>$ The appropriate scaling of the energy in this equation is to ensure that we are working with a high-energy state in the semiclassical limit.

<sup>&</sup>lt;sup>17</sup>In the  $\beta \to \infty$  limit, the fields  $F(\sigma) = f(\sigma)$ 

### FZZT branes: Neumann condition and Schwarzian coherent states

We are now interested in the semi-classical answer for the correlation function

$$\langle E_r | \mathcal{O}_\ell(\sigma_1, \sigma_2) | E_r \rangle$$
 (4.55)

where,  $|E_r\rangle$  corresponds to the local operator discussed in (4.4). This insertion restricts us to the orbit Diff( $S^1$ )/U(1), as was deduced in the previous section and corresponds to the zero mode of a classical solution to Liouville theory with a Dirichlet boundary condition at  $\sigma = 0$ and a Neumann boundary condition at  $\sigma = \beta/2$ . In this case the classical solution [142] can be written as

$$\mathcal{O}_{\ell}^{\theta}(\sigma_1, \sigma_2) = \left(\frac{\pi^2 \theta^2}{\beta_E^2} \frac{f'(\sigma_1) f'(\sigma_2)}{\sin^2\left(\frac{\theta \pi}{\beta_E} \left(f(\sigma_1) - f(\sigma_2)\right)\right)}\right)^{2\ell}$$
(4.56)

The superscript  $\theta$  parametrizes the family of Neumann boundary conditions corresponding to our coherent states. We note that setting  $\theta = 1$  recovers the pure Dirichlet case, explaining the choice of superscript above. Also note that the background temperature for this orbit is taken to be the same as the effective temperature  $T_E = 1/\beta_E$  induced by external states  $|E\rangle$ .

In order to get the Schwarzian correlation function we still need to integrate over the circle diffeomorphism f. We must thus evaluate the path integral

$$\int \frac{\mathscr{D}f}{U(1)} \mathcal{O}_{\ell}^{\theta}(\sigma_1, \sigma_2) e^{-\frac{4\pi C \theta}{\beta} \frac{f'(\sigma_3)}{\tan(\pi \theta)} - C \int d\sigma \{f(\sigma); \sigma\}}. \tag{4.57}$$

where we have explicitly written the path integral in terms of the f fields as opposed to F fields. For  $C \gg 1$ , this expression is again evaluated via saddle point resulting in the same solution as above  $f(\sigma) = \sigma$ , and thus in the matrix element

$$\langle E_r | \mathcal{O}_{\ell}(\sigma_1, \sigma_2) | E_r \rangle = \left[ \left( \frac{\pi}{\beta_{\theta}} \right)^2 \frac{1}{\sin^2 \left( \frac{\pi}{\beta_{\theta}} \sigma_{12} \right)} \right]^{2\ell}$$
(4.58)

with effective temperature

$$T_{\theta} = 1/\beta_{\theta} = \theta \sqrt{\frac{2E}{C}} \,. \tag{4.59}$$

The reader will recall that solutions on this orbit are classified by their monodromy, whence  $\theta \in$ 

 $\mathbb{R}$  corresponds to the elliptic class of solutions while  $\theta = ip \in i\mathbb{R}$  corresponds to the hyperbolic class. The time parameter  $\sigma$  appearing in the correlation function has the interpretation of Euclidean time in the 1D theory, so that the result is thermal for  $\theta \in \mathbb{R}$  and non-thermal for  $\theta \in i\mathbb{R}$ . We note that this is in perfect agreement with the results of [117, 155] who consider the scrambling behavior of the 2D identity block and finds an effective temperature analogous to (4.59) also in the elliptic case (i.e. for operators below the BTZ threshold). It is interesting to note that [156], who study properties of de Sitter horizons, also find the oscillatory to exponential cross-over of the OTOC, which they associate with the different Virasoro coadjoint orbits. A soft-mode action of the Schwarzian type appears in their work as the boundary action of AdS<sub>2</sub>, which has been glued to a dS<sub>2</sub> region in the IR.

We would now like to go on and calculate the semi-classical two-point function of bilocals, which will allow us to extract the OTOC in the pure states  $|\Psi\rangle$ . We will arrive at this result by using the symplectic structure of Alekseev and Shatashvili [120,142], allowing us to compute the semi-classical expectation value of commutators of the relevant operators.

## 4.3.2 Semiclassical OTOC and chaos conjecture

As discussed in [142,144], the standard symplectic form  $\omega = \int d\pi \wedge d\varphi$  subject to the boundary conditions considered in section 4.2.1 gives rise to the Poisson bracket

$$\{f(\sigma_1), f(\sigma_2)\}_{PB} = \frac{1}{4T_0} \left( \frac{\sinh\left(2\sqrt{T_0}\lambda(\sigma_1, \sigma_2)\right)}{\sinh\left(2\pi\sqrt{T_0}\right)} - \frac{\lambda(\sigma_1, \sigma_2)}{\pi} \right), \tag{4.60}$$

$$\lambda(\sigma_1, \sigma_2) = f(\sigma_1) - f(\sigma_2) - \pi\epsilon(\sigma_1 - \sigma_2)$$

between two Schwarzian soft modes. Here  $\epsilon(x) = 2n+1$ ,  $x \in (2\pi n, 2\pi(n+1))$  is the stair step function, which will play no further role in our analysis, while  $T_0$  is the constant representative defined in (4.25). For large separation  $\sigma_1 - \sigma_2$  and evaluated on the saddle point (4.51), this Poisson bracket takes the simple form

$$\{f(\sigma_1), f(\sigma_2)\}_{PB} \sim \frac{\sinh\left(2\sqrt{\frac{2E}{C}T_0}(\sigma_1 - \sigma_2)\right)}{4T_0\sinh\left(2\pi\sqrt{T_0}\right)}$$
(4.61)

Using to the standard Dirac quantization prescription, this then allows us to compute the semi-classical commutator

$$[f(\sigma_1), f(\sigma_2)]_{\text{s.c.}} = -i\hbar \{f(\sigma_1), f(\sigma_2)\}_{\text{PB}}$$

$$(4.62)$$

where we have of course h = 1/C by comparing to the action (4.1). We now explain how this allows us to extract the quantum Lyapunov exponent with respect to our pure states  $|\Psi\rangle$ . The quantum Lyapunov exponent is diagnosed from a correlation function with four time insertions of the type

$$G_{\ell_1,\ell_2}^{\text{OTO}}(t_1, t_2, t_3, t_4) = \langle \Psi | \mathcal{O}_{\ell_1}(t_1, t_2) \mathcal{O}_{\ell_2}(t_3, t_4) | \Psi \rangle, \tag{4.63}$$

where the Lorentzian times are ordered, such that  $t_1 < t_3 < t_2 < t_4$ . This can be obtained as an analytic continuation from the Euclidean correlation function  $\langle \Psi | \mathcal{O}(\sigma_1, \sigma_2) \mathcal{O}(\sigma_3, \sigma_4) | \Psi \rangle$  by defining<sup>18</sup>

$$\sigma_i = it_i + \epsilon_i$$
, with  $\epsilon_1 < \epsilon_3 < \epsilon_2 < \epsilon_4$  (4.64)

The resulting correlation function then depends on the precise analytical structure of the correlator as a function of complex time insertions. The problem was solved in [127] for the thermal OTO by appealing to the *R*-matrix of Ponsot and Teschner [157] together with a plausible ansatz about its behavior in the semiclassical limit. In order to find the OTO in eigenstates we take a different route, which also applies to the thermal case, where it agrees with the answer found in [127]. It would be interesting to further understand how these two methods are related.

Thanks to the semi-classical results we established above, in conjunction with the symplectic form (4.61), we can sidestep this somewhat involved procedure. Before we describe this argument let us introduce some notation. For the purposes of being explicit about analytic continuation it is often useful to formally split up a bilocal operator as  $\mathcal{O}_{\ell}(\sigma_1, \sigma_2) \sim V(\sigma_1)V(\sigma_2)$ ,

$$\sigma_1 = -\frac{\beta}{4} + it_1 \; , \quad \sigma_2 = \frac{\beta}{4} + it_1 \; , \quad \sigma_3 = -\frac{\beta}{4} + it_2 \; , \quad \sigma_4 = \frac{\beta}{4} + it_2 \; .$$

One could consider a similar arrangement by inserting the ETH temperature associated with the pure state, but the above arrangement appears more natural in our context.

<sup>&</sup>lt;sup>18</sup>In the thermal case one instead often displaces the Lorentzian times a quarter turn around the thermal circle

and thus denote the corresponding correlation function

$$\langle \mathcal{O}_{\ell_1}(\sigma_1, \sigma_2) \mathcal{O}_{\ell_2}(\sigma_3, \sigma_4) \rangle \Leftrightarrow \langle V(\sigma_1) V(\sigma_2) W(\sigma_3) W(\sigma_4) \rangle.$$
 (4.65)

This is simply a formal device that makes clear that we may consider any ordering of (Lorentzian) time insertions on all legs, such as the time ordered arrangement  $t_1 < t_2 < t_3 < t_4$ , or the out-of-time ordered one  $t_1 < t_3 < t_2 < t_3$ . The order of arranging the 'split' bilocals simply expresses the corresponding time-order of the 2n times of a correlation function of n bilocal operators.

With this formal device in place, the difference between a time-ordered and an out-oftime-order correlation function is given by the insertion of a commutator

$$G_{\ell_1\ell_2}^{\text{TO}}(t_1, t_3, t_2, t_4) - G_{\ell_1\ell_2}^{\text{OTO}}(t_1, t_2, t_3, t_4) = \langle W(t_1) [W(t_3), V(t_2)] V(t_4) \rangle$$
(4.66)

This relation is elementary, but we can also understand it in terms of the analytic continuation from the Euclidean correlator. The difference between the continuation to a time-ordered and an out-of-time order configuration of Lorentzian times is due to crossing a branch cut in the complex  $\sigma$  plane. The discontinuity across the cut is, once again, given by the insertion of the commutator in the correlation function. We can view the construction of the OTOC from a TOC as a braiding operation, as illustrated in Figure 4.4.

In the case at hand, we can evaluate the commutator by using the Poisson bracket (4.61) together with the various semiclassical saddle points relevant to our pure states (4.51). We thus have

$$G_{\ell_1 \ell_2}^{\text{TO}} - G_{\ell_1 \ell_2}^{\text{OTO}} = \frac{1}{C} \frac{\delta \mathcal{O}_{\ell_1}}{\delta f(t_2)} \frac{\delta \mathcal{O}_{\ell_2}}{\delta f(t_3)} \left\{ f(t_2), f(t_3) \right\}_{\text{PB}} \bigg|_{f = f_{\text{saddle}}}$$

$$\sim \frac{1}{C} \sinh \left( 2\pi \theta \sqrt{\frac{2E}{C}} t_{23} \right) \tag{4.67}$$

The tilde in this expression denotes a time-independent proportionality factor, which includes the normalization of the symplectic form (4.61)  $1/\sin(\pi\theta)$  in the denominator. This factor

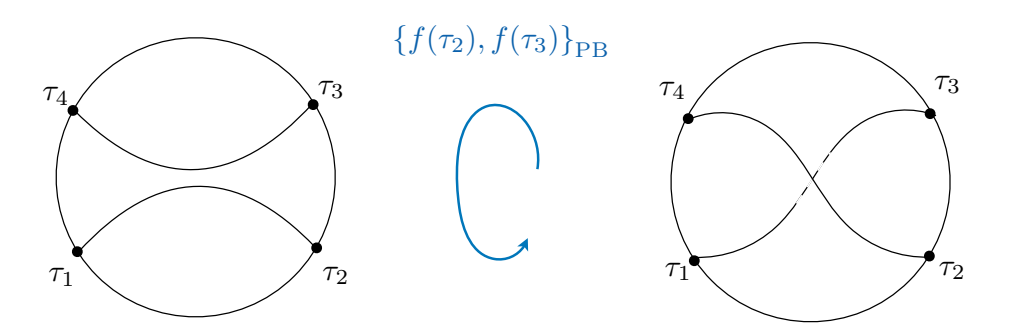


Figure 4.4: Illustration of our computation of the semiclassical OTO by saddle point. In order to get the operator in OTO order as shown, we must twist two of the insertions around each other. Quantum mechanically this corresponds to the 'second-sheet' analytic continuation from Euclidean to Lorentzian times and is equivalent to the insertion of a commutator  $[f(\sigma_1), f(\sigma_2)]$  when writing the operators in terms of integrals over the Goldstone mode f. This commutator can be computed semiclassically using the AS symplectic form to generate the Poisson bracket  $\{f(\sigma_1), f(\sigma_2)\}$  living on the appropriate Virasoro coadjoint orbit (Details in section 4.3.2).

diverges at the parabolic orbit  $\theta = 1$ . We implicitly regulate this UV divergence by introducing an  $\epsilon$  factor, which we view as analogous to the divergent prefactor in [158]. This expression thus tells us that the OTO correlation function behaves maximally chaotically at the appropriate eigenstate temperature

$$\langle \Psi | \mathcal{O}_{\ell_1}(t_1, t_2) \mathcal{O}_{\ell_1}(t_3, t_4) | \Psi \rangle_{\text{OTO}} \sim 1 - \frac{\#}{C} e^{\lambda t_{23}}, \quad \text{with} \quad \lambda = 2\pi/\beta_{\Psi}$$
 (4.68)

where  $|\Psi\rangle$  is either  $|E(k)\rangle$  or one of the coherent states  $|E_r\rangle$  for  $r < \sqrt{2}$ . The former corresponds to parabolic and the latter to elliptic monodromy of the associated Hill's equation. On the other hand, if we dial the parameter r characterizing the boundary state through  $r_c = \sqrt{2}$  we find the non-ergodic OTOC

$$\langle E_r | \mathcal{O}_{\ell_1}(t_1, t_2) \mathcal{O}_{\ell_1}(t_3, t_4) | E_r \rangle_{\text{OTO}} \sim 1 - \frac{\#}{C} e^{i\lambda t_{23}}, \quad \text{with} \quad \lambda = 2\pi \sqrt{\frac{2E}{C}} p$$
 (4.69)

for  $\theta = ip \in i\mathbb{R}$ . We have thus uncovered a phase transition in the scrambling behavior of the Schwarzian theory<sup>19</sup>, whereby the model changes from maximally chaotic behavior

<sup>&</sup>lt;sup>19</sup>And thus also in the IR limit of the SYK model and related many-body systems [23, 24, 111, 159]

with exponentially growing OTOCs to a phase that does not scramble at all and the OTOC behaves in an oscillatory fashion. As was remarked in an analogous two-dimensional CFT context, this is an analytical example of a transition between an ergodic and a non-ergodic phase and as such deserves further study.

#### 4.3.3 An alternative derivation

For the expectation values with respect to the FZZT density operator  $\rho = |E_r\rangle\langle E_r|$  we can obtain the chaos exponent directly from a perturbative quantization of the action (4.34). Since this discussion parallels that in [117, 155, 160], who computed the chaos exponent in thermal states excited by a heavy operator, we will be brief. The idea is to expand the action appearing in the exponent of (4.34) in fluctuations

$$f(\sigma) = \tan\left(\frac{\pi}{\beta_{\text{eff}}} \left(\sigma + \varepsilon(\sigma)\right)\right),$$
 (4.70)

where  $\beta_{\text{eff}}$  is the effective temperature defined in (4.5). We then compute the Euclidean correlation function of two bilocals  $\langle O_{\ell_1}(\sigma_1, \sigma_2) O_{\ell_2}(\sigma_3, \sigma_4) \rangle$  using the propagator of the fluctuation  $\langle \varepsilon(\sigma)\varepsilon(\sigma') \rangle$  given, for example, in [11,12]. The leading perturbative result, continued into the chaos region reads

$$\frac{\langle \mathcal{O}_{\ell_1}(\sigma_1, \sigma_2) \mathcal{O}_{\ell_2}(\sigma_3, \sigma_4) \rangle}{\langle \mathcal{O}_{\ell_1}(\sigma_1, \sigma_2) \rangle \langle \mathcal{O}_{\ell_2}(\sigma_3, \sigma_4) \rangle} \sim -2\pi \frac{\sin\left(\frac{\pi}{\beta_{\text{eff}}}(\sigma_1 + \sigma_2 - \sigma_3 - \sigma_4)\right) + \dots}{\sin\left(\pi \frac{\sigma_{12}}{\beta_{\text{eff}}}\right) \sin\left(\pi \frac{\sigma_{34}}{\beta_{\text{eff}}}\right)}$$
(4.71)

$$\xrightarrow{\sigma_{1,2} \to it \pm \epsilon_{12}} \quad 1 - \frac{\#}{C} \frac{\sinh\left(\frac{2\pi}{\beta_{\text{eff}}}t\right)}{\epsilon_{12}\epsilon_{34}} + \dots \tag{4.72}$$

In the above expressions the ellipsis denotes subleading corrections to exponential behaviour and  $\epsilon_{12}$ ,  $\epsilon_{34}$  originate from the continuation procedure, as indicated. We are keeping them in the final result to play the role of UV regulators [158]. In the second line we have added the leading disconnected contribution which is always present. From this expression we deduce, again, that  $\lambda = \frac{2\pi}{\beta_{\text{eff}}}$ , i.e. that the coherent states are maximally scrambling at the effective temperature deduced from ETH. Of course we must ensure to be in the ergodic region  $(r < \sqrt{2})$  for this result to hold.

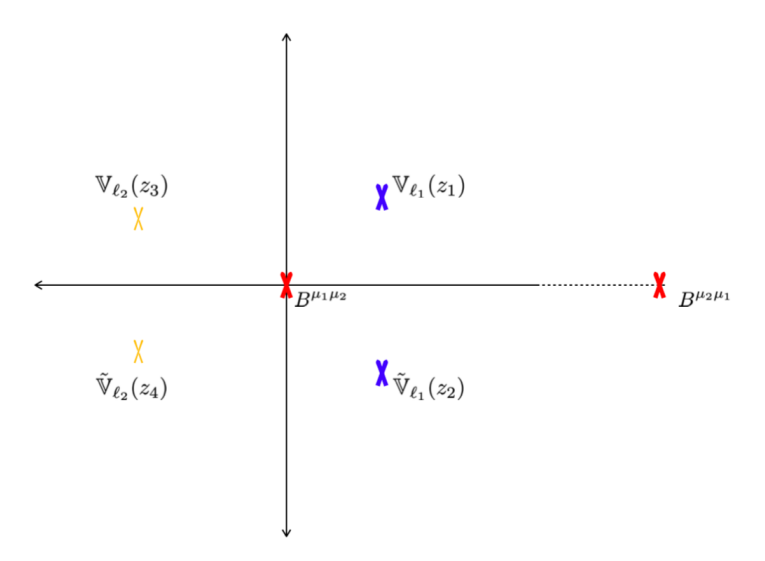


Figure 4.5: The configuration of various insertions on the two-dimensional complex plane that evaluates the bilocal two-point functions with ZZ and FZZT boundary conditions. Operators B are those that impose the ZZ and FZZT boundary conditions on positive and negative real axis respectively. While the tilde-operators are the mirror operators after the doubling trick.

We now describe a computation that exploits the boundary-CFT perspective of [122,123] together with [116] to give yet another derivation of the result above.

As pointed out in [113], the dimensionless coupling of the Schwarzian theory is  $\sim C/\beta$ , and thus the large-C limit is equivalent to a high-temperature limit at fixed C. One may then take the high-temperature limit directly in the Liouville theory before descending to the Schwarzian [113]. We thus want to calculate the two-point function of the Liouville vertex operator in the UHP with appropriate boundary conditions on the real axis. Recall that the boundary states  $|E_T\rangle$  correspond to ZZ boundary conditions on the positive real axis and FZZT boundary conditions on the negative real axis. This means that we are really evaluating a six-point function on the plane in the geometry shown in Figure 4.5. There are boundary operators implementing the ZZ and FZZT boundary conditions at the origin and at infinity, as well as the two physical operators in the UHP and their two mirror operators in the LHP. We formally allow the mirror operators' positions to be arbitrary, as indicated in Figure 4.5. In this way each pair of mirror operators descends to an operator of the type  $\mathcal{O}_{\ell}(\sigma_1, \sigma_2)$  in the Schwarzian limit, notably admitting two arbitrary time insertions  $(\sigma_2 \neq -\sigma_1)$ . It was shown

in [116], under the assumption of identity dominance, that such a six-point function reduces to an effectively thermal result for the four-point function of the vertex operators alone. In the present context identity dominance is no longer an assumption, as it follows from the OPE coefficients of boundary Liouville theory [122, 123]. Hence we evaluate the correlation function by contracting each operator with its mirror operator into the identity, using the boundary OPE derived in [122, 123] and like-wise contract the boundary operators into the identity with the result

$$\frac{\langle \mathcal{O}_{\ell_1}(\sigma_1, \sigma_2) \mathcal{O}_{\ell_2}(\sigma_3, \sigma_4) \rangle_r^{\text{TO}}}{\langle \mathcal{O}_{\ell_1}(\sigma_1, \sigma_2) \rangle_r \langle \mathcal{O}_{\ell_2}(\sigma_3, \sigma_4) \rangle_r} = \mathcal{J}(z) (1 - z)^{2\Delta_{\ell_1}} \mathcal{F}_{\text{id}} \left[ \frac{\Delta_{\ell_1} \Delta_{\ell_2}}{\Delta_{\ell_1} \Delta_{\ell_2}}; 1 - z \right]. \tag{4.73}$$

Here the conformal block is evaluated on the thermal coordinate [79, 116]  $z_i = e^{i\frac{2\pi}{\beta_{\rm eff}}\sigma_i}$  so that the cross ratio takes the form  $z = \frac{\sin\left(\frac{\pi}{\beta_{\rm eff}}\sigma_{13}\right)\sin\left(\frac{\pi}{\beta_{\rm eff}}\sigma_{24}\right)}{\sin\left(\frac{\pi}{\beta_{\rm eff}}\sigma_{23}\right)\sin\left(\frac{\pi}{\beta_{\rm eff}}\sigma_{14}\right)}$  and J is the Jacobian for the coordinate transformation  $\sigma_i \to z_i$  [116] whose specific form plays no further role in this analysis. Contracting each operator with its mirror operator means that  $z \to 1$ . Under the same analytic continuation as above we obtain

$$1 - z \xrightarrow{\sigma_{1,2} \to it \pm \epsilon_{12}} - \frac{\pi^2 \epsilon_{12} \epsilon_{34}}{\beta_{\text{eff}}^2} e^{-\frac{2\pi}{\beta_{\text{eff}}} t}$$

$$(4.74)$$

Furthermore, in order to move from the Euclidean configuration of the  $\sigma_i$  to the Lorentzian OTO configuration imposed by the  $\epsilon_i$ , we moved the cross ratio around the branch point at z = 1, so that now the block is evaluated on the second sheet [116, 158]. In the Schwarzian limit, this gives again, to leading order

$$\frac{\langle \mathcal{O}_{\ell_1}(\sigma_1, \sigma_2) \mathcal{O}_{\ell_2}(\sigma_3, \sigma_4) \rangle_r^{\text{OTO}}}{\langle \mathcal{O}_{\ell_1}(\sigma_1, \sigma_2) \rangle_r \langle \mathcal{O}_{\ell_2}(\sigma_3, \sigma_4) \rangle_r} = 1 - \frac{\#}{C\epsilon_{12}\epsilon_{34}} e^{\frac{2\pi}{\beta_{\text{eff}}}t} + \cdots$$

$$(4.75)$$

Thus once again we find the maximally chaotic behavior (4.68) of the OTOC in pure states. As in (4.72) we should keep in mind that the exponential behavior is true so long as we stay in the range  $r < \sqrt{2}$ . For  $r > \sqrt{2}$  the effective temperature becomes imaginary, and the OTOC oscillates.

The recent papers [117, 155] consider a closely related  $^{20}$  computation in the context of

<sup>&</sup>lt;sup>20</sup>In fact the effective-field-theory of the identity block [161,162] employed in [117] makes the analogy

two-dimensional CFT: they insert two heavy operators at spatial infinity into an already thermal system. The resulting configuration is then again approximately thermal, but at the modified temperature  $\beta_{\text{eff}}$ , depending on the heavy state insertions. The scrambling exponent found in [117,155] takes on the value  $2\pi/\beta_{\text{eff}}$  with respect to this effective temperature, in accordance with the results we find for the Schwarzian theory.

## 4.4 Exact results

In this section we describe how to obtain the exact results for the Schwarzian correlation functions we discussed above semi-classically. We will also show that these expression result from a suitable semi-classical expansion of the full answers, giving a second independent derivation of our results on eigenstates and the behavior of correlation functions therein. Our main technical vehicle to obtain full exact expressions for correlation functions is the descent construction described in section 4.2.1, in other words we will find the Schwarzian answers as limits of those obtained in boundary Liouville theory using the identities (4.45) and (4.47).

## 4.4.1 Computations between ZZ branes

We now use the boundary state perspective to find the one and two-point functions of bilocal operators in the presence of Dirichlet boundary conditions. This will allow us to confirm our semiclassical expectations above, as well as to show the maximal eigenstate chaos conjecture once more from a different perspective. One and two-point functions with Dirichlet conditions have previously been computed by [113,127]. We repeat these calculations for two reasons: firstly to extend those results to include extended ETH as well as the chaos exponent in eigenstates; and secondly, to express everything in our own conventions <sup>21</sup> before moving on to the general case including FZZT states.

even closer, taking the form of a Schwarzian-like description for this object.

<sup>&</sup>lt;sup>21</sup>A caveat for the reader interested in reproducing the detailed calculations: our conventions are fully aligned with [123], but differ in some places from the ones used in [113, 127].

4.4 Exact results 125

#### Bilocal one-point function $\langle ZZ|V_{\ell}(x,\bar{x})|ZZ\rangle$

We are interested in evaluating a particular case of (4.47) with only one operator insertion. Recall, the ZZ-wavefunction can be written as, (4.42),

$$\Psi_{ZZ}(P) := \langle ZZ|P \rangle = 2^{3/4} 2i\pi P \left(\frac{\gamma(b^2)}{8b^2}\right)^{-\frac{iP}{b}} \frac{1}{\Gamma(1 - 2iPb)\Gamma(1 - 2\frac{iP}{b})}.$$
 (4.76)

Putting together the ingredients we assembled in subsection 4.2.3, the expression for the expectation value  $\langle ZZ|V_{\ell}(z,\bar{z})|ZZ\rangle$  reads in full detail

$$2^{3/2} \pi^2 \int dP^2 dR^2 \frac{\left(\frac{\gamma(b^2)}{8b^2}\right)^{i\frac{P-R}{b}}}{\Gamma\left(1+2ibP\right)\Gamma\left(1+2i\frac{P}{b}\right)\Gamma\left(1-2ibR\right)\Gamma\left(1-2i\frac{R}{b}\right)} \langle \nu_R | \mathbb{V}_{\ell}(z,\bar{z}) | \nu_P \rangle \tag{4.77}$$

Let us now start simplifying this expression, starting with the matrix element of the vertex operator between primary states,

$$\langle \nu_{R} | \mathbb{V}_{\ell}(x, \bar{x}) | \nu_{P} \rangle = \langle \nu_{R} | e^{-\frac{4\pi}{a} \left(\frac{\beta}{2} - \sigma\right) L_{0}} \mathbb{V}_{\ell} e^{-\frac{4\pi}{a} \sigma L_{0}} | \nu_{P} \rangle$$

$$= e^{-\frac{2\beta\pi}{a} \Delta_{R}} e^{-\frac{4\pi}{a} \sigma(\Delta_{P} - \Delta_{R})} \langle \nu_{R} | \mathbb{V}_{\ell}(0, 0) | \nu_{P} \rangle$$

$$= e^{-\frac{2\beta\pi}{a} \Delta_{R}} e^{-\frac{4\pi}{a} \sigma(\Delta_{P} - \Delta_{R})} \frac{1}{2b} \int d\varphi \langle \nu_{R} | \varphi \rangle \langle \varphi | \nu_{P} \rangle e^{2\ell\varphi}$$

$$(4.78)$$

where,  $w, \bar{w} = \tau \pm i\sigma$  are the coordinates on the open string; and,  $x, \bar{x} = -i\tau \pm \sigma = -iw$ ,  $-i\bar{w}$  are the coordinates on the dual closed string. We have also used the fact that we are working with a chiral-CFT with only the holomorphic sector. The projection of the wavefunctions on the  $\varphi$ -basis is given by [123],

$$\langle \nu_R | \varphi \rangle = 2 \frac{\left(8b^4\right)^{-i\frac{R}{b}}}{\Gamma\left(2i\frac{R}{b}\right)} K_{-2i\frac{R}{b}} \left(\frac{e^{\varphi/2}}{\sqrt{2}b^2}\right),$$

$$\langle \varphi | \nu_P \rangle = 2 \frac{\left(8b^4\right)^{i\frac{P}{b}}}{\Gamma\left(-2i\frac{P}{b}\right)} K_{2i\frac{P}{b}} \left(\frac{e^{\varphi/2}}{\sqrt{2}b^2}\right).$$

$$(4.79)$$

Thus the matrix element boils down to

$$\langle \nu_R | \mathbb{V}_{\ell}(x,\bar{x}) | \nu_P \rangle = \frac{1}{2b} \left( 8b^4 \right)^{2\ell + i\frac{P-R}{b}} \frac{\Gamma\left( 2\ell \pm \frac{i}{b}(P \pm R) \right)}{\Gamma\left( -2i\frac{P}{b} \right) \Gamma\left( 2i\frac{R}{b} \right) \Gamma(4\ell)} e^{-\frac{2\beta\pi}{a}\Delta_R} e^{-\frac{4\pi}{a}\sigma(\Delta_P - \Delta_R)} . \quad (4.80)$$

In view of our descent to the 1D Schwarzian theory, we need to additionally make the change of variables,  $P = b\mathfrak{p}$ ,  $R = b\mathfrak{r}$ , since, from this point of view, we are interested in the  $b \to 0$  limit. Recall that the operator insertions in Liouville theory corresponding to the bilocal operator insertions in the 1D theory are of the form,

$$\mathbb{V}_{\ell}(x,\bar{x}) = e^{2\ell\varphi} \quad \text{under 1D reduction} \quad \left(\frac{\sqrt{f'(\sigma)f'(-\sigma)}}{|f(\sigma) - f(-\sigma)|}\right)^{2\ell} \tag{4.81}$$

For the most part we are interested in operators satisfying  $\ell \sim \mathcal{O}(1)$ , in which case the conformal dimension of the 2D vertex operator is  $\Delta_{\ell} = 2b\ell (Q - 2b\ell)$ . Since we want the boundary states to be of similar energies as the insertions themselves,  $\Delta_P \sim \Delta_{\ell} \Rightarrow P \sim \pm \frac{Q}{2} \mp 2b\ell$ . Up to the constant shift,  $\frac{Q}{2}$ , which will not matter, we get  $P \sim \mathcal{O}(b)$ . Now we reinsert the expression for the matrix element into the full expectation value (4.77). In anticipation of the  $b \to 0$  limit to come, we already restrict the Ishibashi states to their leading term (the primary state) and write

$$\langle \mathbf{Z}\mathbf{Z}|\mathbb{V}_{\ell}(x,\bar{x})|\mathbf{Z}\mathbf{Z}\rangle = 2^{1/2}b^{3}\left(8b^{4}\right)^{2\ell}\int d\mathfrak{p}^{2}\,d\mathfrak{r}^{2}\,\sinh(2\pi\mathfrak{p})\sinh(2\pi\mathfrak{p})\,e^{-\frac{2\beta\pi}{a}\left(\frac{Q^{2}}{4}+b^{2}\mathfrak{r}^{2}\right)}e^{\frac{4\pi}{a}\sigma\,b^{2}\left(\mathfrak{r}^{2}-\mathfrak{p}^{2}\right)}$$

$$\times\frac{\Gamma\left(2\ell\pm i(\mathfrak{p}\pm\mathfrak{r})\right)}{\Gamma(4\ell)}\left\{\frac{\left(b^{2}\gamma(b^{2})\right)^{i(\mathfrak{p}-\mathfrak{r})}}{\Gamma\left(1+2ib^{2}\mathfrak{p}\right)\Gamma\left(1-2ib^{2}\mathfrak{r}\right)}\right\}.$$

We can now straightforwardly take the limit  $b \to 0$  of the above expression, giving the final result for the expectation value in the form,

$$\langle ZZ|\mathbb{V}_{\ell}(x,\bar{x})|ZZ\rangle = 2^{1/2}b^{3}\left(8b^{4}\right)^{2\ell}e^{-\frac{\pi\beta Q^{2}}{2a}}\int d\mathfrak{p}^{2}d\mathfrak{r}^{2}e^{2\pi(\mathfrak{p}+\mathfrak{r})}e^{-\frac{\beta}{2C}\mathfrak{r}^{2}}e^{\frac{\sigma}{C}(\mathfrak{r}^{2}-\mathfrak{p}^{2})}\frac{\Gamma\left(2\ell\pm i(\mathfrak{p}\pm\mathfrak{r})\right)}{\Gamma(4\ell)}.$$

$$(4.82)$$

In writing (4.82) we have made use of the  $\mathfrak{p} \to -\mathfrak{p}$  and  $\mathfrak{r} \to -\mathfrak{r}$  symmetries of the integrand to convert the hyperbolic sine contributions into exponentials. Also,  $C = a/4\pi b^2$  was defined in previously in (4.31). The expression (4.82) is our final result for the *exact* one-point function.

The zero (1-dimensional) temperature limit of the answer is given by taking  $\beta \to \infty$ . In

<sup>&</sup>lt;sup>22</sup>More accurately, we want to insert a complete set of states for the 1-dimensional theory, which is equivalent to insertion of ZZ branes with energies scaled as described here. On the other hand, as we will see in the next section, the insertion of FZZT states is equivalent to choosing a 'heavy' state.

4.4 Exact results 127

this limit, the  $\mathfrak{r}$  integral condenses to  $\mathfrak{r} = 0$ . Consequently,

$$\langle ZZ|\mathbb{V}_{\ell}(x,\bar{x})|ZZ\rangle_{\beta\to\infty} = \langle \mathcal{O}_{\ell}(2\sigma,0)\rangle_{\beta\to\infty} \sim \int d\mathfrak{p}^2 \, e^{2\pi\mathfrak{p}} \, e^{-\frac{\sigma}{C}\mathfrak{p}^2} \, \frac{\Gamma^2\left(2\ell \pm i(\mathfrak{p})\right)}{\Gamma(4\ell)} \,\,, \tag{4.83}$$

which matches the answer earlier derived in [17, 102, 113, 127].

One can instead compute the correlation functions in the eigenstates,  $|E(\mathfrak{l})\rangle := |\mathfrak{l}\rangle$  of the Schwarzian theory by first projecting out from the superposition of  $|\mathfrak{r}\rangle$  states any state with energy less than  $\mathfrak{l}^2/2C$ . This is achieved by cutting off the  $\mathfrak{r}$  integral as follows,

$$\langle \mathfrak{l} | \mathcal{O}_{\ell}(2\sigma, 0) | \mathfrak{l} \rangle_{\beta \to \infty} \sim \lim_{\beta \to \infty} \int d\mathfrak{p}^{2} \int_{|\mathfrak{r}| \ge |\mathfrak{l}|} d\mathfrak{r}^{2} e^{2\pi(\mathfrak{p}+\mathfrak{r})} e^{-\frac{\beta}{2C}\mathfrak{r}^{2}} e^{\frac{\sigma}{C}(\mathfrak{r}^{2}-\mathfrak{p}^{2})} \frac{\Gamma(2\ell \pm i(\mathfrak{p} \pm \mathfrak{r}))}{\Gamma(4\ell)}$$

$$\sim \mathfrak{l} \sinh(2\pi\mathfrak{l}) \int d\mathfrak{p}^{2} e^{2\pi\mathfrak{p}-\frac{\sigma}{C}(\mathfrak{p}^{2}-\mathfrak{l}^{2})} \frac{\Gamma(2\ell \pm i(\mathfrak{p} \pm \mathfrak{l}))}{\Gamma(4\ell)}$$

$$(4.84)$$

One can think of this cut-off prescription as follows: an ensemble of states,

$$\rho = e^{-\beta H} |\Psi\rangle\langle\Psi| \quad \xrightarrow{\beta \to \infty} \quad |E_{\text{low}}\rangle\langle E_{\text{low}}| \tag{4.85}$$

where  $|E_{\text{low}}\rangle$  is the lowest energy state that appears in the wavefunction  $|\Psi\rangle$ . By introducing the cut-off we work with a wavefunction whose lowest energy state is the one corresponding to  $E_{\text{low}} = E(\mathfrak{l}) = \mathfrak{l}^2/(2C)$ . Taking  $\beta \to \infty$  with the original ZZ wavefunction gives us the vacuum expectation value, (4.83), because the lowest energy state in ZZ-wavefunction corresponds to  $\mathfrak{l} = 0$ .

## Semiclassical limit

Next, let us evaluate the integral appearing in (4.82) in the  $C \sim a/b^2 \to \infty$  limit using the saddle point analysis. We start by performing the following change of variables,  $\mathfrak{p} + \mathfrak{r} = \frac{aM}{b^2}$  and  $\mathfrak{p} - \mathfrak{r} = \omega$ . To evaluate this integral, one may integrate  $\omega$  exactly, noting that is precisely a Mellin-Barnes type integral, [163] and then solve the remaining M integral via saddle point. Keeping only the leading terms as  $C \to \infty$  we find

$$M_* = \frac{2a}{\beta} \tag{4.86}$$

Finally, the semiclassical limit of the correlation function becomes

$$\langle ZZ|V_{\ell}(x,\bar{x})|ZZ\rangle \sim \frac{2^{3/2}M_{\star}^{2}}{2b} \left(8b^{4}\right)^{2\ell} \frac{1}{2b^{2}} \left(2\pi e^{\frac{2C\pi^{2}}{\beta}}\right) \left(\frac{1}{2\sin\left(\frac{2\pi}{\beta}\sigma\right)}\right)^{4\ell} .$$
 (4.87)

To analyze the operator expectation value in the high energy eigenstates, let us consider (4.84) with  $\mathfrak{l} \sim \mathcal{O}(C)$ . In this case, consider  $\mathfrak{p} = \mathfrak{l} + m$ ,

$$\langle \mathfrak{l} | \mathcal{O}_{\ell}(2\sigma,0) | \mathfrak{l} \rangle_{\beta \to \infty} \sim \mathfrak{l} \sinh(2\pi \mathfrak{l}) \int dm \, (\mathfrak{l}+m) e^{2\pi(\mathfrak{l}+m) - \frac{\sigma}{C}(2\mathfrak{l}m+m^2)} \, \frac{\Gamma(2\ell \pm i(2\mathfrak{l}+m)) \, \Gamma(2\ell \pm im)}{\Gamma(4\ell)}$$

$$\sim \mathfrak{l}^2 \sinh(2\pi \mathfrak{l}) (2\mathfrak{l})^{4\ell-1} \int dm \, e^{\pi m - \frac{2\sigma \mathfrak{l}m}{C}} \, \frac{\Gamma(2\ell \pm im)}{\Gamma(4\ell)}$$

$$\sim \left(\frac{1}{2} \frac{1}{i \sin\left(\frac{2\pi \mathfrak{l}}{C}\sigma\right)}\right)^{4\ell} \tag{4.88}$$

The effective temperature due to the heavy state is given by,  $T_{\text{eff}} = \mathfrak{l}/C = \sqrt{2E(\mathfrak{l})/C}$ . This is consistent with the answer that we obtained in (4.54).

## Two-point function of light operators $\langle ZZ|V_{\ell_2}(x_2,\bar{x}_2)V_{\ell_1}(x_1,\bar{x}_1)|ZZ\rangle$

We have now shown that the insertion of ZZ branes in the 2D picture allows us to study Schwarzian expectation values either at finite temperature, or using the projection trick, with respect to the eigenstates of the theory. We now move on to higher-point correlators of operators of weight  $\mathcal{O}(1)$  and the interesting physics associated to them. To this end, we study the time ordered correlation function,  $\langle ZZ|\mathbb{V}_{\ell_2}(x_2,\bar{x}_2)\mathbb{V}_{\ell_1}(x_1,\bar{x}_1)|ZZ\rangle$ . Because of the dimensional reduction combined with the doubling trick described in section 4.2.3, from the 1-dimensional point of view we get a configuration of bilocal operator insertion with  $-\pi < -\sigma_2 < -\sigma_1 < 0 < \sigma_1 < \sigma_2 < \pi$ . In the Liouville theory the expression of this correlation function is,

$$\langle ZZ|\mathbb{V}_{\ell_{2}}(x_{2},\bar{x}_{2})\mathbb{V}_{\ell_{1}}(x_{1},\bar{x}_{1})|ZZ\rangle = 2^{3/2}\pi^{2}\int dP^{2}dR^{2}\frac{\left(\pi\mu\gamma(b^{2})\right)^{i\frac{P-R}{b}}}{\Gamma\left(1+2ibP\right)\Gamma\left(1+2i\frac{P}{b}\right)} \times \frac{\langle\nu_{R}|\mathbb{V}_{\ell_{2}}(x_{2},\bar{x}_{2})\mathbb{V}_{\ell_{1}}(x_{1},\bar{x}_{1})|\nu_{P}\rangle}{\Gamma\left(1-2ibR\right)\Gamma\left(1-2i\frac{R}{b}\right)}$$
(4.89)

4.4 Exact results 129

which, in 1-dimension, reduces to,

$$\sim \int d\mathfrak{p}^2 d\mathfrak{r}^2 d\mathfrak{d}^2 \sinh(2\pi\mathfrak{d}) \sinh(2\pi\mathfrak{p}) \sinh(2\pi\mathfrak{p}) \frac{\Gamma(2\ell_2 \pm i(\mathfrak{r} \pm \mathfrak{d}))}{\Gamma(4\ell_2)} \frac{\Gamma(2\ell_1 \pm i(\mathfrak{d} \pm \mathfrak{p}))}{\Gamma(4\ell_1)}$$

$$\times \exp\left[-\frac{1}{2C} \left(\beta\mathfrak{r}^2 + 2\sigma_2(\mathfrak{d}^2 - \mathfrak{r}^2) + 2\sigma_1(\mathfrak{p}^2 - \mathfrak{d}^2)\right)\right]$$
(4.90)

The Lyapunov exponent for the Schwarzian theory in the thermal ensemble has already been computed from the OTO two-point function of bilocals in [113,127] using the ZZ-brane perspective. Here our main interest is in using the projection trick of section 4.4.1 to instead compute the Lyapunov exponent with respect to the eigenstate density operator  $|E\rangle\langle E|$ , which is the main object of interest here. Applying the projection trick discussed previously to (4.90) results in the expression,

$$\sim \lim_{\beta \to \infty} \int d\mathfrak{p}^2 d\mathfrak{d}^2 \int_{|\mathfrak{r}| \ge |\mathfrak{l}|} d\mathfrak{r}^2 \sinh(2\pi\mathfrak{d}) \sinh(2\pi\mathfrak{p}) \sinh(2\pi\mathfrak{p}) \frac{\Gamma(2\ell_2 \pm i(\mathfrak{r} \pm \mathfrak{d}))}{\Gamma(4\ell_2)} \frac{\Gamma(2\ell_1 \pm i(\mathfrak{d} \pm \mathfrak{p}))}{\Gamma(4\ell_1)}$$

$$\times \exp\left[-\frac{1}{2C} \left(\beta\mathfrak{r}^2 + 2\sigma_2(\mathfrak{d}^2 - \mathfrak{r}^2) + 2\sigma_1(\mathfrak{p}^2 - \mathfrak{d}^2)\right)\right]$$

$$\sim \mathfrak{l} \sinh(2\pi\mathfrak{l}) \int d\mathfrak{p}^2 d\mathfrak{d}^2 \sinh(2\pi\mathfrak{d}) \sinh(2\pi\mathfrak{p}) \frac{\Gamma(2\ell_2 \pm i(\mathfrak{l} \pm \mathfrak{d}))}{\Gamma(4\ell_2)} \frac{\Gamma(2\ell_1 \pm i(\mathfrak{d} \pm \mathfrak{p}))}{\Gamma(4\ell_1)}$$

$$\times \exp\left[-\frac{1}{2C} \left(2\sigma_2(\mathfrak{d}^2 - \mathfrak{l}^2) + 2\sigma_1(\mathfrak{p}^2 - \mathfrak{d}^2)\right)\right] \tag{4.91}$$

In order to make contact with our semi-classical results on chaos in eigenstate 4.3.2 we also need an expression for the OTO version of the above. This can be formally achieved by insertion the R-matrix of [157], analogous to the thermal case worked out in [127],

$$\langle ZZ|\mathbb{V}_{\ell_{2}}(x_{2},\bar{x}_{2})\mathbb{V}_{\ell_{1}}(x_{1},\bar{x}_{1})|ZZ\rangle_{OTOC} =$$

$$\int d\mathfrak{p}d\mathfrak{r}d\mathfrak{p}_{s}d\mathfrak{p}_{t}C(-\mathfrak{r},2\ell_{2},\mathfrak{p}_{s})C(-\mathfrak{p}_{s},2\ell_{1},\mathfrak{p})\,\Psi_{ZZ}(b\mathfrak{r})\Psi_{ZZ}(-b\mathfrak{p})$$

$$\times R_{\mathfrak{p}_{s}\mathfrak{p}_{t}}\left[\begin{smallmatrix} 2\ell_{2}&2\ell_{1}\\\mathfrak{r}&\mathfrak{p}\end{smallmatrix}\right]\mathcal{F}_{\mathfrak{p}_{t}}\left[\begin{smallmatrix} 2\ell_{1}&2\ell_{2}\\\mathfrak{r}&\mathfrak{p}\end{smallmatrix}\right]\mathcal{F}_{\mathfrak{p}_{s}}\left[\begin{smallmatrix} 2\ell_{2}&2\ell_{1}\\\mathfrak{r}&\mathfrak{p}\end{smallmatrix}\right]\mathcal{F}_{\mathfrak{p}_{s}}\left[\begin{smallmatrix} 2\ell_{2}&2\ell_{1}\\\mathfrak{r}&\mathfrak{p}\end{smallmatrix}\right]. \tag{4.92}$$

where  $C(y_1, y_2, y_3)$  is the DOZZ three-point function, [164, 165]. After reduction to 1-dimension we obtain a final answer,

$$\frac{\langle O_{\ell_{2}}(\sigma_{3}, \sigma_{4}) O_{\ell_{1}}(\sigma_{1}, \sigma_{2}) \rangle}{\langle O_{\ell_{2}}(\sigma_{3}, \sigma_{4}) \rangle \langle O_{\ell_{1}}(\sigma_{1}, \sigma_{2}) \rangle} \sim \int d\mathfrak{p}^{2} d\mathfrak{r}^{2} d\mathfrak{p}_{s}^{2} d\mathfrak{p}_{t}^{2} \sinh(2\pi\mathfrak{p}) \sinh(2\pi\mathfrak{p}) \sinh(2\pi\mathfrak{p}_{s}) \sinh(2\pi\mathfrak{p}_{s}) \sinh(2\pi\mathfrak{p}_{t}) 
\times R_{\mathfrak{p}_{s}\mathfrak{p}_{t}} \begin{bmatrix} 2\ell_{2} 2\ell_{1} \\ \mathfrak{r} & \mathfrak{p} \end{bmatrix} \exp \left[ -\frac{1}{2C} \left( \mathfrak{p}^{2} (\beta - \sigma_{41}) - \mathfrak{p}_{t}^{2} \sigma_{31} - \mathfrak{r}^{2} \sigma_{32} - \mathfrak{p}_{s}^{2} \sigma_{41} \right) \right] 
\times \frac{\sqrt{\Gamma(2\ell_{1} \pm i(\mathfrak{p} \pm \mathfrak{p}_{t}))\Gamma(2\ell_{2} \pm i(\mathfrak{r} \pm \mathfrak{p}_{t}))\Gamma(2\ell_{1} \pm i(\mathfrak{r} \pm \mathfrak{p}_{s}))\Gamma(2\ell_{2} \pm i(\mathfrak{p} \pm \mathfrak{p}_{s}))}}{\Gamma(4\ell_{1})\Gamma(4\ell_{2})} \tag{4.93}$$

In the above and subsequent equations, we have generalized the placement of the operators to arbitrary points  $\sigma_i$ , with the ordering,  $-\beta/2 < \sigma_1 < \sigma_2 < \sigma_3 < \sigma_4 < \beta$ . The R-matrix,  $R_{\mathfrak{p}_s\mathfrak{p}_t}\left[\begin{smallmatrix} 2\ell_2 & 2\ell_1 \\ \mathfrak{r} & \mathfrak{p} \end{smallmatrix}\right]$  is related to the 6-j symbols of  $SL(2,\mathbb{R})$ . Its expression is rather daunting and we refer the reader to Appendix B of [127].

However, we can bypass this procedure by appealing to our results in section 4.3.3 and express the OTO correlation function in terms of the identity Virasoro block

$$\frac{\langle \mathcal{O}_{\ell_1}(\sigma_1, \sigma_2) \mathcal{O}_{\ell_2}(\sigma_3, \sigma_4) \rangle}{\langle \mathcal{O}_{\ell_1}(\sigma_1, \sigma_2) \rangle \langle \mathcal{O}_{\ell_2}(\sigma_3, \sigma_4) \rangle} \sim y^{2\Delta_{\ell_1}} \mathcal{F}_{id} \left[ \frac{\Delta_{\ell_1}}{\Delta_{\ell_1}} \frac{\Delta_{\ell_2}}{\Delta_{\ell_2}}; y \right], \tag{4.94}$$

where y = 1 - z, as defined in (4.73) and (4.74) above. Note that we had to pass to the semiclassical limit  $C \to \infty$  in order to establish this result. We see, once more, that the large-C expansion of the full result (4.92) agrees with our direct semiclassical evaluation, confirming that the eigenstates of the Schwarzian are maximally scrambling with Lyapunov exponent  $2\pi/\beta_{\text{eff}}$ .

## Heavy-light two-point function $\langle ZZ|V_{\ell^H}(x_1,\bar{x}_1)V_{\ell^L}(x_2,\bar{x}_2)|ZZ\rangle$

We next want to study the effect of inserting heavy operators on the (effective) temperature as perceived by light operators. We evaluate the 4-point function, (4.90), with a heavy operator,  $\mathbb{V}_{\ell_1} = \mathbb{V}_{\ell^H}$  with  $\ell^H \sim C$  and a light operator  $\mathbb{V}_{\ell_2} = \mathbb{V}_{\ell^L}$  with  $\ell^L \sim 1$ , in the classical limit to study ETH. Since the dimensionless parameter in our problem is  $C/\beta$ , the classical zero temperature limit can be taken in two ways:  $C/\beta \to \infty$  with  $\beta$  fixed, followed by  $\beta \to \infty$ ; or, by taking  $C, \beta \to \infty$  simultaneously such that  $\mathfrak{C} = C/\beta$  is finite followed by  $\mathfrak{C} \to \infty$ . We find that the thermal behaviour of this 4-point function depends on the order of limits.

4.4 Exact results 131

# $C/\beta \to \infty$ with $\beta$ fixed, followed by $\beta \to \infty$

In this limit, we perform a change of variables  $\mathfrak{r}^2 = \mathfrak{d}^2 + m$ . Consequently, the  $\mathfrak{p}, \mathfrak{d}$  integrals are performed using saddle point analysis while the m integral is done using the Mellin-Barnes technique discussed above.

$$\sim \int d\mathfrak{p}^2 d\mathfrak{d}^2 \,\mathfrak{d}^{4\ell^L} \sinh\left(2\pi\mathfrak{p}\right) \sinh\left(2\pi\mathfrak{d}\right) \frac{\Gamma\left(2\ell^H \pm i(\mathfrak{p} \pm \mathfrak{d})\right)}{\Gamma(4\ell^H)} \times \exp\left[-\frac{1}{2C}\left(\beta\mathfrak{d}^2 + 2\sigma_1\left(\mathfrak{p}^2 - \mathfrak{d}^2\right)\right)\right] \times \left[\frac{\mathfrak{d}}{\sin\left(\frac{\mathfrak{d}}{2C}\left(\beta - 2\sigma_2\right)\right)}\right]^{4\ell^L}$$
(4.95)

The saddle point equations, in the variables  $\mathfrak{p}$  and  $\mathfrak{d}$ , of the above integral are,

$$\tan(x\omega) = -\frac{4\omega\ell_{sc}}{4\tilde{\omega}^2 - 4\omega^2 + \ell_{sc}^2} \qquad \text{assuming} \qquad 4\tilde{\omega}^2 - 4\omega^2 + \ell_{sc}^2 \neq 0$$
 (4.96a)

$$\tan\left(\tilde{\omega}(\beta - x)\right) = -\frac{4\tilde{\omega}\ell_{sc}}{4\omega^2 - 4\tilde{\omega}^2 + \ell_{sc}^2} \quad \text{assuming} \quad 4\omega^2 - 4\tilde{\omega}^2 + \ell_{sc}^2 \neq 0 . \quad (4.96b)$$

For simplicity, here we have scaled the variables as follows,

$$\omega = \frac{\mathfrak{d}}{2C}, \quad \tilde{\omega} = \frac{\mathfrak{p}}{2C}, \quad \ell_{sc} = \frac{2\ell^H}{C}, \quad x = 2\sigma_1 .$$
 (4.97)

While these equations are transcendental and thus not exactly solvable, we can find the solutions for  $\omega, \tilde{\omega}$  is special limits. Note that the solutions of these variables depend on the separation of the heavy insertions, x. We take  $x = \beta/2$ . At this value of x, both equations are equivalent to

$$\tan\left(\frac{\beta}{2}\omega\right) = -\frac{4\omega}{\ell_{sc}} \ . \tag{4.98}$$

For very large values of  $\ell_{sc}$ , the solutions of this equation are given by,

$$\omega_n = 2n \frac{\pi}{\beta} - \mathfrak{c}_n , \quad \text{where, } \mathfrak{c}_n = \frac{16\pi n}{\beta(\beta \ell_{sc} + 8)} , \quad n \in \mathbb{Z} ,$$

$$\Rightarrow T_{\text{eff}} = \frac{1}{\beta_{\text{eff}}} = \frac{\omega_n}{\pi} = \frac{2nT\ell_{sc}}{\ell_{sc} + 8T} . \tag{4.99}$$

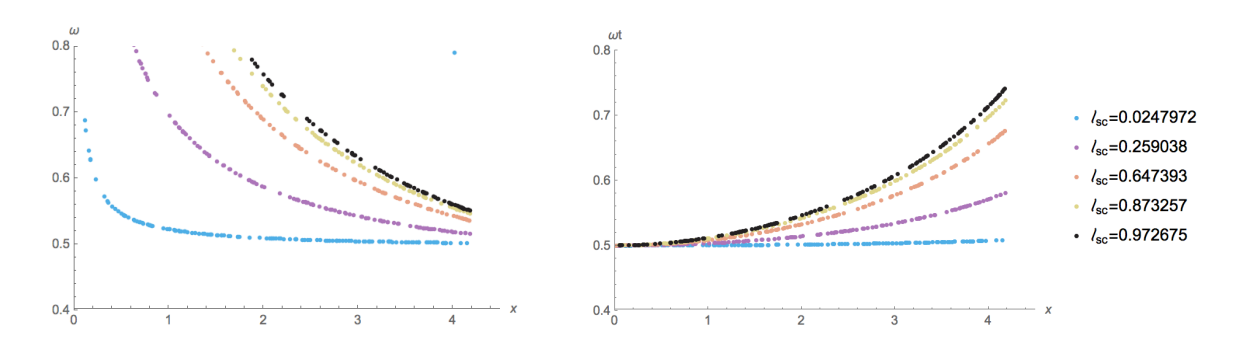


Figure 4.6: Plots for increasing values of  $\ell_{sc}$  demonstrate that the solution for  $\omega$  (left) and  $\tilde{\omega}$  (right) for a given x increases with increasing  $\ell_{sc}$ . In the above plot, C = 567.605,  $\beta = 2\pi$ . The solution for  $x = \beta$  is  $\omega = \pi/\beta$  for all values of  $\ell_{sc}$ . While the solution for x = 0 is  $\tilde{\omega} = \pi/\beta$  for all values of  $\ell_{sc}$ .

Here,  $T = 1/\beta$  is the background temperature that we began with;  $T_{\text{eff}} = 1/\beta_{\text{eff}}$  is the effective temperature perceived by the light operator in the presence of the heavy insertions,

$$\frac{\langle \mathcal{O}_{\ell^H} \mathcal{O}_{\ell^L} \mathcal{O}_{\ell^L} \mathcal{O}_{\ell^H} \rangle}{\langle \mathcal{O}_{\ell^H} \mathcal{O}_{\ell^H} \rangle} \sim \left( \frac{\pi}{\beta_{\text{eff}} \sin\left(\frac{2\pi\sigma_2}{\beta_{\text{eff}}}\right)} \right)^{4\ell^L} .$$
(4.100)

The  $\ell_{sc} \to 0$  limit leaves only n=1 as a physical solution; for all other solutions,  $\ell_{sc} \to 0$  limit leaves an unphysical 'residual' temperature. An observant reader may point out that for low enough values of  $\ell_{sc}$ ,  $T_{\rm eff} < T$ , but that is outside the validity of the above approximation. Moreover, the asymptotic temperature at large  $\ell_{sc}$  provides an upper-bound on the effective temperature. This is simply because we do not expect an operator with smaller  $\ell_{sc}$  to create a thermal state at a higher temperature than an operator with higher  $\ell_{sc}$ . The more general solution for the effective temperature needs to be computed numerically, and can be inferred from Figure 4.6. Note that the effective temperature due to the presence of the heavy operators is always greater than the background temperature,  $T=1/\beta$  that we start with. However, the effective temperature uniformly approaches zero as the background temperature  $T \to 0$ . This is similar to the result for the FZZT brane that we obtained in section 4.3 in that the effective temperature is proportional to the background temperature.

4.4 Exact results 133

### $\mathfrak{C} = C/\beta$ is finite followed by $\mathfrak{C} \to \infty$

Correlation functions in this other limit were studied in [113] and we include their result for completeness of presentation. In their analysis they found that the four point function (two point function of the bilinears) does not show ETH, as the correlation function actually becomes periodic in real time. Written in Euclidean time, they find [113]

$$\frac{\langle \mathcal{O}_{\ell^H} \mathcal{O}_{\ell^L} \mathcal{O}_{\ell^H} \mathcal{O}_{\ell^H} \rangle}{\langle \mathcal{O}_{\ell^H} \mathcal{O}_{\ell^H} \rangle} \sim \left( \frac{\pi}{\beta_{\text{eff}} \sinh\left(\frac{2\pi\sigma_2}{\beta_{\text{eff}}}\right)} \right)^{2\ell^L}, \qquad \beta_{\text{eff}} = \frac{2\pi}{\ell_{sc}} . \tag{4.101}$$

Drawing analogy with AdS<sub>3</sub>/CFT<sub>2</sub> correspondence, this correlation function behaves like a correlation function computed in thermal AdS<sub>3</sub>. It would be interesting to obtain an analogous bulk interpretation for the case of AdS<sub>2</sub>.

#### 4.4.2 Computations between ZZ and FZZT branes

We now use the relationship between 2D Liouville theory and the Schwarzian in the presence of FZZT branes. This allows us to write down the full Schwarzian correlation functions in the presence of coherent states of the type (4.4). As we shall see, their leading semiclassical limits will once more confirm our previous results obtained by other means.

#### Bilocal one-point function $\langle FZZT|V_{\ell}(x,\bar{x})|ZZ\rangle$

In this section we compute the special case of (4.45) with a single operator insertion using the FZZT-wavefunction given by (4.42),

$$\Psi_{FZZT}^{(s)}(P) \coloneqq \langle \text{FZZT}|P\rangle = e^{2i\pi Ps} \left[ -\frac{i}{2\pi P} \left( \frac{\gamma(b^2)}{8b^2} \right)^{-\frac{iP}{b}} \Gamma\left(1 + 2iPb\right) \Gamma\left(1 + 2\frac{iP}{b}\right) \right]$$
(4.102)

Recall, the variable s is related to the parameter r that labels the FZZT branes by equation (4.46). We are now ready to put together all the ingredients to compute the expectation value of a bilocal operator with respect to the FZZT boundary state. We start by writing

down the full expression for  $\langle \mathbb{V}_{\ell}(x,\bar{x}) \rangle_r := \langle \text{FZZT} | \mathbb{V}_{\ell}(x,\bar{x}) | \text{ZZ} \rangle$ , which takes the form

$$\langle \mathbb{V}_{\ell}(x,\bar{x}) \rangle_{r} = -2^{3/4} \int dP \, dR \, \frac{P}{R} e^{2\pi i Rs} \frac{\left(\frac{\gamma(b^{2})}{8b^{2}}\right)^{i\frac{P-R}{b}} \Gamma\left(1+2ibR\right) \Gamma\left(1+2i\frac{R}{b}\right)}{\Gamma\left(1+2ibP\right) \Gamma\left(1+2i\frac{P}{b}\right)} \left\langle \nu_{R} | \mathbb{V}_{\ell}(x,\bar{x}) | \nu_{P} \right\rangle$$

$$(4.103)$$

This expression differs from the pure ZZ one only in the measure factor where, roughly speaking, a ZZ brane corresponds to an insertion of  $\sinh(2\pi\mathfrak{p})$ , while an FZZT brane corresponds to an insertion of  $\cos(2\pi\mathfrak{p})$ . Once again, using (4.80), and performing the same kind of manipulations as for the pure ZZ case above, we can write,

$$\langle \mathbb{V}_{\ell}(x,\bar{x}) \rangle_{r} = -\frac{2^{3/4}}{2b} \left(8b^{4}\right)^{2\ell} \frac{b^{2}}{\pi} e^{-\frac{\pi\beta Q^{2}}{4a}} \int d\mathfrak{p}^{2} d\mathfrak{r} \, e^{2\pi(i\mathfrak{r}\hat{s}+\mathfrak{p})} \, e^{-\frac{\beta}{2C}\mathfrak{r}^{2}} e^{\frac{\sigma}{C}(\mathfrak{r}^{2}-\mathfrak{p}^{2})} \, \frac{\Gamma\left(2\ell \pm i(\mathfrak{p} \pm \mathfrak{r})\right)}{\Gamma(4\ell)} \, . \tag{4.104}$$

Above, we have introduced a rescaled  $\hat{s} = s b$  parameter for the FZZT brane. This scales the energy of the FZZT brane in an appropriate fashion from the 1D perspective. This can be easily seen by recalling that s is related to the parameter r in the boundary term, (4.13) by,

$$\cosh^{2}(\pi bs) = \frac{r^{2}}{2\pi b^{2}} \sin(\pi b^{2})$$

$$\downarrow b \to 0$$

$$1 + \frac{\pi^{2}b^{2}s^{2}}{2} \approx \frac{r^{2}}{2}$$
(4.105)

In the  $b \to 0$  limit, RHS of the above equation is an  $\mathcal{O}(1)$  parameter, therefore  $s \sim \frac{1}{b}$  which justifies our redefinition,  $s = \hat{s}/b$ .

Evaluating (4.104) using the saddle point integration method described above we get,

$$\langle \text{FZZT} | \mathbb{V}_{\ell}(x, \bar{x}) | \text{ZZ} \rangle \sim \left( \frac{1}{2 \sinh\left(\frac{2\pi}{\beta} \hat{s} \sigma\right)} \right)^{4\ell} .$$
 (4.106)

Since  $\sigma$  is indeed Euclidean time in the Schwarzian theory, this result is thermal for the orbit when  $\hat{s} \in i\mathbb{R}$  and non-thermal if  $\hat{s} \in \mathbb{R}$ . In the former case it is thermal at the effective temperature  $\beta_{\text{eff}} = \beta/\hat{s}$ . A similar result in 2D CFT was recently found in [117, 155].

4.4 Exact results 135

#### Bilocal two-point function $\langle FZZT|V_{\ell_2}(x_2,\bar{x}_2)V_{\ell_1}(x_1,\bar{x}_1)|ZZ\rangle$

Like in the previous case, we next compute the 2-point correlation function of the bilocal operators. From the perspective of 2-dimensional Liouville theory it is given by,

$$\langle \text{FZZT} | \mathbb{V}_{\ell_{2}}(x_{2}, \bar{x}_{2}) \mathbb{V}_{\ell_{1}}(x_{1}, \bar{x}_{1}) | \text{ZZ} \rangle = -2^{3/4} \int dP \, dR \frac{P}{R} e^{2\pi i R s} \left( \pi \mu \gamma(b^{2}) \right)^{i \frac{P-R}{b}} \\ \times \frac{\Gamma(1 + 2ibR) \Gamma\left(1 + 2i\frac{R}{b}\right)}{\Gamma(1 + 2ibP) \Gamma\left(1 + 2i\frac{P}{b}\right)} \langle \nu_{R} | \mathbb{V}_{\ell_{2}}(x_{2}, \bar{x}_{2}) \mathbb{V}_{\ell_{1}}(x_{1}, \bar{x}_{1}) | \nu_{P} \rangle , \quad (4.107)$$

and in 1-dimension, this expression reduces to,

$$\sim \int d\mathbf{r} d\mathbf{p}^2 d\mathbf{d}^2 e^{2\pi i \mathbf{r} \hat{\mathbf{s}}} \sinh (2\pi \mathbf{p}) \sinh (2\pi \mathbf{d}) \frac{\Gamma(2\ell^2 \pm i(\mathbf{r} \pm \mathbf{d}))}{\Gamma(4\ell^2)} \frac{\Gamma(2\ell^1 \pm i(\mathbf{d} \pm \mathbf{p}))}{\Gamma(4\ell^1)}$$

$$\times \exp \left[ -\frac{1}{2C} \left( \beta \mathbf{r}^2 + 2\sigma_2(\mathbf{d}^2 - \mathbf{r}^2) + 2\sigma_1(\mathbf{p}^2 - \mathbf{d}^2) \right) \right]. \tag{4.108}$$

Moreover, we can also compute the out-of-time-ordered correlation functions using the R-matrices. The exact expression for such an OTOC is given by,

$$\frac{\langle O_{\ell_{2}}(\sigma_{3}, \sigma_{4}) O_{\ell_{1}}(\sigma_{1}, \sigma_{2}) \rangle}{\langle O_{\ell_{2}}(\sigma_{3}, \sigma_{4}) \rangle \langle O_{\ell_{1}}(\sigma_{1}, \sigma_{2}) \rangle} \sim \int d\mathfrak{p}^{2} d\mathfrak{r} d\mathfrak{p}_{s}^{2} d\mathfrak{p}_{t}^{2} \sinh(2\pi\mathfrak{p}) \cos(2\pi\mathfrak{r}\hat{s}) \sinh(2\pi\mathfrak{p}_{s}) \sinh(2\pi\mathfrak{p}_{s}) \sinh(2\pi\mathfrak{p}_{t})$$

$$\times R_{\mathfrak{p}_{s}\mathfrak{p}_{t}} \begin{bmatrix} 2\ell_{2} 2\ell_{1} \\ \mathfrak{r} & \mathfrak{p} \end{bmatrix} \exp \left[ -\frac{1}{2C} \left( \mathfrak{p}^{2} (\beta - \sigma_{41}) - \mathfrak{p}_{t}^{2} \sigma_{31} - \mathfrak{r}^{2} \sigma_{32} - \mathfrak{p}_{s}^{2} \sigma_{41} \right) \right]$$

$$\times \frac{\sqrt{\Gamma(2\ell_{1} \pm i(\mathfrak{p} \pm \mathfrak{p}_{t})) \Gamma(2\ell_{2} \pm i(\mathfrak{r} \pm \mathfrak{p}_{t})) \Gamma(2\ell_{1} \pm i(\mathfrak{r} \pm \mathfrak{p}_{s})) \Gamma(2\ell_{2} \pm i(\mathfrak{p} \pm \mathfrak{p}_{s}))}}{\Gamma(4\ell_{1}) \Gamma(4\ell_{2})} \tag{4.109}$$

Once again, we bypass the exact computation of this integral and resort to the analysis of section 4.3.2 to argue that the Lyapunov exponent in this scenario will be given by  $\lambda = 2\pi/\beta_{\text{eff}}$  where  $\beta_{\text{eff}} = \beta/\hat{s}$ .

## 4.4.3 Computations between two FZZT branes

Before moving on to the discussions section, for completeness we would like to gather exact results for correlation functions in the presence of FZZT branes at both ends, proceeding along similar lines as above.

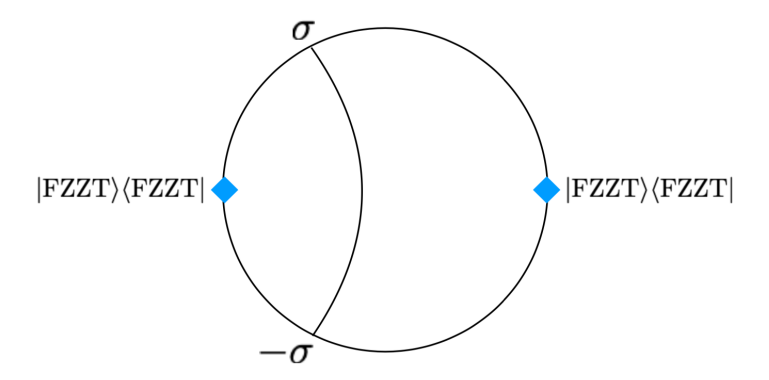


Figure 4.7: The configuration of the insertions in the case of two FZZT operators.

$$\langle \text{FZZT} | \mathbb{V}_{\ell}(x, \bar{x}) | \text{FZZT} \rangle$$

This correlation function corresponds to one with two insertions of FZZT operators as shown in Figure 4.7. Using the FZZT wavefunctions in (4.42), we can write this one-point function of the bilocal operator as follows,

$$\langle \text{FZZT} | \mathbb{V}_{\ell}(x, \bar{x}) | \text{FZZT} \rangle = \frac{1}{4\pi^{2}} \int dP \, dR \, \frac{1}{PR} e^{2\pi i (s \, R - s' \, P)} \left( \frac{\gamma(b^{2})}{8b^{2}} \right)^{i \frac{P - R}{b}} \\
\times \left[ \Gamma\left(1 + 2ibR\right) \Gamma\left(1 + 2i\frac{R}{b}\right) \Gamma\left(1 - 2ibP\right) \Gamma\left(1 - 2i\frac{P}{b}\right) \right] \langle \nu_{R} | \mathbb{V}_{\ell}(z, \bar{z}) | \nu_{P} \rangle . \tag{4.110}$$

Once again, using (4.80), we can write,

$$\langle \text{FZZT} | \mathbb{V}_{\ell}(x, \bar{x}) | \text{FZZT} \rangle = \frac{1}{2b} \left( 8b^4 \right)^{2\ell} \frac{1}{\pi^2} e^{-\frac{2\beta\pi}{a} \frac{Q^2}{4}} \int d\mathfrak{p} \, d\mathfrak{r} \cos(2\pi \hat{s}\mathfrak{r}) \cos(2\pi \hat{s}'\mathfrak{p}) \\ \times \frac{\Gamma\left( 2\ell \pm i(\mathfrak{p} \pm \mathfrak{r}) \right)}{\Gamma(4\ell)} \, e^{-\frac{\beta}{2C} \mathfrak{r}^2} e^{\frac{\sigma}{C} (\mathfrak{r}^2 - \mathfrak{p}^2)} \,. \tag{4.111}$$

Above, we have introduced rescaled  $\hat{s}, \hat{s}' = sb, s'b$  parameters for both the FZZT branes. Lastly, the saddle point evaluation of (4.111) in the  $C \to \infty$  limit gives,

$$\langle \text{FZZT} | \mathbb{V}_{\ell}(x, \bar{x}) | \text{FZZT} \rangle \sim \left( \frac{1}{2 \sinh \left( 2\pi \hat{s} + \frac{2\pi}{\beta} \left( \hat{s}' - \hat{s} - i \right) \sigma \right)} \right)^{4\ell}$$
 (4.112)

4.5 Discussion 137

state	2D picture	class	ETH	λ
$ E(k)\rangle$	ZZ	parabolic	<b>✓</b>	$2\pi T_{ m ETH}$
$ E_{r^-}\rangle$	FZZT	elliptic	<b>✓</b>	$2\pi T_{ m ETH}$
$ E_{r^+}\rangle$	FZZT	hyperbolic	X	$\in i\mathbb{R}$
$\mathcal{O}_{\ell_H} 0 angle$	ZZ	parabolic	<b>/</b>	

Figure 4.8: Panoramic summary of the pure states studied in this Chapter and their thermal properties. We see that in all cases where the system behaves thermally it satisfies maximal extended ETH (we did not compute the Lyapunov exponent in the last line of this table). The states  $|E_{r^{\pm}}\rangle$  denote the coherent FZZT states for  $r \gtrsim \sqrt{2}$ . The grey tick mark indicates that the states in question show only a weak form of ETH.

#### 4.5 Discussion

We have undertaken a detailed study of the behavior of pure states of the Schwarzian theory as defined by the path integral (4.1). A table showing the different classes of states considered and their thermal properties is given in Figure 4.8. Let us briefly review what has been established. From a many-body perspective this Chapter should be understood in conjunction with the numerical results of Chapter 2 and the analytical results of Chapter 3 to give a complete picture of the thermal properties of pure states of the SYK model. These studies taken together explicitly demonstrate the applicability of ETH both for the tower of massive states by studying the asymptotics of OPE coefficients in Chapter 3, as well as for the Schwarzian sector in the present Chapter, by employing a combination of methods, all of which are ultimately linked to the Virasoro symmetry which shows up via the orbits of Diff(S<sup>1</sup>). This is yet another demonstration of the usefulness of the SYK and SYK-like models as controllable theoretical laboratories of strongly coupled quantum chaotic systems. At the same time, these models serve as simple examples of holographic duality and the applicability of ETH has important implications for the physics of the dual black holes, as discussed in section 4.1.1.

It is natural to ask whether a more detailed investigation could unearth a story similar to the case of large-c 2D CFT, where sub-leading corrections necessitate a more refined analysis of thermalization to the generalized Gibbs ensemble of KdV charges (see, for example [81,166–170]). To this end, we note that we have the exact results of many relevant quantities at our disposal (see section 4.4), so one could in principle undertake a systematic expansion in large-C to address this question. A second important angle is the maximal extended ETH conjecture made here and in Chapter 2: the IR limit of the SYK model as well as other similar many-body theories (such as the melonic tensor models) scramble with the maximally allowed exponent  $2\pi/\beta_{\text{eff}}$  predicted from the ETH as applied to simple operators. It would be interesting to further explore whether there are universal critical phenomena associated to the ergodic / non-ergodic transition established here, and linked to the critical parabolic orbit of Virasoro. A possible connection between ETH and the Lyapunov behavior was first suggested in [45] and later formalized in [171], who point out the general structure of non-Gaussianities this implies for the statistics of off-diagonal matrix elements in the energy basis. It would be of interest to compute these non-Gaussianities explicitly in the present model, but for this we would need to extend our results to off-diagonal matrix elements.

Such an expansion of the exact results would naturally be of interest also in discussion of how the correlation function deviates from semi-classical bulk EFT expectations, as discussed in various recent analyses, such as for example [6, 7, 56, 172].

It is interesting to note that an ergodic to non-ergodic phase transition was also found in [61, 173] within pure states of the SYK model. However, the connection with the pure states of the above paper is presently not clear and begs a more detailed analysis.

An interesting aspect with potentially important ramifications for holography is the close connection between ETH and approximate quantum error correction pointed out in [174]. Combining their results with what has been established in this work, implies as a corollary that heavy eigenstates of SYK-like models (more precisely their IR Schwarzian limit) form an approximate quantum error correcting code (AQECC). It would be very interesting to investigate what more can be said about the properties of the AQECC hosted by the eigenstates of SYK-like models in the light of the OTOC version of ETH we found. Recent investigations linking ETH to AQECC in chaotic theories, including holographic ones, have appeared

4.5 Discussion 139

in [175], while [176] link complexity of time evolution to ETH-type behavior.

An alternative approach to relate spectral statistics and Lyapunov behavior is developed in [177–179] who introduce new measures of quantum chaos defined in terms of the random nature of matrices of correlation functions of all the operators in a system. Given the exact results developed in this work, it would be interesting to attempt compute these measures in the Schwarzian theory.

We would like to end by reiterating an important remark about our results demonstrating ETH. For a complete proof of eigenstate thermalization in a system it is indispensable to demonstrate the exponential suppression of the off-diagonal matrix elements with respect to the diagonal terms. This was addressed numerically in Chapter 2, as well as analytically in the conformal limit in Chapter 3. Our present work focused on the study of the diagonal terms only, so it would be interesting to generalize our techniques to allow the determination of the behavior of the off-diagonal terms.

# **Bibliography**

- [1] S. W. Hawking, "Breakdown of predictability in gravitational collapse," *Physical Review D* **14** no. 10, (1976) 2460.
- [2] A. Almheiri, D. Marolf, J. Polchinski, and J. Sully, "Black Holes: Complementarity Or Firewalls?," *JHEP* **02** (2013) 062, arXiv:1207.3123 [hep-th].
- [3] J. Deutsch, "Quantum statistical mechanics in a closed system," *Physical Review A* 43 no. 4, (1991) 2046.
- [4] M. Srednicki, "Chaos and quantum thermalization," Physical Review E 50 no. 2, (1994) 888.
- [5] A. L. Fitzpatrick, J. Kaplan, M. T. Walters, and J. Wang, "Hawking from Catalan," arXiv:1510.00014 [hep-th].
- [6] A. L. Fitzpatrick, J. Kaplan, D. Li, and J. Wang, "On information loss in AdS<sub>3</sub>/CFT<sub>2</sub>," JHEP 05 (2016) 109, arXiv:1603.08925 [hep-th].
- [7] T. Anous, T. Hartman, A. Rovai, and J. Sonner, "Black Hole Collapse in the 1/c Expansion," *JHEP* 07 (2016) 123, arXiv:1603.04856 [hep-th].
- [8] T. Anous, T. Hartman, A. Rovai, and J. Sonner, "From Conformal Blocks to Path Integrals in the Vaidya Geometry," arXiv:1706.02668 [hep-th].

[9] A. Kitaev, "A simple model of quantum holography." Talks at KITP, April 7, 2015 and May 27, 2015.

- [10] S. Sachdev, "Bekenstein-Hawking Entropy and Strange Metals," Phys. Rev. X5 no. 4, (2015) 041025, arXiv:1506.05111 [hep-th].
- [11] J. Maldacena and D. Stanford, "Remarks on the Sachdev-Ye-Kitaev model," *Phys. Rev.* **D94** no. 10, (2016) 106002, arXiv:1604.07818 [hep-th].
- [12] J. Maldacena, D. Stanford, and Z. Yang, "Conformal symmetry and its breaking in two dimensional Nearly Anti-de-Sitter space," PTEP 2016 no. 12, (2016) 12C104, arXiv:1606.01857 [hep-th].
- [13] S. Sachdev and J. Ye, "Gapless spin fluid ground state in a random, quantum Heisenberg magnet," Phys. Rev. Lett. 70 (1993) 3339, arXiv:cond-mat/9212030 [cond-mat].
- [14] J. Polchinski and V. Rosenhaus, "The Spectrum in the Sachdev-Ye-Kitaev Model," JHEP 04 (2016) 001, arXiv:1601.06768 [hep-th].
- [15] J. Maldacena, S. H. Shenker, and D. Stanford, "A bound on chaos," JHEP 08 (2016) 106, arXiv:1503.01409 [hep-th].
- [16] D. Bagrets, A. Altland, and A. Kamenev, "Sachdev-Ye-Kitaev model as Liouville quantum mechanics," 2016.
- [17] D. Bagrets, A. Altland, and A. Kamenev, "Power-law out of time order correlation functions in the SYK model," *Nucl. Phys.* B921 (2017) 727-752, arXiv:1702.08902 [cond-mat.str-el].
- [18] I. Danshita, M. Hanada, and M. Tezuka, "Creating and probing the Sachdev-Ye-Kitaev model with ultracold gases: Towards experimental studies of quantum gravity," arXiv:1606.02454 [cond-mat.quant-gas].
- [19] L. García-Álvarez, I. L. Egusquiza, L. Lamata, A. del Campo, J. Sonner, and E. Solano, "Digital Quantum Simulation of Minimal AdS/CFT," Phys. Rev. Lett. in press (2016), arXiv:1607.08560 [quant-ph].

[20] D. I. Pikulin and M. Franz, "Black hole on a chip: proposal for a physical realization of the SYK model in a solid-state system," *Phys. Rev.* X7 no. 3, (2017) 031006, arXiv:1702.04426 [cond-mat.dis-nn].

- [21] A. Chew, A. Essin, and J. Alicea, "Approximating the Sachdev-Ye-Kitaev model with Majorana wires," arXiv:1703.06890 [cond-mat.dis-nn].
- [22] L. D'Alessio, Y. Kafri, A. Polkovnikov, and M. Rigol, "From Quantum Chaos and Eigenstate Thermalization to Statistical Mechanics and Thermodynamics," *Adv. Phys.* **65** no. 3, (2016) 239–362, arXiv:1509.06411 [cond-mat.stat-mech].
- [23] E. Witten, "An SYK-Like Model Without Disorder," arXiv:1610.09758 [hep-th].
- [24] I. R. Klebanov and G. Tarnopolsky, "Uncolored random tensors, melon diagrams, and the Sachdev-Ye-Kitaev models," *Phys. Rev.* D95 no. 4, (2017) 046004, arXiv:1611.08915 [hep-th].
- [25] R. Gurau, "The complete 1/N expansion of a SYK-like tensor model," Nucl. Phys. B916 (2017) 386-401, arXiv:1611.04032 [hep-th].
- [26] S. Khlebnikov and M. Kruczenski, "Thermalization of isolated quantum systems," arXiv:1312.4612 [cond-mat.stat-mech].
- [27] D. A. Trunin, "Pedagogical introduction to SYK model and 2D Dilaton Gravity," arXiv:2002.12187 [hep-th].
- [28] G. Sárosi, "AdS<sub>2</sub> holography and the SYK model," PoS Modave2017 (2018) 001, arXiv:1711.08482 [hep-th].
- [29] M. Rigol, V. Dunjko, and M. Olshanii, "Thermalization and its mechanism for generic isolated quantum systems," *Nature* 452 (2008) 854-858, arXiv:0708.1324 [cond-mat].
- [30] V. Arnold, Mathematical Methods of Classical Mechanics. Springer, 1989.
- [31] L. A. Bunimovich, "On the ergodic properties of nowhere dispersing billiards," Comm. Math. Phys. 65 (1979) 295–312.

[32] O. Bohigas, M. Giannoni, and C. Schmit, "Characterization of chaotic quantum spectra and universality of level fluctuation laws," *Phys. Rev. Lett.* **52** (1983) .

- [33] T. M. Berry, M. V., "Level clustering in the regular spectrum," Proc. R. Soc. Lond. A 356 (1977).
- [34] R. R. Pandet, A., "Level spacings for harmonic-oscillator systems," Phys. Rev. A 43 (1991) .
- [35] M. Srednicki, "Thermal fluctuations in quantized chaotic systems," J. Phys. A 29 (1996) L75-L79, arXiv:chao-dyn/9511001.
- [36] M. Srednicki, "The approach to thermal equilibrium in quantized chaotic systems," Journal of Physics A 32 no. 7, (1999).
- [37] R. Nandkishore and D. A. Huse, "Many body localization and thermalization in quantum statistical mechanics," *Ann. Rev. Condensed Matter Phys.* **6** (2015) 15–38, arXiv:1404.0686 [cond-mat.stat-mech].
- [38] M. Feingold and A. Peres, "Distribution of matrix elements of chaotic systems," Phys. Rev. A 34 (Jul, 1986) 591-595. https://link.aps.org/doi/10.1103/PhysRevA.34.591.
- [39] B. Eckhardt, S. Fishman, J. Keating, O. Agam, J. Main, and K. Müller, "Approach to ergodicity in quantum wave functions," *Phys. Rev. E* **52** no. 6, (1995) .
- [40] A. S. Wijn, B. Hess, and B. V. Fine, "Largest Lyapunov Exponents for Lattices of Interacting Classical Spins," *Phys. Rev. Lett* **109** (2012), arXiv:1205.2901.
- [41] I. L. Aleiner and A. I. Larkin, "Divergence of classical trajectories and weak localization," *Phys. Rev. B* **54** (1996) .
- [42] A. Romero-Bermúdez, K. Schalm, and V. Scopelliti, "Regularization dependence of the OTOC. Which Lyapunov spectrum is the physical one?," *JHEP* 07 (2019) 107, arXiv:1903.09595 [hep-th].

- [43] Y. Sekino and L. Susskind, "Fast Scramblers," JHEP 10 (2008) 065, arXiv:0808.2096 [hep-th].
- [44] V. Rosenhaus, "An Introduction to the SYK Model," arXiv:1807.03334 [hep-th].
- [45] J. Sonner and M. Vielma, "Eigenstate Thermalization in the Sachdev-Ye-Kitaev Model," JHEP 11 (2017) 149, arXiv:1707.08013 [hep-th].
- [46] W. Fu and S. Sachdev, "Numerical study of fermion and boson models with infinite-range random interactions," *Phys. Rev.* B94 no. 3, (2016) 035135, arXiv:1603.05246 [cond-mat.str-el].
- [47] O. Parcollet and A. Georges, "Non-fermi-liquid regime of a doped mott insulator," Phys. Rev. B 59 (Feb, 1999) 5341-5360. https://link.aps.org/doi/10.1103/PhysRevB.59.5341.
- [48] A. Jevicki, K. Suzuki, and J. Yoon, "Bi-Local Holography in the SYK Model," JHEP 07 (2016) 007, arXiv:1603.06246 [hep-th].
- [49] D. J. Gross and V. Rosenhaus, "The Bulk Dual of SYK: Cubic Couplings," JHEP 05 (2017) 092, arXiv:1702.08016 [hep-th].
- [50] A. Jevicki and K. Suzuki, "Bi-Local Holography in the SYK Model: Perturbations," JHEP 11 (2016) 046, arXiv:1608.07567 [hep-th].
- [51] S. Dartois, H. Erbin, and S. Mondal, "Conformality of 1/N corrections in SYK-like models," arXiv:1706.00412 [hep-th].
- [52] S. H. Shenker and D. Stanford, "Black holes and the butterfly effect," JHEP 03 (2014) 067, arXiv:1306.0622 [hep-th].
- [53] M. Rigol, "Quantum quenches and thermalization in one-dimensional fermionic systems," Phys. Rev. A 80 (Nov, 2009) 053607. https://link.aps.org/doi/10.1103/PhysRevA.80.053607.
- [54] W. Beugeling, R. Moessner, and M. Haque, "Off-diagonal matrix elements of local operators in many-body quantum systems," *Physical Review E* 91 no. 1, (2015) 012144.

[55] A. M. García-García and J. J. M. Verbaarschot, "Spectral and thermodynamic properties of the Sachdev-Ye-Kitaev model," *Phys. Rev.* D94 no. 12, (2016) 126010, arXiv:1610.03816 [hep-th].

- [56] J. S. Cotler, G. Gur-Ari, M. Hanada, J. Polchinski, P. Saad, S. H. Shenker, D. Stanford, A. Streicher, and M. Tezuka, "Black Holes and Random Matrices," JHEP 05 (2017) 118, arXiv:1611.04650 [hep-th].
- [57] R. A. Davison, W. Fu, A. Georges, Y. Gu, K. Jensen, and S. Sachdev, "Thermoelectric transport in disordered metals without quasiparticles: The Sachdev-Ye-Kitaev models and holography," *Phys. Rev.* B95 no. 15, (2017) 155131, arXiv:1612.00849 [cond-mat.str-el].
- [58] A. del Campo, J. Molina-Vilaplana, and J. Sonner, "Scrambling the spectral form factor: unitarity constraints and exact results," *Phys. Rev.* D95 no. 12, (2017) 126008, arXiv:1702.04350 [hep-th].
- [59] E. Brézin and S. Hikami, "Spectral form factor in a random matrix theory," Phys. Rev. E 55 (Apr, 1997) 4067–4083. https://link.aps.org/doi/10.1103/PhysRevE.55.4067.
- [60] M. Távora, E. Torres-Herrera, and L. F. Santos, "Inevitable power-law behavior of isolated many-body quantum systems and how it anticipates thermalization," *Physical Review A* 94 no. 4, (2016) 041603.
- [61] I. Kourkoulou and J. Maldacena, "Pure states in the SYK model and nearly- $AdS_2$  gravity," arXiv:1707.02325 [hep-th].
- [62] C. Krishnan and K. V. P. Kumar, "Towards a Finite-N Hologram," arXiv:1706.05364 [hep-th].
- [63] R. Jackiw, "Lower Dimensional Gravity," Nucl. Phys. **B252** (1985) 343–356.
- [64] C. Teitelboim, "Gravitation and Hamiltonian Structure in Two Space-Time Dimensions," Phys. Lett. 126B (1983) 41–45.

[65] A. Almheiri and J. Polchinski, "Models of AdS<sub>2</sub> backreaction and holography," JHEP 11 (2015) 014, arXiv:1402.6334 [hep-th].

- [66] K. Jensen, "Chaos in AdS<sub>2</sub> Holography," Phys. Rev. Lett. 117 no. 11, (2016) 111601, arXiv:1605.06098 [hep-th].
- [67] G. Mandal, P. Nayak, and S. R. Wadia, "Coadjoint orbit action of Virasoro group and two-dimensional quantum gravity dual to SYK/tensor models," arXiv:1702.04266 [hep-th].
- [68] M. Taylor, "Generalized conformal structure, dilaton gravity and SYK," arXiv:1706.07812 [hep-th].
- [69] S. R. Das, A. Jevicki, and K. Suzuki, "Three Dimensional View of the SYK/AdS Duality," JHEP 09 (2017) 017, arXiv:1704.07208 [hep-th].
- [70] F. Ferrari, "The Large D Limit of Planar Diagrams," arXiv:1701.01171 [hep-th].
- [71] K. Papadodimas and S. Raju, "Black Hole Interior in the Holographic Correspondence and the Information Paradox," *Phys. Rev. Lett.* 112 no. 5, (2014) 051301, arXiv:1310.6334 [hep-th].
- [72] J. M. Maldacena, "Eternal Black Holes in Anti-de Sitter," JHEP 04 (2003) 021, arXiv:hep-th/0106112 [hep-th].
- [73] J. Maldacena and L. Susskind, "Cool horizons for entangled black holes," Fortsch. Phys. 61 (2013) 781-811, arXiv:1306.0533 [hep-th].
- [74] K. Jensen and A. Karch, "Holographic Dual of an Einstein-Podolsky-Rosen Pair has a Wormhole," *Phys. Rev. Lett.* **111** no. 21, (2013) 211602, arXiv:1307.1132 [hep-th].
- [75] J. Sonner, "Holographic Schwinger Effect and the Geometry of Entanglement," *Phys. Rev. Lett.* **111** no. 21, (2013) 211603, arXiv:1307.6850 [hep-th].
- [76] D. Marolf and J. Polchinski, "Gauge/Gravity Duality and the Black Hole Interior," Phys. Rev. Lett. 111 (2013) 171301, arXiv:1307.4706 [hep-th].

[77] V. Balasubramanian, M. Berkooz, S. F. Ross, and J. Simon, "Black Holes, Entanglement and Random Matrices," Class. Quant. Grav. 31 (2014) 185009, arXiv:1404.6198 [hep-th].

- [78] K. Papadodimas and S. Raju, "An Infalling Observer in AdS/CFT," JHEP 10 (2013) 212, arXiv:1211.6767 [hep-th].
- [79] A. L. Fitzpatrick, J. Kaplan, and M. T. Walters, "Virasoro Conformal Blocks and Thermality from Classical Background Fields," *JHEP* 11 (2015) 200, arXiv:1501.05315 [hep-th].
- [80] N. Lashkari, A. Dymarsky, and H. Liu, "Eigenstate Thermalization Hypothesis in Conformal Field Theory," arXiv:1610.00302 [hep-th].
- [81] P. Basu, D. Das, S. Datta, and S. Pal, "On thermality of CFT eigenstates," arXiv:1705.03001 [hep-th].
- [82] D. Anninos, T. Anous, and F. Denef, "Disordered Quivers and Cold Horizons," JHEP 12 (2016) 071, arXiv:1603.00453 [hep-th].
- [83] W. Fu, D. Gaiotto, J. Maldacena, and S. Sachdev, "Supersymmetric Sachdev-Ye-Kitaev models," *Phys. Rev.* **D95** no. 2, (2017) 026009, arXiv:1610.08917 [hep-th]. [Addendum: Phys. Rev.D95,no.6,069904(2017)].
- [84] T. Li, J. Liu, Y. Xin, and Y. Zhou, "Supersymmetric SYK model and random matrix theory," arXiv:1702.01738 [hep-th].
- [85] M. Berkooz, P. Narayan, M. Rozali, and J. Simón, "Higher Dimensional Generalizations of the SYK Model," JHEP 01 (2017) 138, arXiv:1610.02422 [hep-th].
- [86] C. Peng, M. Spradlin, and A. Volovich, "A Supersymmetric SYK-like Tensor Model," JHEP 05 (2017) 062, arXiv:1612.03851 [hep-th].
- [87] C. Krishnan, S. Sanyal, and P. N. Bala Subramanian, "Quantum Chaos and Holographic Tensor Models," *JHEP* **03** (2017) 056, arXiv:1612.06330 [hep-th].

[88] P. Nayak, J. Sonner, and M. Vielma, "Eigenstate Thermalisation in the Conformal Sachdev-Ye-Kitaev Model: an Analytic Approach," arXiv:1903.00478 [hep-th].

- [89] J. Engelsöy, T. G. Mertens, and H. Verlinde, "An investigation of AdS<sub>2</sub> backreaction and holography," *JHEP* **07** (2016) 139, arXiv:1606.03438 [hep-th].
- [90] M. Cvetič and I. Papadimitriou, "AdS<sub>2</sub> holographic dictionary," JHEP 12 (2016) 008, arXiv:1608.07018 [hep-th]. [Erratum: JHEP01,120(2017)].
- [91] P. Nayak, A. Shukla, R. M. Soni, S. P. Trivedi, and V. Vishal, "On the Dynamics of Near-Extremal Black Holes," JHEP 09 (2018) 048, arXiv:1802.09547 [hep-th].
- [92] F. Larsen, "A nAttractor Mechanism for nAdS<sub>2</sub>/nCFT<sub>1</sub> Holography," arXiv:1806.06330 [hep-th].
- [93] A. Castro, F. Larsen, and I. Papadimitriou, "5D rotating black holes and the nAdS<sub>2</sub>/nCFT<sub>1</sub> correspondence," *JHEP* **10** (2018) 042, arXiv:1807.06988 [hep-th].
- [94] U. Moitra, S. P. Trivedi, and V. Vishal, "Near-Extremal Near-Horizons," arXiv:1808.08239 [hep-th].
- [95] Y.-Z. Li, S.-L. Li, and H. Lu, "Exact Embeddings of Jt Gravity in Strings and M-theory," Eur. Phys. J. C78 no. 9, (2018) 791, arXiv:1804.09742 [hep-th].
- [96] F. Larsen and Y. Zeng, "Black Hole Spectroscopy and AdS<sub>2</sub> Holography," arXiv:1811.01288 [hep-th].
- [97] R. R. Poojary, "BTZ Dynamics and Chaos," arXiv:1812.10073 [hep-th].
- [98] M. Franz and M. Rozali, "Mimicking Black Hole Event Horizons in Atomic and Solid-State Systems," *Nature Rev. Mater.* **3** (2018) 491–501, arXiv:1808.00541 [cond-mat.str-el].
- [99] A. Dymarsky, "Bound on Eigenstate Thermalization from Transport," arXiv:1804.08626 [cond-mat.stat-mech].
- [100] D. J. Gross and V. Rosenhaus, "A line of CFTs: from generalized free fields to SYK," JHEP 07 (2017) 086, arXiv:1706.07015 [hep-th].

[101] A. Kitaev and S. J. Suh, "The Soft Mode in the Sachdev-Ye-Kitaev Model and Its Gravity Dual," *JHEP* 05 (2018) 183, arXiv:1711.08467 [hep-th].

- [102] D. Bagrets, A. Altland, and A. Kamenev, "Sachdev-Ye-Kitaev model as Liouville quantum mechanics," *Nucl. Phys.* **B911** (2016) 191–205, arXiv:1607.00694 [cond-mat.str-el].
- [103] R. de Mello Koch, A. Jevicki, K. Suzuki, and J. Yoon, "AdS Maps and Diagrams of Bi-Local Holography," arXiv:1810.02332 [hep-th].
- [104] A. Kitaev, "A simple model of quantum holography, Talks at KITP, April 7, and May 27, 2015,".
- [105] D. J. Gross and V. Rosenhaus, "All point correlation functions in SYK," JHEP 12 (2017) 148, arXiv:1710.08113 [hep-th].
- [106] V. Balasubramanian and S. F. Ross, "Holographic particle detection," *Phys. Rev.* **D61** (2000) 044007, arXiv:hep-th/9906226 [hep-th].
- [107] O. Aharony, S. S. Gubser, J. M. Maldacena, H. Ooguri, and Y. Oz, "Large N field theories, string theory and gravity," *Phys. Rept.* 323 (2000) 183–386, arXiv:hep-th/9905111 [hep-th].
- [108] A. Belin, C. A. Keller, and I. G. Zadeh, "Genus two partition functions and Rényi entropies of large c conformal field theories," J. Phys. A50 no. 43, (2017) 435401, arXiv:1704.08250 [hep-th].
- [109] V. Balasubramanian, B. Craps, B. Czech, and G. Sárosi, "Echoes of chaos from string theory black holes," *JHEP* **03** (2017) 154, arXiv:1612.04334 [hep-th].
- [110] P. Nayak, J. Sonner, and M. Vielma, "Extended Eigenstate Thermalization and the role of FZZT branes in the Schwarzian theory," *JHEP* 03 (2020) 168, arXiv:1907.10061 [hep-th].
- [111] R. Gurau, "The 1/N Expansion of Colored Tensor Models," *Annales Henri Poincare*12 (2011) 829–847, arXiv:1011.2726 [gr-qc].

[112] G. Turiaci and H. Verlinde, "On CFT and Quantum Chaos," JHEP 12 (2016) 110, arXiv:1603.03020 [hep-th].

- [113] H. T. Lam, T. G. Mertens, G. J. Turiaci, and H. Verlinde, "Shockwave S-Matrix from Schwarzian Quantum Mechanics," JHEP 11 (2018) 182, arXiv:1804.09834 [hep-th].
- [114] S. Banerjee, J.-W. Brijan, and G. Vos, "On the Universality of Late-Time Correlators in Semi-Classical 2D CFTs," *JHEP* **08** (2018) 047, arXiv:1805.06464 [hep-th].
- [115] G. Vos, "Vacuum Block Thermalization in Semi-Classical 2D CFT," *JHEP* **02** (2019) 022, arXiv:1810.03630 [hep-th].
- [116] T. Anous and J. Sonner, "Phases of Scrambling in Eigenstates," arXiv:1903.03143 [hep-th].
- [117] K. Jensen, "Scrambling in Nearly Thermalized States at Large Central Charge," arXiv:1906.05852 [hep-th].
- [118] N. Lashkari, A. Dymarsky, and H. Liu, "Universality of Quantum Information in Chaotic CFTs," *JHEP* **03** (2018) 070, arXiv:1710.10458 [hep-th].
- [119] J. De Boer, R. Van Breukelen, S. F. Lokhande, K. Papadodimas, and E. Verlinde, "Probing Typical Black Hole Microstates," arXiv:1901.08527 [hep-th].
- [120] A. Alekseev and S. L. Shatashvili, "Path Integral Quantization of the Coadjoint Orbits of the Virasoro Group and 2D Gravity," Nucl. Phys. B323 (1989) 719–733.
- [121] A. Alekseev and S. L. Shatashvili, "From Geometric Quantization to Conformal Field Theory," Commun. Math. Phys. 128 (1990) 197–212. [,22(1990)].
- [122] V. Fateev, A. B. Zamolodchikov, and A. B. Zamolodchikov, "Boundary Liouville Field Theory. 1. Boundary State and Boundary Two Point Function," arXiv:hep-th/0001012 [hep-th].
- [123] A. B. Zamolodchikov and A. B. Zamolodchikov, "Liouville Field Theory on a Pseudosphere," arXiv:hep-th/0101152 [hep-th].

[124] P. Saad, S. H. Shenker, and D. Stanford, "JT Gravity as a Matrix Integral," arXiv:1903.11115 [hep-th].

- [125] A. Altland and D. Bagrets, "Quantum Ergodicity in the Syk Model," *Nucl. Phys.* **B930** (2018) 45–68, arXiv:1712.05073 [cond-mat.str-el].
- [126] P. Saad, S. H. Shenker, and D. Stanford, "A Semiclassical Ramp in Syk and in Gravity," arXiv:1806.06840 [hep-th].
- [127] T. G. Mertens, G. J. Turiaci, and H. L. Verlinde, "Solving the Schwarzian via the Conformal Bootstrap," *JHEP* 08 (2017) 136, arXiv:1705.08408 [hep-th].
- [128] J. de Boer, R. Van Breukelen, S. F. Lokhande, K. Papadodimas, and E. Verlinde, "On the Interior Geometry of a Typical Black Hole Microstate," *JHEP* 05 (2019) 010, arXiv:1804.10580 [hep-th].
- [129] J. M. Deutsch, "Quantum statistical mechanics in a closed system," *Phys. Rev. A* 43 (Feb, 1991) 2046–2049. https://link.aps.org/doi/10.1103/PhysRevA.43.2046.
- [130] M. Srednicki, "Chaos and quantum thermalization," *Phys. Rev. E* **50** (Aug, 1994) 888–901. https://link.aps.org/doi/10.1103/PhysRevE.50.888.
- [131] X. O. Camanho, J. D. Edelstein, J. Maldacena, and A. Zhiboedov, "Causality Constraints on Corrections to the Graviton Three-Point Coupling," *JHEP* 02 (2016) 020, arXiv:1407.5597 [hep-th].
- [132] N. Afkhami-Jeddi, T. Hartman, S. Kundu, and A. Tajdini, "Einstein Gravity 3-Point Functions from Conformal Field Theory," JHEP 12 (2017) 049, arXiv:1610.09378 [hep-th].
- [133] A. Belin, D. M. Hofman, and G. Mathys, "Einstein gravity from ANEC correlators," arXiv:1904.05892 [hep-th].
- [134] M. Kologlu, P. Kravchuk, D. Simmons-Duffin, and A. Zhiboedov, "Shocks, Superconvergence, and a Stringy Equivalence Principle," arXiv:1904.05905 [hep-th].

[135] F. M. Haehl, R. Loganayagam, P. Narayan, and M. Rangamani, "Classification of Out-Of-Time-Order Correlators," SciPost Phys. 6 no. 1, (2019) 001, arXiv:1701.02820 [hep-th].

- [136] F. M. Haehl and M. Rozali, "Fine Grained Chaos in AdS<sub>2</sub> Gravity," Phys. Rev. Lett.
  120 no. 12, (2018) 121601, arXiv:1712.04963 [hep-th].
- [137] T. G. Mertens and G. J. Turiaci, "Defects in Jackiw-Teitelboim Quantum Gravity," arXiv:1904.05228 [hep-th].
- [138] N. Seiberg and D. Shih, "Minimal String Theory," Comptes Rendus Physique 6 (2005) 165-174, arXiv:hep-th/0409306 [hep-th].
- [139] E. J. Martinec, "The Annular Report on Noncritical String Theory," arXiv:hep-th/0305148 [hep-th].
- [140] T. G. Mertens, "The Schwarzian theory origins," JHEP 05 (2018) 036, arXiv:1801.09605 [hep-th].
- [141] J. Teschner, "Remarks on Liouville Theory with Boundary," *PoS* tmr2000 (2000) 041, arXiv:hep-th/0009138 [hep-th].
- [142] H. Dorn and G. Jorjadze, "Boundary Liouville Theory: Hamiltonian Description and Quantization," SIGMA 3 (2007) 012, arXiv:hep-th/0610197 [hep-th].
- [143] J. L. Cardy, "Conformal Invariance and Surface Critical Behavior," Nucl. Phys. B240 (1984) 514–532.
- [144] H. Dorn and G. Jorjadze, "Operator Approach to Boundary Liouville Theory," Annals Phys. 323 (2008) 2799–2839, arXiv:0801.3206 [hep-th].
- [145] W. Magnus and S. Winkler, Hill's Equation. Interscience Publishers, a division of John Wiley & Sons, New York, London, Sydney, 1966.
- [146] E. Witten, "Coadjoint Orbits of the Virasoro Group," Commun. Math. Phys. 114(1988) 1.

[147] A. B. Zamolodchikov, "Conformal Scalar Field on the Hyperelliptic Curve and Critical Ashkin-Teller Multipoint Correlation Functions," Nucl. Phys. B285 (1987) 481–503.

- [148] T. Hartman, "Entanglement Entropy at Large Central Charge," arXiv:1303.6955 [hep-th].
- [149] J. Gervais and A. Neveu, "The dual string spectrum in polyakov's quantization (i)," Nuclear Physics B 199 no. 1, (1982) 59 - 76. http://www.sciencedirect.com/science/article/pii/0550321382905661.
- [150] J.-L. Gervais and A. Neveu, "Dual string spectrum in polyakov's quantization (ii). mode separation," Nuclear Physics B 209 no. 1, (1982) 125 – 145. http://www.sciencedirect.com/science/article/pii/0550321382901055.
- [151] D. Stanford and E. Witten, "Fermionic Localization of the Schwarzian Theory,"

  JHEP 10 (2017) 008, arXiv:1703.04612 [hep-th].
- [152] Y. Nakayama, "Liouville Field Theory: a Decade After the Revolution," *Int. J. Mod. Phys.* A19 (2004) 2771–2930, arXiv:hep-th/0402009 [hep-th].
- [153] N. Ishibashi, "The Boundary and Crosscap States in Conformal Field Theories," Mod. Phys. Lett. A4 (1989) 251.
- [154] T. Onogi and N. Ishibashi, "Conformal Field Theories on Surfaces with Boundaries and Crosscaps," Mod. Phys. Lett. A4 (1989) 161. [Erratum: Mod. Phys. Lett.A4,885(1989)].
- [155] J. R. David, T. J. Hollowood, S. Khetrapal, and S. P. Kumar, "Chaos Bound in Bershadsky-Polyakov Theory," arXiv:1906.00667 [hep-th].
- [156] D. Anninos, D. A. Galante, and D. M. Hofman, "De Sitter Horizons & Holographic Liquids," arXiv:1811.08153 [hep-th].
- [157] B. Ponsot and J. Teschner, "Liouville Bootstrap via Harmonic Analysis on a Noncompact Quantum Group," arXiv:hep-th/9911110 [hep-th].

[158] D. A. Roberts and D. Stanford, "Two-dimensional conformal field theory and the butterfly effect," *Phys. Rev. Lett.* 115 no. 13, (2015) 131603, arXiv:1412.5123 [hep-th].

- [159] V. Bonzom, R. Gurau, A. Riello, and V. Rivasseau, "Critical Behavior of Colored Tensor Models in the Large N Limit," Nucl. Phys. B853 (2011) 174–195, arXiv:1105.3122 [hep-th].
- [160] J. Yoon, "A Bound on Chaos from Stability," arXiv:1905.08815 [hep-th].
- [161] J. Cotler and K. Jensen, "A theory of reparameterizations for AdS<sub>3</sub> gravity," *JHEP*02 (2019) 079, arXiv:1808.03263 [hep-th].
- [162] F. M. Haehl and M. Rozali, "Effective Field Theory for Chaotic CFTs," JHEP 10 (2018) 118, arXiv:1808.02898 [hep-th].
- [163] I. S. Gradshteyn and I. M. Ryzhik, Table of integrals, series, and products. Elsevier/Academic Press, Amsterdam, seventh ed., 2007.
- [164] H. Dorn and H. J. Otto, "Two and Three Point Functions in Liouville Theory," *Nucl. Phys.* **B429** (1994) 375–388, arXiv:hep-th/9403141 [hep-th].
- [165] A. B. Zamolodchikov and A. B. Zamolodchikov, "Structure Constants and Conformal Bootstrap in Liouville Field Theory," Nucl. Phys. B477 (1996) 577–605, arXiv:hep-th/9506136 [hep-th].
- [166] A. Dymarsky and K. Pavlenko, "Generalized Gibbs Ensemble of 2D CFTs at Large Central Charge in the Thermodynamic Limit," *JHEP* 01 (2019) 098, arXiv:1810.11025 [hep-th].
- [167] S. Datta, P. Kraus, and B. Michel, "Typicality and Thermality in 2D CFT," arXiv:1904.00668 [hep-th].
- [168] A. Maloney, G. S. Ng, S. F. Ross, and I. Tsiares, "Generalized Gibbs Ensemble and the Statistics of Kdv Charges in 2D CFT," JHEP 03 (2019) 075, arXiv:1810.11054 [hep-th].

[169] A. Maloney, G. S. Ng, S. F. Ross, and I. Tsiares, "Thermal Correlation Functions of Kdv Charges in 2D CFT," JHEP 02 (2019) 044, arXiv:1810.11053 [hep-th].

- [170] A. Dymarsky and K. Pavlenko, "Generalized Eigenstate Thermalization in 2D CFTs," arXiv:1903.03559 [hep-th].
- [171] L. Foini and J. Kurchan, "Eigenstate Thermalization Hypothesis and Out of Time Order Correlators," *Phys. Rev.* **E99** no. 4, (2019) 042139, arXiv:1803.10658 [cond-mat.stat-mech].
- [172] N. Iizuka and J. Polchinski, "A Matrix Model for Black Hole Thermalization," *JHEP* 10 (2008) 028, arXiv:0801.3657 [hep-th].
- [173] A. Dhar, A. Gaikwad, L. K. Joshi, G. Mandal, and S. R. Wadia, "Gravitational collapse in SYK models and Choptuik-like phenomenon," arXiv:1812.03979 [hep-th].
- [174] F. G. S. L. Brandao, E. Crosson, M. B. Şahinoğlu, and J. Bowen, "Quantum Error Correcting Codes in Eigenstates of Translation-Invariant Spin Chains," arXiv:1710.04631 [quant-ph].
- [175] N. Bao and N. Cheng, "Eigenstate Thermalization Hypothesis and Approximate Quantum Error Correction," arXiv:1906.03669 [hep-th].
- [176] V. Balasubramanian, M. Decross, A. Kar, and O. Parrikar, "Quantum Complexity of Time Evolution with Chaotic Hamiltonians," arXiv:1905.05765 [hep-th].
- [177] M. Hanada, H. Shimada, and M. Tezuka, "Universality in Chaos: Lyapunov Spectrum and Random Matrix Theory," *Phys. Rev.* E97 no. 2, (2018) 022224, arXiv:1702.06935 [hep-th].
- [178] H. Gharibyan, M. Hanada, B. Swingle, and M. Tezuka, "Quantum Lyapunov Spectrum," *JHEP* **04** (2019) 082, arXiv:1809.01671 [quant-ph].
- [179] H. Gharibyan, M. Hanada, B. Swingle, and M. Tezuka, "A Characterization of Quantum Chaos by Two-Point Correlation Functions," arXiv:1902.11086
  [quant-ph].